The Dissertation Committee for Scott David Auerbach Certifies that this is the approved version of the following dissertation:

Analysis of Mutations in the Kinesin Motor That Decouple ATPase Activity and Microtubule Interaction

Committee:

Kenneth A Johnson, Supervisor

Marvin L. Hackert

Brent L. Iverson

Theresa J. O'Halloran

Christian P. Whitman

Analysis of Mutations in the Kinesin Motor That Decouple ATPase Activity and Microtubule Interaction

by

Scott David Auerbach, B.A.

Dissertation

Presented to the Faculty of the Graduate School of

The University of Texas at Austin

in Partial Fulfillment

of the Requirements

for the Degree of

Doctor of Philosophy

The University of Texas at Austin

December 2004

Analysis of Mutations in the Kinesin Motor that Decouple ATPase Activity and Microtubule Interaction

Publication No._____

Scott David Auerbach, Ph.D.

The University of Texas at Austin, 2004

Supervisor: Kenneth A. Johnson

Conventional kinesin is a dimeric, microtubule-dependent motor whose activity is tightly coupled to ATP hydrolysis. Mutations that might affect the coupling between ATPase and motor activities of kinesin were predicted to fall within the gamma-phosphate sensor apparatus, a set of domains in the protein believed to detect the phosphorylation state of the bound nucleotide and mechanically transmit the information via conformational change to the microtubule-binding domain. An additional element, the relay helix, has been postulated to undergo axial translation, rotation, and/or elongation, in response to the loss of the gamma phosphate from the bound nucleotide, and serve as intermediary between nucleotide- and microtubule-binding sites.

An N-terminal truncation of rat conventional kinesin was examined using steady- and transient-state kinetic methods. Rate constants for ATP and microtubule binding were determined, as well as those for microtubule-dependent ADP and phosphate release. The dimeric state of the motor in solution was confirmed using analytical ultracentrifugation. Conserved residues within the gamma phosphate sensor were selected for mutagenesis. The residue E237 is believed to form a transient salt bridge with R204 when the motor is in the ATP state, based on crystal structure analysis, and the mutations E237A and E237D were examined using transient state kinetic methods. Both mutants showed > 10-fold reduction in steady-state ATPase activity, although rate constants for ATP and microtubule binding, as well as ADP release were little affected. These results suggested a disruption in the catalysis step caused by the mutations. An electrostatic interaction between E200 and R204 may also form in response to changes in nucleotide phosphorylation state, however, E200D and E200A mutants were scarcely compromised in steady-state ATPase activity, and this was attributed to a reduction in the rate constants governing product release. Finally, the N256K mutation caused a >1000-fold reduction in the rate of ADP release and a ~100-fold reduction in the steady-state ATPase rate. N256 falls within the relay helix, although the mechanism by which the N256K defect arises cannot yet be determined.

Table of Contents

List of Tables

List of Figures

List of Schemes

CHAPTER 1

Introduction

Kinetic analyses of the ATPase activity of rat kinesin, as well as a set of active-site mutants of the motor, are described in this work. The experiments performed were designed to examine pre-steady-state kinetics of kinesin-microtubule interaction, ATP binding, ATP hydrolysis, and product release. The techniques employed to not measure the force generated by the motor, nor the displacement of kinesin along the microtubule during substrate processing. ATP hydrolysis does, however, provide the free energy required for the directional movement of kinesin. Additionally, the interaction between kinesin and the microtubule filament to which it is bound influences ATPase activity. Kinesin, in short, is a force-generating enzyme whose biochemical and mechanical behaviors are tightly coordinated. What follows in this chapter describes features of kinesin biophysics and biochemistry that are relevant to the experiments described in the remainder of this work.

OVERVIEW OF MOTOR PROTEINS

The ability to exert directed and regulated mechanical force is one without which most complex forms of life would scarcely be possible. The process of intracellular transport requires the ability to discriminate a target object from among an ensemble of cellular components, and convey it through the cytoplasm. Regulation of this activity enables a cell to achieve the spatial and temporal distribution of macromolecules and organelles required for the successful execution of physiological tasks. Active transport mechanisms can mediate an accelerated redistribution of components over distances

across which simple diffusion would provide ineffective conveyance. Motor proteins, like other enzymes, can be specific for substrates, can provide a fulfillment of physiological goals more rapidly than can unassisted thermodynamic processes, and can be regulated in time according to the needs of the cell. They differ from typical enzymes in that the primary product of their activity is physical work rather than newly synthesized or disassembled molecules; their activities, however, are governed by the same underlying principles as are all enzymes.

The movement of a molecular load against hydrostatic friction requires that the object be pushed away from, pulled towards, or slid across another. The intracellular environment provides structures, in the form of the various components of the cytoskeleton, which can serve as anchors or tracks, upon or against which molecular motors exert force. Three families of molecular motors exist, which rely on either microtubules or actin filaments as mechanical support structures. The kinesins, dyneins, and myosins comprise a "molecular motor toolbox" fashioned by evolution, from which eukaryotic cells select to service their various motility needs [1]. Dyneins and kinesins utilize microtubules as a track along which loads are carried, whereas the myosins rely on actin for this purpose.

Phylogenetic analysis of the motor proteins allows for the identification of multiple classes within each. The myosin superfamily consists of 15 classes [2;3], the kinesins, 9 classes [4], and the dyneins, 3 classes [5]. All of the motor proteins share several features. First, each binds specifically to a cytoskeletal polymer, upon which its motile ability is dependent; myosin binds to actin, dynein and kinesin to microtubules. Second, the movement of each on its polymer track requires the hydrolysis of ATP. Those motor proteins serving as force-generating engines and bear structures intended for cargo binding, such that force may be exerted between cargo and cytoskeleton.

Several unusual classes of motor proteins are believed to perform roles that have diverged from that of motility, or perhaps represent ancestral functions. One such class is that of the MCAKs (mitotic centromere-associated kinesins), which are thought to bind to the ends of microtubules and destabilize them [6;7], forming part of the cellular apparatus responsible for microtubule assembly, maintenance, and disassembly. Like other motor proteins, the MCAKs are ATPases. Another kinesin-like protein, Xklp1, a member of the chromokinesin class responsible for chromosome-microtubule interactions and spindle pole extension, has been shown to inhibit microtubule disassembly [8]. Likewise, some myosins exist which may not function primarily as molecular motors. The myosin classes III and IX may have forfeited motility roles in exchange for those of cell signaling [9], or perhaps represent a myosin progenitor lacking force-generation capability, resembling more closely the structurally similar G-proteins, components of the signal transduction machinery in eukaryotes. Class III myosin, first identified as ninaC mutants in *Drosophila*, plays a role in photoreceptor signal transduction [10] and may have a protein kinase activity [11]. Myosin IX, identified in human, rat, and *C. elegans*, is a membrane-associated protein expressed in many cell types [12]. Although the exact signaling role played by myosin IX has yet to be determined, considerable evidence suggests that it functions as a Rho GTPase activating protein (RhoGAP) [13], a class of proteins that negatively regulates members of the Rho subfamily of small G-proteins. Since active Rho can trigger the formation of stress fibers, focal adhesions, and activate various actin-related processes, myosin IX may help organize and regulate the actin cytoskeleton [14].

OVERVIEW OF KINESIN STRUCTURE

Conventional kinesin was first identified in the giant axons of squid, and was shown capable of inducing ATP-dependent microtubule movement in a microscopic gliding assay [15;16]. It is an anterograde (forward-moving, in this case, moving towards the axon end and away from the cell body), plus-end directed microtubule motor responsible for the transport of vesicles along axons. Rat conventional kinesin, typically represented as a dimeric protein of elongated form, 955 residues (per monomer) in length, can be depicted as a dimer of mutually entwined α-helices forming a coiled-coil structure, flanked on both ends with N- and C-terminal globular domains [17]. Since the discovery of this archetype, related proteins from higher and lower eukaryotes have been identified, yielding an ensemble known as the kinesin superfamily [1;4]. The method of maximum parsimony applied to the analysis of sequence data from 144 kinesin motor domains generated a phylogenetic tree revealing 9 kinesin classes [4], as well as orphans not readily categorized. This superfamily has also been subdivided into 5 subgroups based on common tertiary and quaternary structural similarities across entire motor molecules [1], and 3 subgroups (KinN, KinC, and KinI), based on the placement of the catalytic core of the motor within the entire protein sequence (N-terminal, C-terminal and Internal placement) [18].

Considerable structural variation among the kinesins revolves about a central theme. Every kinesin bears a catalytic core, a globular motor domain of conserved sequence and structure, responsible for microtubule binding and ATP hydrolysis (figure 1.1). The remainder of the protein is of size and structure that varies between classes. In the crystal structure of a rat dimeric kinesin I (conventional kinesin) 379 N-terminal residue fragment, the N-terminal catalytic core, or head, is a globular structure of ~330 residues [19]. In this domain are found the features responsible for microtubule binding,

Figure 1.1: Crystal structure of rat conventional kinesin, with neck helices, neck linkers, and microtubule binding domains highlighted.

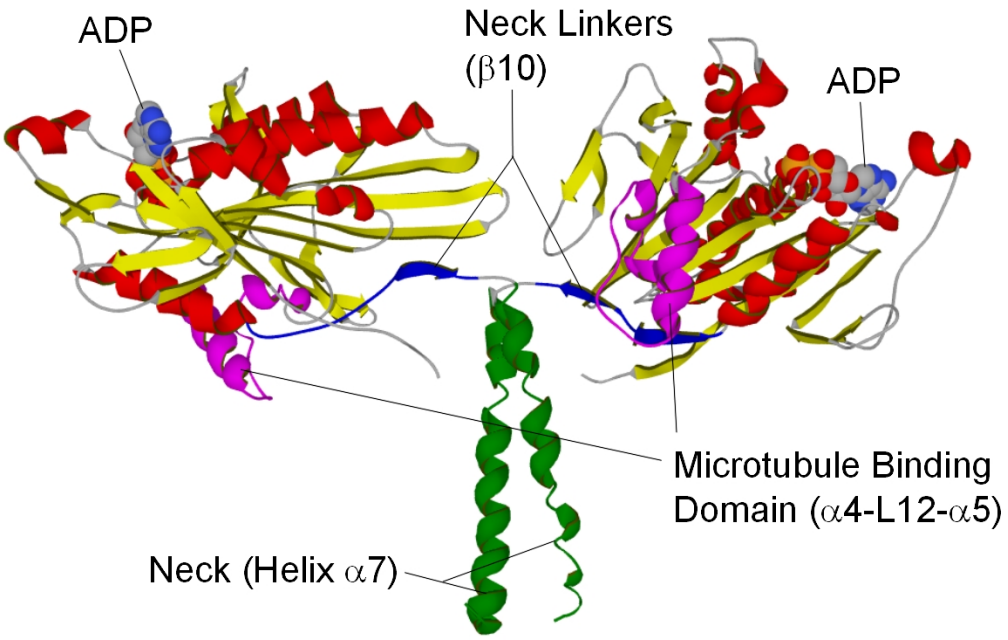

as well as for ATP binding and hydrolysis. The motor domain is sufficient for microtubule-activated ATP hydrolysis; the expression and purification of a 340 residue N-terminal truncation of *Drosophila* conventional kinesin from an *E. coli* expression system yields a protein that can hydrolyze ATP in a microtubule-dependent manner [20].

The monomers associate by virtue of interactions taking place between two parallel C-terminal α-helices, designated α7, extending to residue 379, which terminates the structure. This region is called the neck. Intervening between the neck and the catalytic core is the "neck linker", a 12-residue strand of primarily β-sheet structure, which appears in the crystal structure as docked to the core [19]. Kinesin dimerization requires the presence of the neck; a 366 residue N-terminal fragment of *Drosophila* conventional kinesin, lacking the neck, is monomeric [21]. The neck visible in the crystal structure contains 5 predicted heptad repeats, common to coiled-coil structures involved in the higher-order assembly of a diverse set of proteins [22], and the two component α-helices appear tilted 20° relative to one another, also typical of coiled-coil structures. Neck sequences are conserved within certain classes, are absent from others, and are less well conserved throughout the kinesin superfamily than are those of the catalytic core.

A coiled-coil domain called the stalk is separated from the neck by a flexible hinge region. The presence of this hinge structure, one of two punctuating the stalk, suggests that the neck is a functional domain. A second set of features within the neck suggests a contribution of the neck to the dynamics of kinesin motility that is distinct from that made by the stalk. The interactions between the parallel α7 helices of the two subunits in the dimer, ideally consisting entirely of those occurring among hydrophobic residues in the heptad repeats, are disrupted by the presence of three non-ideal residues, which serve to weaken the interaction [23;24]. Specific interactions among neck residues

at the junction between the neck and neck linker may inhibit unzipping of the coiled-coil neck domain [25]

The coiled-coil of the stalk in conventional kinesin is disrupted twice along its length by disordered regions where glycine and proline residues disrupt the α-helical structure and create a region of flexibility [17;26]. The presence of the first hinge, located roughly between residues 370 and 410 in rat brain kinesin, impacts the kinetics of kinesin motility. Deletion of the hinge from fungal kinesin produced a motor with reduced gliding velocity, suggesting that the hinge may be part of the functional motor domain [27]. The hinge may also play an important role in linking microtubule-dependent motility with cargo transport. A microtubule tethered to a glass surface by a single molecule of kinesin is capable of a 360° rotation due to Brownian motion in the absence of ATP hydrolysis, suggesting that kinesin's stalk has a torsional flexibility, most likely contributed by the hinges [28]. Such flexibility may be important in enabling several kinesin motors to propel a single organelle along a microtubule without being oriented along a common axis, as is myosin.

In conventional kinesin, a second hinge is present further down the stalk, creating a bending site roughly midway along its length (around residue 570 in conventional kinesin) as revealed by electron microscopy [29]. The second hinge is implicated in the folding behavior exhibited by conventional kinesin, as investigated by electron microscopy and sedimentation analysis [30;31]. At low ionic strength, kinesin adopts a folded conformation that becomes relaxed as the ionic strength is raised. The folding of conventional kinesin is an autoregulatory mechanism, thought to be of relevance to *in vivo* function; reduction of ionic strength from moderate (50 mM KCl) to low (5 mM KCl) causes a reversible ~ 90-fold reduction in the bimolecular ATPase rate constant of microtubule-activated full-length *Drosophila* kinesin, and this effect is dependent upon

the presence of the C-terminal 15 residues from the 960-residue long protein [32;33] as well as a functional second hinge [34]. Acidification of kinesin in cell extracts from pH 7.2 to 6.8 also increases microtubule-dependent motor activity, although sedimentation behavior is not affected [35]. Folded kinesin is inhibited in its ability to form productive microtubule complexes, perhaps due to an interaction between the C-terminus and the motor domain, brought into contact by hinge-mediated conformational change, although pH dependence experiments suggest that stalk folding is necessary but not sufficient for kinesin inhibition.

The structure of the C-terminus of conventional kinesin is complex, including a coiled region followed by a C-terminal globular domain. This portion of the stalk contains binding sites for accessory proteins [35;36] and, at least in the case of *Neurospora*, be mediated by the binding of cellular cargo as well [37]. In metazoans, a conventional kinesin dimer has associated with it two 60-70 kDa proteins called kinesin light chains [38], which bind to the heavy (motor) chain at its tail. The light chain may interact with and bind to receptor elements on cargo via six tetratricopeptide repeats [35], a common protein-protein interaction motif [39]. Light chains are also required for the complete inhibition of kinesin activity under restrictive conditions [35].

Mechanisms of kinesin regulation *in vivo* are likely to include phosphorylation [40]. The phosphorylation of kinesin light chains in neurons leads to release of membrane-bound organelles from kinesin and a reduction in kinesin-dependent motility [41]. Similarly, the mitotic centromere-associated kinesin (MCAK) is a phosphoprotein, and is regulated by the protein kinase Aurora B in *Xenopus* [42;43]. Kinesin phosphorylation may be necessary for glucose-stimulated release of insulin from pancreatic beta cells, since stimulation of cultured cells with calcium results in an accumulation of the phosphorylated kinesin heavy chain [44]. It is suggested from these

and similar observations, as well as studies concerning the salt- and pH-dependent folding states of kinesin, that kinesin undergoes regulation of its cargo binding and microtubule-dependent motility by several mechanisms.

The structure of conventional kinesin, having been reviewed in the preceding section, the functional relevance of its various features, as well as the mechanisms by which kinesin performs its tasks, are better understood with adjacent examination of the various members of the kinesin superfamily. Additionally, several predictions concerning the kinetics of conventional kinesin motility find their source in the analysis of related non-kinesin proteins. The myosin motor family, being of structural and functional similarity and presumed evolutionary kinship, warrants attention; the G-proteins, components of the cell signaling apparatus in eukaryotes, share surprising structural homology with the motor domains of the kinesins and myosins, are likewise deserving of scrutiny [45-47]. What follows, therefore, is a brief review of these two protein families insofar as they pertain to kinesin motor function.

RELEVANCE OF UNCONVENTIONAL KINESINS AND MUSCLE MYOSIN

The structure of conventional kinesin represents one of several variations on a central theme. Conventional kinesin, the motor responsible for fast axonal transport, was the first of this class of motor protein to be discovered, and remains one of the most thoroughly characterized. Kinesin superfamily genes are represented in every eukaryotic genome examined, ranging in number from 6 genes in *S. cerevisiae* to 45 found in the human genome [1;48]. Members of this family are implicated in the transport of vesicles and organelles [49], as well as a variety of other microtubule-dependent processes, such as meiotic and mitotic chromosome movement [50], microtubule dynamics, as in the case of MCAKs [51], as well as the maintenance and function of cilia and flagella [52;53].

Several members of the kinesin superfamily have been examined by x-ray crystallography; in each case, only a fragment consisting of the catalytic core, sometimes extended to include part of the neck, has been crystallized and examined. Structures of rat conventional kinesin in both dimeric and monomeric forms (with and without a portion of the neck domain required for dimerization) have been solved [19;54]. Human conventional kinesin has been crystallized under different conditions, revealing conformational state variations of possible mechanistic significance [45;55]. The catalytic cores of several unconventional kinesins have also been examined.

The Ncd (Nonclaret disjunction) protein from *Drosophila* is necessary for meiotic spindle assembly and stabilization [56;57]. With a design that departs from that of conventional kinesin by the C-terminal placement of its motor domain, Ncd nevertheless has a catalytic core that shares ~ 40% sequence identity with its conventional kinesin counterpart, and the three-dimensional structures of the two domains are nearly superimposable [58]. Like conventional kinesin, Ncd is a dimer in solution. Ncd, as well as all other kinesin-related proteins with C-terminal motor domains (the KinC group) also distinguishes itself from conventional kinesin by the direction of its movement on the microtubule track, towards the minus end, opposite from that taken by conventional kinesin [59]. Examination of the structure of Ncd coupled with kinetic analysis has provided insight into the determinants of kinesin directionality, as well as the mechanism by which unidirectional movement is achieved [60;61]. Additionally, analyses of mutations that disrupt the microtubule-dependent motility of Ncd are relevant to the understanding of mechanisms common to kinesin superfamily members [62;63].

The Kar3 protein is another kinesin-related protein from *S. cerevisiae* for whose catalytic core a structure has been determined by x-ray crystallography [64]. Kar3 plays a role in yeast mitosis, and is required for karyogamy (nuclear fusion). Like *Drosophila*

Ncd, it is a minus-end directed microtubule motor with a C-terminal motor domain, and has the additional feature of promoting the disassembly of microtubules from their minus ends, reminiscent of the MCAKs [65]. The examination of crystal structures of Kar3 mutants defective in microtubule-activated ATPase activity has revealed domain reorganizations within the catalytic core thought to accompany changes in the occupancy of the nucleotide binding site and phosphorylation of the nucleotide when bound [66].

Of the solved kinesin crystal structures, only one contains an ATP analog in its active site [67], the remainder being ADP co-crystals, containing the product of substrate hydrolysis. The ADP-bound state is associated with microtubule detachment, and free kinesin in the absence of microtubules is found in this state. A void exists, therefore, in the corpus of kinesin structural information, which might otherwise reveal the conformational changes precipitated by ATP binding and hydrolysis. Corresponding information from myosin, crystallized with bound ADP, non-hydrolysable nucleotide pseudosubstrates, and transition state analogs, illuminate myosin's motility mechanism [68;69]. The crystal structure of the kinesin-related protein Kif1A, bound to the non-hydrolysable ATP analog AMP-PCP, represents a unique picture of a kinesin in mid-stride [67;70]. Kif1A, like conventional kinesin, is an anterograde, plus-end directed microtubule motor in neurons, responsible for vesicle transport. It is, however, monomeric, belonging to the only class of monomeric motors within the kinesin superfamily, and the mechanism by which it moves along its microtubule track is likely to differ substantially from that of dimeric motors, despite the presence of the well-conserved catalytic core common to the kinesin superfamily [71].

The mechanism of movement and force production by kinesin is likely to share features with that of muscle myosin, an actin-dependent motor protein whose 180 residue catalytic core bears structural resemblance to that of kinesin and G-proteins ($p21^{ras}$, EF-

Tu, G-tα), preserving several structural elements in various states of modification. The interaction between myosin and its actin polymer track resembles that of kinesin and microtubules insofar as many events in the motility process of one appears to have a counterpart in the other. Differences between the two systems include the polymer specificity of each motor, as well as the timing and order of events in their motility cycles. The dynamics of force production by kinesin and myosin reflect the differences in the timing and sequence of mechano-chemical events characteristic of each motor. Most significantly are differences in duty ratio, defined as the fraction of the motility cycle during which a motor domain is attached to its polymer [72;73]. In the following section, the duty ratios and processivities of motor proteins will be examined.

PROCESSIVITY

Conventional kinesin is a processive motor [74-76]. Processivity describes the ability of a molecular motor to move across its polymer substrate without dissociation; a highly processive motor will execute many repetitions of its motility cycle while remaining bound to its track, while a nonprocessive motor dissociates after each step. Estimates of the processivity of dimeric kinesin have been made using *in-vitro* microtubule gliding and single molecule visualization assays, in which the distance traveled by a kinesin molecule along a microtubule track can be measured [77;78]. These experiments measured kinesin travel lengths of several micrometers before dissociation, which predicted hundreds of ATP hydrolysis events in a processive run. The kinetics of nucleotide processing by kinesin-microtubule complexes, including ATP binding, hydrolysis, and the release of product, allow an indirect determination of processivity [75;76;79]. Although estimated values of kinesin's processivity vary, the evidence supports two conclusions. First, that processive movement of a truncated *Drosophila*

conventional kinesin dimer (without the C-terminal inhibitory domain or associated light chains) hydrolyzes more than 10 (perhaps over 100) molecules of ATP subsequent to each kinesin-microtubule association event. Second, that processivity is dependent upon dimerization, since no evidence supports processive movement of conventional kinesin lacking the neck dimerization domain.

Muscle myosin (myosin II) is nonprocessive, despite its structural and functional similarities with kinesin. This difference reflects the tasks each motor performs; a single kinesin molecule might be called upon to transport a cargo item over millimeter distances or greater, whereas muscle myosin acts in bundles that may contain hundreds of molecules exerting force over comparatively short distances [80]. The duty ratios of the two proteins differ, a reflection of the tasks each performs. Since, in muscle thick filaments, many myosin molecules will act without synchronization upon a single thin filament actin molecule, each myosin-actin crossbridge should be short-lived, dissociating immediately after its mechanically productive dwell time in order to reduce the drag that would accompany static association. The small duty ratio of muscle myosin is reflected in observations made on single molecules. Although capable of exerting force upon an actin filament, a single myosin molecule is unable to move actin in an *in vitro* gliding assay, and cannot seek and attach to successive actin binding sites even under negligible mechanical loads [81-83]. Muscle myosin, like conventional kinesin, is a dimer; yet single-headed proteolytic S1 myosin subfragments can move actin in motility assays, suggesting that the two heads of the dimer act independently [84;85]. The temporal relationship between ATP hydrolysis and polymer binding by muscle myosin is likewise distinct from that evident in conventional kinesin; this topic will be further addressed in a subsequent section.

Not every member of the kinesin superfamily is processive, and not every myosin is nonprocessive. The minus-end directed *Drosophila* microtubule motor Ncd resembles myosin II in that, despite being a dimer, it lacks the processivity of conventional kinesin [86;87]. Models that relate kinesin processivity to the coordinated action of the two microtubule-interacting catalytic cores in a dimer can easily accommodate the shortcomings of the Ncd dimer; however, the existence of processive monomeric kinesins, such as the Kif1A protein, suggests the existence of multiple mechanisms for similar processes [88;89]. The myosins exhibit a diversity of mechanisms for force generation as well, and some have developed the capacity for processive movement. A cytoplasmic myosin, myosin V, is a processive actin-dependent motor that transports vesicles, organelles, and RNA [90;91]. Like conventional kinesin, myosin V is a dimer of two identical subunits, associating by virtue of a coiled-coil element that is terminated by motor domains that interact with actin and hydrolyze ATP. Thus, in the related families of the myosins and kinesins are found apparent solutions to the problem of how to move loads along protein polymers without dissociating, which have been applied in some instances where warranted, omitted where unnecessary or counterproductive.

Mechanisms proposed for unidirectional and processive movement of conventional kinesin take into account possible modifications that might permit nonprocessive movement by related motors such as Ncd and muscle myosin. The high duty ratio of conventional kinesin, coupled with the presence of two catalytic cores in the dimer, each with a microtubule binding domain, suggests an alternating site model, in which one head of kinesin remains tightly associated with a microtubule while the other is free to seek its next binding site [79;92;93]. While several variations on the theme have been proposed, all mechanisms suggested for conventional kinesin motility, as well as those for myosin V and other cooperative dimeric motors, share several features. First,

kinesin binds to discrete binding sites on the surface of a microtubule, which are distributed at regular intervals according to the dimensions of an αβ-tubulin dimer. Second, force generation by conventional kinesin is achieved through conformational changes in the kinesin dimer as a whole, not through force-generating conformational changes in each motor domain. Third, the microtubule-binding domain has a variable affinity for its target, and this affinity is modulated by the occupancy of the nucleotide-binding site. Fourth, the activity of each head of the dimer must be coordinated with that of the other in order to ensure unidirectional processive movement.

MICROTUBULE INTERACTION

An understanding of the mechanics of kinesin movement begins with one of the structure of a microtubule. Microtubules are components of the eukaryotic cytoskeleton, and are essential elements in mitotic spindles, flagella and cilia. Acting with microtubule-dependent motor proteins, microtubules are essential for the spatial organization of cellular components. A microtubule is a hollow cylindrical array of αβ-tubulin dimers arranged in a head-to-tail configuration [94]. The α and β subunits of tubulin are homologous proteins of ~55 KDa that, when laid end to end, form a protofilament with a periodicity equal to the distance spanned by a tubulin dimer, or about 8.0 nm. The most commonly encountered form of the microtubule *in vivo* is composed of 13 protofilaments arranged around a hollow core like barrel staves, forming a cylinder with an outer diameter of 25 nm [95;96].

A microtubule is a polar structure, whose ends are distinct in structure and behavior [94;96]. In a microtubule, the parallel alignment of protofilaments, composed of αβ-tubulin subunits laid end-to-end, presents α-tubulin at one end and β-tubulin at the other. These two ends, designated the minus- and the plus-end, respectively, differ in the

dynamics with which they grow and shrink through the addition and removal of additional tubulin dimers. The elongation of a single microtubule protofilament at the plus end is accompanied by tubulin-catalyzed GTP hydrolysis, which is then followed by the addition of a soluble αβ-tubulin dimer to the lattice. The plus ends are also subject to rapid depolymerization, making the microtubule an unstable structure, subject to alternating phases of growth and shrinkage. Microtubule dynamics *in vivo* are regulated by a set of microtubule-associated proteins that can either stabilize the plus end, or promote its depolymerization [97]. In contrast to the plus ends, the minus ends of microtubules are slow-growing *in vitro*, while *in vivo* are thought to be static, typically associated with complex microtubule organizing centers (MTOCs), which serve as nucleation sites for microtubule assembly.

The structure of tubulin has been solved to progressively higher resolutions by electron crystallography of zinc-induced tubulin sheets stabilized with taxol [98-100]. Images of microtubule-motor complexes visualized by cryo-electron microscopy soon followed, and have since revealed with increasing resolution the conformations adopted by microtubule-bound kinesin and kinesin-related motors. The method of cryo-electron microscopy permits high-resolution imaging of rapidly frozen (vitrified) samples by electron crystallography, and is particularly suited to 2-dimensional molecular arrays and macromolecules with helical symmetry [101;102]. Early 3-dimensional reconstructions of monomeric Ncd motor heads bound to tubulin sheets indicated that the motor domains make contacts with both α- and β-tubulin subunits at the surface of a single protofilament, such that one binding site exists at the interface between successive tubulin dimers [103]. This finding suggests that the spacing of motor-domain binding sites along the surface of a microtubule is equal to the lengthwise periodicity of the protofilament, or 8 nm.

Given the homology between the microtubule binding domains in Ncd and conventional kinesin, it is unremarkable that microtubules decorated with monomeric heads from the latter motor protein display a similar distribution [104]. An intermediate complex between dimeric conventional kinesin and a bound microtubule is suggested, in which the kinesin dimer adopts an extended conformation that permits both heads to simultaneously contact two successive binding sites, 8 nm apart, on a microtubule protofilament. Such an intermediate would allow processive movement, which requires at least one kinesin head to be bound at any given time, and demands the existence of a doubly bound transient. Reconstructed 3-dimensional images at 25 Å resolution of dimeric kinesin bound to microtubules show such a conformation [105], consistent with interpretations of earlier imaging data [106]. This conformation appears in the presence of the nonhydrolyzable nucleotide analog AMP-PCP, while kinesin-ADP appears in images from several laboratories to form only one attachment with the microtubule protofilament, leaving one head unbound [105;107;108]. Nucleotide-free kinesin, prepared by apyrase treatment, also forms the extended doubly bound conformation. The dimeric nonprocessive motor Ncd, in contrast, fails to adopt the proposed intermediate conformation under equivalent conditions, binding instead with a stoichiometry of one Ncd dimer per tubulin dimer, with one head bound and the other tethered [109;110]. The doubly bound state seen among conventional kinesin dimers attached to microtubules is believed to represent a rigor condition necessary for processive movement, and unnecessary for the motility of nonprocessive motors such as Ncd.

Images of conventional kinesin bound to microtubules also indicate that the dimer interacts with binding sites on a single microtubule protofilament, suggesting that a conventional kinesin motor performs a 1-dimensional walk along one protofilament at the surface of a 13-protofilament microtubule. This model is supported by the results of *in-*

vitro microtubule gliding assays, which showed that the path followed by conventional kinesin conforms to the non-helical protofilament axis of the microtubule [111]. In light of these observations, it is unlikely that conventional kinesin makes use of adjacent protofilaments for motility, taking parallel, "biped-like" steps along the microtubule surface. Instead, it probably walks on a single protofilament as if on a macromolecular tightrope. Models describing the details of this walk seek to address the conformational changes, occurring at scales encompassing secondary through quaternary structure, which accompany each step.

The ratio of motile speed and ATPase rate exhibited by conventional kinesin in motion on a microtubule track at low mechanical loads provides an estimate of the fuel consumption rate of the unburdened motor, being approximately one ATP hydrolyzed for each 8 nm step taken [112;113]. In optical force trapping experiments in which resistive force could be applied to single microtubule-bound kinesin molecules, the relationship between applied drag force and observed k_{cat} for kinesin ATPase activity was found to be consistent with a simple model in which ATPase activity and stepping are tightly coupled [114;115]. Tight coupling of ATP hydrolysis and force generation in the dynamics of this motor contradicts a thermal ratchet hypothesis of energy transduction, by which the free energy of nucleotide hydrolysis serves merely to provide a unidirectional bias to the otherwise random fluctuations in motor conformation, rather than driving a specific conformational change [116]. Thus, the existence, but not the identity, of a single force-generating substep in the mechano-chemical cycle of conventional kinesin is inferred.

A body of evidence supports a "hand-over-hand" model of conventional kinesin movement, whereby an 8-nm advance is achieved when the trailing head detaches from its binding site on the microtubule, and rebinds to a site upstream from the remaining bound head [117-120]. The trailing head is portrayed in this model as advancing 16 nm

(the distance spanned by two αβ-tubulin dimers) along the microtubule protofilament, thereby propelling the center of mass of the kinesin dimer 8 nm towards the plus end of the microtubule. Strong support for a hand-over-hand model comes from the biophysical examination of a heterodimeric conventional kinesin variant, with one head impaired in ATPase activity due to mutation [120]. The mutant heterodimer took alternating fast and slow steps, which was interpreted indicating alternating biochemical roles for the two heads, consistent with an alternating site, hand-over-hand stepping process. The model favored by the results of these studies is done so at the expense of an alternative "inchworm" model, which describes a motor dimer whose heads never exchange positions, but instead move forward in cycles that are out of phase, the trailing head taking an 8 nm step only after the leading one has already advanced. The inchworm model predicts that conventional kinesin should produce no torsional force during movement, since only the distance between the two heads varies during the motile cycle, while the hand-over-hand model requires a symmetric exchange of head positions, rotating the dimer about an axis normal to the microtubule. In an experiment designed to visualize any rotational movement of conventional kinesin in motion on a microtubule, no torsional force was detected, providing support to the inchworm model [121].

To resolve these contradictory findings, a distinction can be made between two possible classes of hand-over-hand mechanisms. A symmetric model, in which each step yields a kinesin-microtubule complex which is indistinguishable from the one preceding it, except that the kinesin dimer has been rotated such that the heads are now interchanged, and the dimer itself is 8 nm closer to the plus end of the microtubule, is contradicted by observations made concerning the absence of dimer rotation during translocation [121]. Symmetric hand-over-hand walking is expected to result in an alternating series of 180º rotations and reversals by the motor with each step, but this was

not detected. To accommodate these observations, a modified, asymmetric hand-over-hand model has been proposed, in which torsion is alternately absorbed and released by the dimer as it takes successive steps, yielding two distinguishable complexes, the identity of which depends upon which head has taken the lead position [105;119]. The steps taken by an asymmetrically walking kinesin dimer have been described as more closely resembling a "limping" than a walking process [122]. In optical trapping experiments, truncated *Drosophila* kinesin exhibits a detectable limp, or alternation between long and short dwell times, whereas native squid kinesin does not [119].

The processive, actin-dependent motor myosin V appears to propel itself using a hand-over-hand mechanism reminiscent of conventional kinesin [123;124]. However, the microtubule-dependent movement of the monomeric KIF1A motor, also processive, cannot be explained by such a mechanism. Nevertheless, the interaction between microtubules and the motor domain of KIF1A is most likely similar to that which occurs when conventional kinesin binds, given the similarity between the motor domains of the two proteins, which share 43% sequence identity. Unlike conventional kinesin, KIF1A takes steps whose sizes are multiples of 8 nm, Gaussian-distributed with a standard deviation of 15 nm, almost twice that of the step size [89]. The movement of this motor is described as a random walk, biased towards the microtubule plus end, but with frequent backwards steps taken. The force generated by KIF1A is at least an order of magnitude smaller than that from conventional kinesin (~0.15 pN vs. ~6 pN), reflecting the relative inefficiency of the force-generating mechanism employed by KIF1A.

The possible relationship between the mechanism by which KIF1A generates force and that governing force-generation in other kinesins is complicated by the presence of structural elements in KIF1A that appear to be unique to its class. A lysine-rich loop (the K-loop) near the microtubule-binding region of the motor domain may

stabilize the interaction between microtubule and motor, assist processivity, and perform a function in KIF1A motility that is absent from other motors [67;125]. Cryo-electron microscopy images of KIF1A bound to microtubules in the presence of either ADP or the nonhydrolyzable ATP analog AMP-PNP reveal a ~20º clockwise rotation of the ADP-state motor along an axis normal to the plane of interface between motor and microtubule [67]. The tip of the core in the ATP state is displaced towards the plus end of the microtubule because of this rotation. A similar effect is observed in the dimeric nonprocessive motor Ncd; somewhat surprising, since the plus-end displacement apparently triggered by ATP binding is in a direction opposite to that of the motor's overall movement [110]. Although the ATP-induced rotation and plus-end displacement is likely to be a feature common to the conserved kinetic cores of the various kinesins, directionality is determined by elements outside this domain.

DIRECTIONALITY AND THE NECK DOMAIN

Experimental evidence suggests that kinesin directionality is determined by the neck structure and placement. The construction and analysis of chimeric kinesins, containing motor domains from a kinesin of one polarity fused to necks from those of the opposite polarity suggest that directionality is determined only by the source of the neck, irrespective of the catalytic core; dimeric conventional kinesin whose catalytic core has been replaced with that of Ncd retains its plus-end directionality [126]. The inverse chimera, with the catalytic core of conventional kinesin and the neck of Ncd, moved towards the minus-end of the microtubule, but directionality could be reversed by point mutations in the neck [127]. One unusual Ncd variant, with a single neck residue change, exhibits both plus- and minus-end movement, changing directions at random, but moving in each case with near-wild-type velocity [63]. Thus, the default direction of kinesin

movement appears to be oriented towards the microtubule plus end, but can be reversed via an alternate mechanism of force transduction afforded by wild-type Ncd neck sequences, added N-terminal to the kinetic core.

These experiments illustrate the determinants of kinesin directional preference. The opposing paths taken by conventional kinesin and Ncd along the microtubule protofilament cannot be attributed to differences in binding site recognition by the respective motor domains; the Ncd-specific course-reversing modifications in the basic kinesin plan do not include the replacement of the microtubule binding region with one with inverted recognition, so as to point the motor in the opposite direction [128]. Image reconstructions of Ncd-microtubule complexes reveal a motor that is bound only by one head under both nucleotide-free and ATP-like (AMP-PNP) conditions, differing substantially from the observed conformation of conventional kinesin, doubly-bound under equivalent conditions [109;129;130]. The structural change induced by ATP binding appears primarily in the conformation of the neck, pointing towards the microtubule plus end in the absence of nucleotide, and towards the minus end under ATP-like conditions [130]. It is therefore likely that Ncd delivers its power stroke through the nucleotide-dependent conformational change in the orientation of the coiled-coil neck, directed towards vaulting bound cargo in the direction of the microtubule minus end. Ncd thus achieves minus-end movement at the expense of the more efficient hand-over-hand walking mechanism employed by conventional kinesin.

A single-headed N-terminal truncated conventional kinesin as been reported to exhibit nonprocessive, plus-end directed movement, despite lacking the K-loop present in monomeric KIF1A, or the capacity for cooperative kinetics possessed by the dimer [131]. Like KIF1A, this movement appears as a biased random walk, with backwards steps dispersed among forward, and further indicates the “default” direction of a kinesin

catalytic core, in the absence of neck sequences, as being oriented towards the microtubule plus end. The occupancy of the nucleotide binding pocket, whether by ATP, ADP, or neither, effects changes in the conformation of the catalytic core which influence its orientation upon, and affinity for the microtubule binding site. Additional conformational changes in the neck domain are responsible for directionality, and in conventional kinesin, cooperative mechanochemistry of the two heads that is necessary for processive movement. The nature and timing of these conformational changes have been at least partly elucidated using structural, spectroscopic, and kinetic data.

THE NUCLEOTIDE BINDING POCKET, SWITCH I AND SWITCH II

The catalytic core of conventional kinesin can be loosely described as consisting of a central β-sheet structure that divides two regions of α-helical composition. The residues making contact with the microtubule lay almost entirely on one side of the β-sheet that divides the domain, as determined by alanine-scanning mutagenesis [132]. The nucleotide-binding pocket, visible in crystallographic images, is found on the other side. The sequence and structure of the nucleotide-binding pocket is conserved not only among members of the kinesin superfamily, but across kinesins, myosins and G-proteins as well [133]. The active sites of motor proteins are rendered additionally complex over those of other enzymes by the requirement that they not only catalyze their respective biochemical reactions, but that they transduce the energy released into mechanical work, specifically directed towards conformational changes elsewhere in the protein that will result in the generation of force applied in an appropriate direction. In processive dimeric conventional kinesin, the activities of the two active sites suffer the further constraints placed upon them by the necessity of mutual coordination. Ironically, the mechanism by

which ATP is hydrolyzed by these proteins seems to be the least understood of these processes.

The catalytic mechanism by which these myosin and kinesin hydrolyze their respective nucleotides have resisted rigorous biochemical characterization, and there is no firm agreement on what it might be [134;135]. Since no proton acceptor lies within a distance from the cleavable P-O bond sufficient for base catalysis, it is likely that an activated water molecule within an extensive hydration network in the active site, visible in the crystal structures of myosin and kinesin, is responsible for proton abstraction [66;69]. In one model for myosin ATP hydrolysis, based on x-ray crystallographic structures of the motor in "pre-hydrolysis" (ATP-like) and transition-state forms, a "two-water hypothesis" is proposed, in which charge separation is achieved via a chain of immobilized water molecules, yielding a transition state that ultimately results in β-γ phosphate bond cleavage [134]. Equivalent mechanisms are proposed for the G-protein $p21^{ras}$ and *E. coli* EF-Tu [136;137]. Evidence for a similar mechanism in kinesin awaits the successful crystallization of the protein bound to the appropriate ATP analogs, but the similarities between myosin and kinesin active sites suggests that the mechanisms might be similar.

Four structural elements, conserved among myosins, G-proteins, and kinesins, interact with bound nucleotide, recognize changes in active-site occupancy, and mechanically link them with those portions of the protein responsible for the execution of various intra- and intermolecular transactions required for motility [128;138;139]. Two of these elements, N2 and N3, corresponding to Switch I and Switch II described in the G-proteins $p21^{ras}$ and *E. coli* EF-Tu, comprise a γ-phosphate sensor apparatus [140]. The N1 and N4 elements make stabilizing contacts with the α- and β-phosphates of the bound nucleotide, and the adenine ring, respectively. Of these four structures, the two switching

elements, Switch I and II, appear to play the most significant role in coordinating the conformational transitions of the motor as a whole, and have consequently received the most attention in the literature. Figure 1.2A and 1.2B illustrate the positions of the four structures relative to bound nucleotide.

Switch I (consensus sequence NxxSSR) and II (consensus sequence DxxGxE) are short peptide stretches conserved among the myosins and kinesins. Crystal structures of myosin appear in three distinct conformations, depending on crystallization conditions, as well as the identity of the bound nucleotide [141-145]. These conformations distinguish themselves from one another primarily in the positions of four structural elements, one of which is the γ-phosphate sensor apparatus, containing Switch I and II. It is suspected that rearrangements in this element, being directly coupled to the chemistry that transpires in the nearby active site, serve as initiators for those in the remaining three, which are mechanically downstream [128;133;138;146]. The binding of GTP to the small GTPases $p21^{ras}$, EF-Tu, and G-tα, appears to be accompanied by a closure of the nucleotide-binding pocket, which is relieved upon hydrolysis of the nucleotide. These two structural states, termed "opened" and "closed", are distinguishable in myosin not by binding pocket closure, but by the formation of a salt bridge visible only in the closed, ADP-AlF_4^- (ATP-like) state, between Switch I arginine and Switch II aspartic acid [142;143]. Myosin in the ATP-bound state is short-lived, yielding quickly to an ADP + P_i state after hydrolysis, and the affinity of the motor domain for actin is weak. The salt bridge visible in this crystal structure is broken in the structures of nucleotide-free myosin (the "near-rigor" state), and myosin-ADP (the detached state) [68;147]. Interestingly, in the structure of myosin-ADP-VO_4 (the "transition state"), the γ-phosphate sensor salt bridge has likewise failed to form [145].

Figure 1.2A: Structure of the nucleotide binding pocket

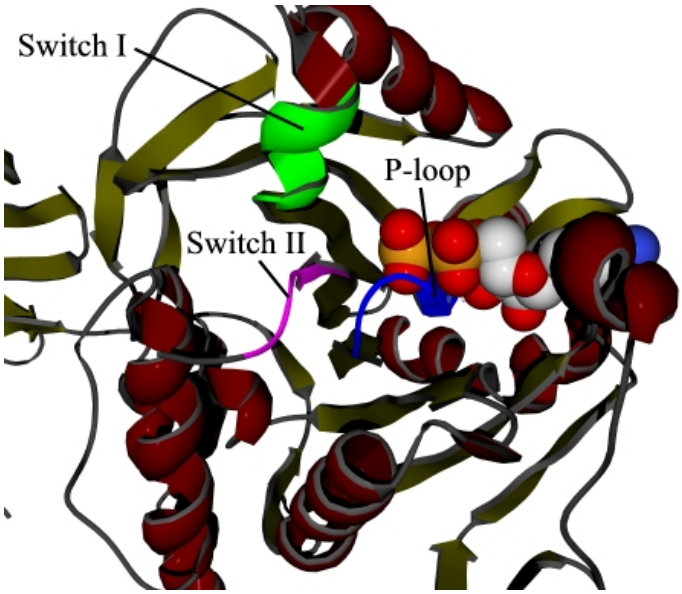

Figure 1.2B: Alternate view of the nucleotide binding pocket, showing Glu237-R204 salt bridge [133]

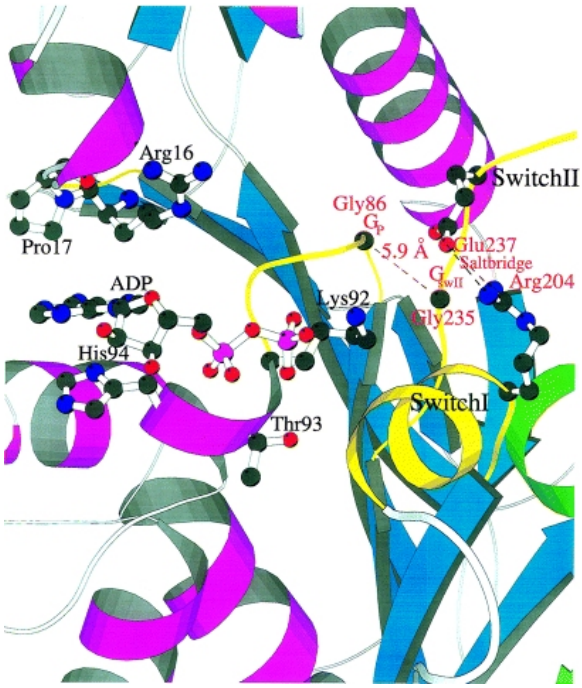

Among the kinesins, distinct nucleotide-dependent conformational changes are poorly understood, since only one structure (KIF1A) has been solved in a true ATP-like state, containing a non-hydrolyzable ATP analog in its active site [67;70]. This structure reveals distinct conformational changes over its ADP-bound counterpart, particularly in the Switch II cluster, which includes the Switch II stretch, as well as a loop and α-helix immediately N-terminal to it. This helix, α4, also called the Relay Helix, exhibits a piston-like behavior apparent in myosin crystallographic images, translating along its axis in response to alternate phosphorylation states of the bound nucleotide [69;142;143]. Surprisingly, the conformation of the Switch II cluster shows variability even among kinesins crystallized with ADP. Crystal structures of rat and human conventional kinesins, nearly identical in sequence, nevertheless reveal distinct Switch II cluster conformations, with the structure of the former most closely resembling that of the KIF1A-AMPPNP co-crystal [45;54]. A low energy barrier between multiple kinesin states in the absence of microtubules, permitting condition-dependent alternate crystallization configurations, may explain these findings [128;148].

These studies identify movement of the Switch II complex as being the source of the observed state transition. In crystal structures of myosin bound to various ATP analogs, as well as those of the various kinesins, it has become evident that the Switch II complex provides a mechanical linkage between the nucleotide binding pocket and the microtubule-binding domain, and may undergo rotation and translation in response to nucleotide hydrolysis and phosphate release [45;54;58;64]. There is the additional possibility that helix α4 (the Relay Helix), N-terminal to Switch II, may undergo a nucleotide-dependent change in it's length, elongating by recruiting residues from the adjacent loop L11 [64].

QUESTIONS TO BE ADDRESSED

The kinetics of *Drosophila* conventional kinesin have been studied using transient-state kinetic methods [20;74;75;79;92;93;149-152]. However, rat conventional kinesin currently holds greater promise for studies concerning structure-function relationships, since its crystal structure has been solved, whereas that of *Drosophila* conventional kinesin has not [19]. Thus, the first set of experiments described in the present study examine the kinetic mechanism of rat conventional kinesin ATPase activity in order to establish a baseline against which the activities of mutant kinesins can be compared, as well as to uncover any differences between the kinetic behaviors of the rat and *Drosophila* enzymes. We then prepared several kinesin mutants that were of potential relevance to the mechanism by which the active site of kinesin is mechanically linked with the microtubule-binding domain. Mutations were prepared at both Switch I R204 and Switch II E237, two residues that are believed to form a transient salt bridge during the motility cycle. A third residue, Switch I E200, was identified by examination of the crystal structure as being capable of participating in an electrostatic interaction with R204, and was chosen for mutagenesis. Finally, a mutation N-terminal to Switch II, N256K, was prepared and examined. This mutation, at a residue that is conserved among the kinesins, corresponds to a mutation identified as decoupling ATP hydrolysis and microtubule-binding activities in the kinesin-like motor Kar3 [62].

CHAPTER 2

Materials and Methods

MATERIALS

Reagents. BLR(DE3), the *Escherichia coli* strain used for protein expression, was obtained from Novagen Inc. (Madison, WI). *E. coli* strain XL1-Blue was from Stratagene (La Jolla, CA). QIAprep Plasmid DNA extraction kits were purchased from Qiagen Inc. (Valencia, CA). The QuickChange Site-Directed Mutagenesis Kit was purchased from Stratagene (La Jolla, CA). Bio-Rex 70 resin (75-150 μm wet bead size) and Bio-Gel P-4 Gel (45-90 μm particle size) were purchased from BioRad Laboratories (Hercules, CA). DEAE-, Q-, and S-Sepharose Fast Flow chromatography resin were from Amersham Biosciences Corp. (Piscataway, NJ). Taxol (paclitaxel) was purchased from Sigma Chemical Co. (St. Louis, MO). Radiolabeled ATP ([α^{32}P]ATP, >3000 Ci/mmol) was from Perkin Elmer (Boston, MA). Phosphocreatine, creatine phosphokinase (300 u/mg), purine nucleoside phosphorylase (PNPase), 7-methylguanosine, isopropylthiogalactopyranoside (IPTG), and nucleotides (ATP, GTP, dATP, dCTP, dGTP, TTP) were purchased from Sigma Chemical Co. (St. Louis, MO). *N*-methylisatoic anhydride and *N*-[2-(1-maleimidyl)ethyl]-7-diethylaminocoumarin-3-carboxamide (MDCC) were from Molecular Probes (Eugene, OR). PEI-cellulose F TLC and silica gel 60 F_{254} plates (EM Science) were purchased from VWR Scientific (West Chester, PA). Other chemicals were from Sigma Chemical Co. (St. Louis, MO) or Fisher Scientific (Pittsburgh, PA).

Media and Buffers. The following media and buffers were used for the experiments described: PBS (8 g/L NaCl, 0.2 g/L KCl, 1.44 g/L Na_2HPO_4, 0.24 g/L KH_2PO_4, pH 7.4); LB broth (10 g/L bacto-tryptone, 5 g/L bacto-yeast extract, 10 g/L NaCl); Terrific Broth (12 g bacto-tryptone, 24 g bacto-yeast extract, 4 ml glycerol per liter); TG-plus minimal medium (120 mM Tris-HCl, pH 7.2, 80 mM NaCl, 20 mM KCl, 20 mM NH_4Cl, 3 mM Na_2SO_4, 100 mg/L L-arginine-HCl, 50 mg/L L-leucine, 40 mg/L L-histidine-HCl, 20 mg/L L-methionine, 30 mg/L L-tryptophan, 20 mg/L adenosine, 10 μM $FeSO_4$, 0.2 mM $MgSO_4$, 0.2 mM $CaCl_2$, 10 mg/L thiamine); Buffer A (30 mM HEPES, pH 7.2, 4 mM $MgCl_2$, 0.1 mM EDTA, 20 μM ATP); Buffer B (50 mM Tris-HCl, pH 8.2, 4 mM $MgCl_2$, 0.1 mM EDTA, 20 μM ATP); ATPase Buffer (40 mM HEPES, pH 7.2 with KOH, 5 mM magnesium acetate, 50 mM potassium acetate, 0.1 mM EDTA, 0.1 mM EGTA, 0.5 mM DTT); PM buffer (100 mM Na-PIPES, pH 6.6, 4 mM magnesium acetate, 1 mM EGTA). Each buffer's pH was adjusted at the temperature at which it was to be used.

Construction of pKHC407A and Mutant Derivatives. The plasmid used in the expression and purification of an N-terminal fragment of rat conventional kinesin heavy chain was derived from pKHC406 [153], a gift from Scott Brady (University of Texas Southwestern Medical Center, Dallas TX). The C-terminal polyhistidine tag encoded in the plasmid was removed by substitution of the first non-kinesin codon in the open reading frame of the plasmid with a nonsense codon, using site-directed mutagenesis [154]. Kinesin mutants were likewise generated using PCR-mediated codon substitution. Oligonucleotides for site-directed mutagenesis were purchased from Integrated DNA Technologies (Coralville, IA). For removal of the polyhistidine tag, the complementary primers

5’-CACCTGTGGTTGACTAGCTTGCGGCCGCAC-3’ and

5’-GTGCGGCCGCAAGCTAGTCAACCACAGGTG-3’

were used. The resulting plasmid, pKHC407A, expresses an N-terminal fragment of rat conventional kinesin terminating at asp407. A QuickChange Site-Directed Mutagenesis Kit, obtained from Stratagene (La Jolla, CA), was used, as well as a GeneAmp PCR System 2400 from Perkin Elmer (Boston, MA) for polymerase chain reaction [155]. Temperature cycles were as recommended by the kit manufacturer: 95ºC (30 s), 55ºC (1 min), and 68ºC (6 min) for 16 cycles. Mutations were introduced into pKHC407A using site directed mutagenesis and primer pairs described in table 1.1:

Table 2.1: *Primers used for mutagenesis*

N256K	5’-GATGAAGCTAAAAATATCAAAAAGTCTTTGTCTGCTCTTGG-3’ 5’-CCAAGAGCAGACAAAGACTTTTTGATATTTTTAGCTTCATC-3’
E200A	5’-GACAAACATGAACGCACACAGCTCCAGG-3’ 5’-CCTGGAGCTGTGTGCGTTCATGTTTGTC-3’
E200D	5’-GACAAACATGAACGATCACAGCTCCAGG-3’ 5’-CCTGGAGCTGTGATCGTTCATGTTTGTC-3’
E237A	5’-GATTTGGCTGGGAGTGCAAAGGTCAGCAAAACTGG-3’ 5’-CCAGTTTTGCTGACCTTTGCACTCCCAGCCAAATC-3’
E237D	5’-GATTTGGCTGGGAGTGATAAGGTCAGCAAAACTGG-3’ 5’-CCAGTTTTGCTGACCTTATCACTCCCAGCCAAATC-3’

Expression of Kinesin. The pKHC406 plasmid and its derivatives are based on the IPTG-inducible pET expression vector [156-158]. In these vectors, an open reading frame to be expressed is under the control of a T7 promoter, with T7 RNA polymerase supplied in *trans* from an IPTG-inducible operator on the bacterial chromosome. Colonies of transformed *E. coli* BLR(DE3) were grown overnight with shaking at 37ºC in 2 L LB broth plus 1% dextrose, 50 μg/mL kanamycin and 10 μg/mL tetracycline. Cells were centrifuged and resuspended in 4 L Terrific Broth, where growth was allowed to continue for 1 hour at 37ºC. The culture was then induced with the addition of 0.4 mM IPTG, and further incubated at 20ºC with shaking for 4 hours. Cells were then harvested, washed once in PBS, and centrifuged again. Approximately 20 g of cells were obtained using this procedure. Cells were frozen in liquid nitrogen and stored at -80ºC.

Purification of Kinesin. Kinesin preparations were kept on ice or at 4ºC. Cells from 4 L induced culture were resuspended in 50 mL Buffer A plus 95 mM NaCl, 1 mM EDTA, 1 mM EGTA, 0.5 mM PMSF, 0.5 μg/mL leupeptin, 0.25 μg/mL lysozyme. The suspension was disrupted using a Branson Sonifier model 450 (VWR, West Chester, PA), for 4 bursts on ice, power setting 4, 20 sec/burst. The lysate was then cleared by centrifuging (Beckman JA-25.50 rotor, 23,000 × g, 30 minutes), and loaded onto a 34 mL BioRex70 column (2 cm^2 × 17 cm) pre-equilibrated with Buffer A plus 95 mM NaCl. This and all subsequent column chromatography operations were conducted at a flow rate of 1 mL/minute. The column was washed with 3 column volumes of the equilibrium buffer. Elution of protein was performed using a 4-column volume gradient spanning 95 mM to 485 mM NaCl, and 4-mL fractions were collected. The fractions were evaluated by SDS-PAGE, and kinesin appeared as an abundant ~45.5 kDa protein. Fractions that contained kinesin were pooled and dialyzed for 2 hours against 1 L Buffer B plus 95 mM

NaCl. The dialyzed kinesin was then loaded at onto a 10-mL Q-sepharose column (2 cm^2 × 5 cm) pre-equilibrated with the same buffer. After a 3-column volume wash, kinesin was eluted with a 6-column volume gradient from 95 to 475 mM NaCl, and 2.5 mL fractions were collected. Fractions were evaluated by SDS-PAGE, and those in which a ~45.5 kDa protein was predominant were selected and pooled. The pooled fractions were dialyzed twice for 2 hours apiece against 1 L of Buffer A plus 40 mM NaCl. After dialysis, the preparation was loaded onto a 3 mL Q-sepharose column (0.8 cm^2 × 3.75 cm), pre-equilibrated with the same buffer, and the column washed with 3 column volumes. Elution was done with a 3-column volume gradient spanning 40 to 240 mM NaCl, and 2 mL fractions were collected. Those fractions containing kinesin, as judged by SDS-PAGE, were dialyzed twice for 2 hours apiece against ATPase buffer plus 0.1 μM ATP. Purified kinesin was then dispensed into 50-100 μL aliquots, snap-frozen in liquid N_2, and stored at -80ºC. Before use, thawed kinesin aliquots were centrifuged (Heraeus Biofuge, 15,000 × g, 10 minutes) to remover debris and precipitants.

Mammalian Brain Tubulin and Microtubule Preparation. Tubulin was extracted from bovine brain tissue by exploiting the temperature-dependent and reversible polymerization of the protein into microtubules [159;160]. Microtubule-associated proteins were then removed by DEAE chromatography [161;162]. Microtubules were stored at -80°C as centrifuged pellets. On the day of each experiment, pellets were thawed and resuspended in PEM buffer plus 1 mM GTP to a concentration of 10-15 mg/mL and depolymerized on ice for 20 minutes. Aggregates were removed by centrifugation (Heraeus Biofuge, 15,000 × g, 15 minutes). Taxol was added stepwise to concentrations of 0.2, 2 and 20 μM, with 10-minute incubations at 34°C subsequent to each addition. The solution was then diluted 10-fold with PEM buffer plus 10 μM taxol

to stabilize the microtubules, and further incubated at 34°C for 10 minutes. After centrifugation (Beckman JA-25.50 rotor, 39,000 × g, 30 minutes, 4°C), the microtubule pellet was resuspended in ATPase buffer plus 20 μM taxol. Microtubules were passed 10-50 times through a 25G $^{5}/_{8}$ syringe needle to maximize homogeneity. Microtubule concentration was determined using the method of Bradford [163], and reported molar concentrations of microtubules refer to the concentrations of αβ-tubulin dimer (M.W. of 110 kDa) in a given preparation of polymerized, taxol-stabilized microtubules.

Nucleotide Analogs. *N*-methylanthraniloyl (mant) derivatives of ATP and ADP were synthesized as described [164;165]. The products were purified by DEAE sepharose chromatography. The crude product of a reaction between 1 mmol nucleotide and excess methyisatoic anhydride was purified by ion-exchange chromatography using a 100 mL DEAE sepharose column (8.0 cm^2 × 12.5 cm), and eluted with an ammonium bicarbonate gradient from 20 to 800 mM. Product purity was evaluated by thin layer chromatography, using silica gel 60 F_{254} and a 1-propanol/NH_4OH/H_2O mobile phase. Spectrophotometric properties of the products were evaluated and conformed to published values. 2'(3')-mantADP and 2'(3')-mantATP are reported to have an A_{255}/A_{356} ratio of approximately 4.0, reflecting the optical densities of the *N*-methylanthraniloyl and adenine moieties [164].

Phosphate Sensor. Phosphate release experiments measured the rate at which inorganic phosphate is released from kinesin, and relied on an engineered *E. coli* phosphate binding protein (PBP-A179C) covalently coupled to a fluorescent dye *N*-[2-(1-maleimidyl)ethyl]-7-diethylaminocoumarin-3-carboxamide (MDCC) [166;167]. The tagged protein exhibits fluorescence at 465 nm that is modulated by the binding of

inorganic phosphate such that its fluorescence in the phosphate-bound state is ~7 times that in the free state [166]. The expression system for the protein component, consisting of the *E. coli* strain ANCC75 containing a pBR322-derived plasmid into which the modified phoS gene directing the production of PBP-A197C has been cloned, was obtained from M. Webb (National Institute for Medical Research, London, UK). To express PBP-A179C, the expressing strain was grown overnight in 1 L TG-plus medium containing high (0.64 mM KH_2PO_4) inorganic phosphate at 37°C with shaking. This culture was then centrifuged (Beckman JLA-16.250 rotor, 1,300 × g, 30 minutes), and the pellet resuspended in 1 L of TG-plus medium supplemented with low (64 μM KH_2PO_4) inorganic phosphate, and grown 12 hours at 37°C with shaking.

Periplasmic PBP-A197C protein was released from the cells by osmotic shock [168]. Conjugation of the protein with MDCC, and subsequent purification of the phosphate sensor were performed as described in by Brune et al. [167]. The concentration of MDCC-PBP-A197C was determined spectrophotometrically, assuming an extinction coefficient at 280 nm of 68,575 $M^{-1}cm^{-1}$. This value represents the sum of contributions from the protein itself, whose extinction coefficient was estimated from amino acid composition [169], and the reported contribution of the fluorophore [166]. To minimize contaminating phosphate in the preparation, a "phosphate mop" was introduced into it before freezing, consisting of 200 μM 7-methylguanosine and 0.2 units/mL purine nucleoside phosphorylase, which sequesters inorganic phosphate by the synthesis of ribose-1-phosphate from 7-methylguanosine. MDCC-PBP-A197C containing the phosphate mop was divided into 100 μL aliquots, snap-frozen in liquid N_2, and stored at -80°C.

METHODS

SDS-PAGE. Fractionation of proteins under denaturing conditions was done with slab gels using the buffer formulation of Laemmli (Laemmli 1970). Stacking and separating components of the gels were 3 and 8% acrylamide, respectively. Staining was done using Coomassie brilliant blue R (Fairbanks 1971). Pre-mixed molecular weight standards (Bio-Rad Laboratories, Hercules, CA), contained myosin (209 kDa), β-galactosidase (124 kDa), BSA (80 kDa), ovalbumin (49.1 kDa), carbonic anhydrase (34.8 kDa), trypsin inhibitor (28.9 kDa), lysozyme (20.6 kDa), and aprotinin (7.1 kDa).

Protein Concentration Determination. The concentration of kinesin was estimated spectrophotometrically, and that of active kinesin determined by active site titration using a phosphocreatine kinase coupled enzyme assay (see below). The extinction coefficient at 280 nm of kinesin KHC407 was estimated at 27,960 $M^{-1}cm^{-1}$, based on amino acid composition [169]. This estimate takes into account the contribution of one molecule of ATP per kinesin monomer. Concentrations of microtubules were determined immediately before use by the method of Bradford, using BSA concentration standards [163].

Phosphocreatine Kinase Coupled Enzyme Assay. A determination of active kinesin concentration was made by measuring the time-dependent dissociation of kinesin-bound ADP. The dissociation rate of the hydrolyzed nucleotide could also measured by this technique. Phosphocreatine kinase, upon mixing with kinesin-[α^{32}P]ADP, can only regenerate the nucleotide triphosphate from free nucleotide diphosphate, leaving kinesin-bound nucleotide unmodified. Thus, [α^{32}P]ADP is converted to [α^{32}P]ATP at a rate equivalent to that at which it is released form the kinesin nucleotide pocket, given a

phosphocreatine kinase concentration sufficient such that the rate of nucleotide release from kinesin is the rate-limiting step in the reaction sequence [170]. Rebinding of [α^{32}P]ATP is prevented by the inclusion of cold ATP.

In the assay, a preparation of kinesin, of estimated concentration between 10 and 30 μM, is mixed with [α^{32}P]ATP at a concentration twice that of kinesin. The mixture is incubated for 30 minutes to allow nucleotide exchange between solution and active site, and hydrolysis of the nucleotide triphosphate. The reaction is initiated by mixing 5 μL labeled kinesin with 20 μL of a chase solution consisting of 0.3 mg/mL phosphocreatine kinase, 4 mM phosphocreatine and 5 mM Mg-ATP in ATPase buffer. Reaction times ranged from 0 to 840 seconds. The reaction is terminated after a designated interval with the addition of 25 μL 2 N HCl, which quenches the reaction. This was immediately followed by 12 μL 2 M Tris-3 M NaOH to neutralize the mixture, and 50 μL chloroform to denature the proteins. The assay was performed at room temperature (22°C). Nucleotide products were separated by PEI-cellulose thin layer chromatography, developed with 0.6 M KH_2PO_4 pH 3.4. Finally, [α^{32}P]ATP and [α^{32}P]ADP were visualized and quantified using a Molecular Dynamics Storm 860 phosphorimager and ImageQuant software (Amersham Biosciences, Little Chalfont, Buckinghamshire, UK).

The fraction of radiolabeled nucleotide in the hydrolyzed diphosphate form, representing the fraction of that remaining bound to kinesin after the reaction interval, was plotted against time, and the data could then be fit by nonlinear regression using GraFit (Erithacus Software, Horley, Surrey, UK) to a single exponential model of the form $[ADP]/([ADP] + [ATP]) = A \cdot \exp(-k \cdot t) + C$, where A and k are the amplitude and rate constant governing nucleotide release, respectively. Active site concentration, corresponding to the concentration of active kinesin monomer, was determined using the equation $[kinesin] = ([ATP] \cdot A)/(1 - A)$, where [ATP] is the concentration of [α^{32}P]ATP

used in the initial kinesin labeling. The equation takes into account a postulated augmentation of the added radiolabeled nucleotide by ADP bound to the active sites of the added kinesin. The value of C was typically less than 8% of that of A, and was regarded as inconsequential to the calculation of active site concentration.

Steady-State ATPase Assays. The hydrolysis of [α^{32}P]ATP by kinesin-microtubule complex was monitored by mixing labeled nucleotide with the enzyme, quenching the reaction after a predetermined time, separating the products on a TLC plate, and measuring the hydrolysis of the labeled nucleotide by standard radiation monitoring techniques. Kinesin-microtubule complex, of selected component concentrations, was prepared in ATPase buffer, to a volume of 2 mL. For evaluation of multiple ATP concentrations, a series of dilutions of the nucleotide were prepared and spiked with in invariant quantity of [α^{32}P]ATP, thus ensuring an equivalent signal/volume ratio for each. To initiate each reaction, 150 μL of kinesin-microtubule complex was rapidly mixed with 50 μL radiolabled ATP. At each designated time point, 25 μL of the reaction were withdrawn, quenched by mixing with 25 μL 2 N HCl, neutralized by the addition of 12 μL 2 M Tris-3 M NaOH, and denatured by the addition of 50 μL chloroform. Finished samples, prior to analysis by thin layer chromatography, were centrifuged (Heraeus Biofuge, 15,000 × g, 5 minutes) to remove precipitants. These assays were performed at room temperature (22°C). Nucleotide products were separated by PEI-cellulose thin layer chromatography, developed with 0.6 M KH_2PO_4 pH 3.4. Finally, [α^{32}P]ATP and [α^{32}P]ADP were visualized and quantified using a Molecular Dynamics Storm 860 phosphorimager and ImageQuant software (Amersham Biosciences, Little Chalfont, Buckinghamshire, UK).

The steady-state rate of ATP hydrolysis is reflected in the initial velocity of the reaction, before it is affected by substrate depletion or product inhibition. The time-dependent appearance of [α^{32}P]ADP was plotted versus time, and the data were fit by nonlinear regression using Excel (Microsoft Corp., Redmond, WA) to a third-order polynomial. This fit serves only to provide a convenient method for extracting the initial velocity of the reaction, according to the coefficient of the linear term. Velocity data for a range of substrate concentrations were then plotted using GraFit (Erithacus Software, Horley, Surrey, UK) and fit to a hyperbolic model $k_{obs} = k_{cat}[ATP]/(K_{m\text{-}ATP} + [ATP]) + C$ to determine values of k_{cat} and $K_{m\text{-}ATP}$.

Analytical Ultracentrifugation. To determine whether KHC407A exists as a dimer in solution, a sedimentation equilibrium experiment was performed. A Beckman-Coulter Optima XL-1 analytical ultracentrifuge was used, fitted with an AnTi60 rotor and absorbance optics. Using 3 6-channel charcoal-filled Epon centerpieces, 9 kinesin concentrations could be evaluated simultaneously. Rotor speed was 13,000 rpm and run temperature was 24°C. Equilibrium data were collected at 230 nm at a spacing of 0.003 cm with 5 averages in a step scan mode. Data sets were collected at 2 hour intervals between 16 and 22 hours after run initiation, and equilibrium verified by comparing successive scans. Optical data was edited in Excel (Microsoft Corp., Redmond, WA) to extract data from individual channels, and analyzed by nonlinear least-squares fitting to a self-association scheme using NONLIN [171]. NONLIN was obtained from the Center for Analytical Ultracentrifugation of Macromolecular Assemblies at University of Texas Health Science Center at San Antonio. The program fits to the reduced molecular weight of the protein, given by $\sigma = M(1-\bar{v}\rho)\omega^2 / RT$, where M is the molecular weight of the monomer, $\bar{v}$ the partial specific volume, ρ the solvent density, and ω the rotor angular

velocity. An estimate of 0.7350 $cm \cdot g^{-1}$ for the partial specific volume of the kinesin monomer was made based on amino acid sequence contribution, taking into account a contribution of -0.0030 $cm \cdot g^{-1}$ made by the bound ADP. Solvent density was determined volumetrically to be 1.0056 $g \cdot cm^{-1}$.

Kinesin dilutions were selected to cover a 20-fold concentration range, and concentration was expressed as active site concentration, determined by the phosphocreatine kinase coupled enzyme assay. The extinction coefficient ε at 230 nm, the wavelength monitored during the analytical ultracentrifugation experiment, of KHC407A, was determined at 31,260 $M^{-1}cm^{-1}$, and this figure was used to convert the apparent association constants determined by NONLIN from optical density units to those of molarity according to the relationship $K_2(M^{-1}) = K_2(abs^{-1}) \times (1.2\varepsilon/2)$, where 1.2 is the optical path length in centimeters of the rotor centerpiece. NONLIN was used to fit equilibrium optical profiles of the sample channels to a simple monomer-dimer association reaction, with no assumed nonideality. Graphical representation of data, curve-fitting, and residuals was performed using GraFit (Erithacus Software, Horley, Surrey, UK).

Rapid Quench Experiments. Transient-state kinetic analysis of kinesin ATPase in ATPase buffer was performed at 35°C, reflecting the temperature of the mammalian brain. A KinTek chemical quench flow instrument (KinTek Corp., Austin, TX), was used in these experiments, permitting the rapid reaction initiation by mixing of enzyme and substrate, followed by termination within milliseconds by acid quenching (Johnson 1983). Kinesin-microtubule complex was loaded into one 15 μL sample loop of the device, and the lableled substrate [α^{32}P]ATP in the other 15 μL sample loop. The reaction is initiated when the contents of the loops are displaced into a common delay

line by ATPase buffer rapidly introduced from syringes driven by a computer controlled stepper motor. The duration of the reaction is determined by the length of time spent in the delay line, controlled by the stepper motor. Upon leaving the delay line, the reaction mixture is quenched by the introduction of 80 μL 2 N HCl, after which the quenched mixture is expelled into a sample tube. Sample preparation is completed by the addition of 28 μL 2 M Tris-3 M NaOH and 100 μL chloroform, to neutralize the solution and denature the kinesin. After centrifuging (Heraeus Biofuge, 15,000 × g, 5 minutes), 1.5 μL of each sample was examined by PEI-cellulose thin layer chromatography, developed with 0.6 M KH_2PO_4 pH 3.4. Finally, [α^{32}P]ATP and [α^{32}P]ADP were visualized and quantified using a Molecular Dynamics Storm 860 phosphorimager and ImageQuant software (Amersham Biosciences, Little Chalfont, Buckinghamshire, UK).

Data from this experiment was plotted as concentration of ADP released versus time, and a simple linear model was fit to the curve using GraFit (Erithacus Software, Horley, Surrey, UK). The burst amplitude of this reaction, indiscernible from the data directly, was inferred to be equal to the y-intercept divided by the active monomer concentration. A burst curve was subsequently generated which would describe the reaction depicted in scheme 2.1 using the kinetic simulation software KINSIM [172;173]. The expected shape of a burst curve is expected to contain an exponential and a linear phase, described by the equation $[ADP] = A \cdot \exp(-k_{obs}t) + k_{ss}t + C$, where A is the observed amplitude, k_{obs} is the observed rate constant for the exponential phase, k_{ss} the constant governing the linear phase, and C a background correction constant. A value for the apparent second-order rate constant k_1 for ATP binding to kinesin was selected based on the results of mantATP-binding experiments (see below). The burst phase of the curve was considered to have occurred before the first time point, and could be estimated by the ratio of the y-intercept and the enzyme concentration. Theoretical work defines the

relationships $A = [k_2/(k_2 + k_3)]^2$ and $k_{cat} = k_2k_3/(k_2 + k_3)$, and solving these two equations given the assumptions made provided estimates for k_2 and k_3 [174]. Graphs were made using GraFit software.

Scheme 2.1: *ATP hydrolysis by preformed kinesin-microtubule complex*

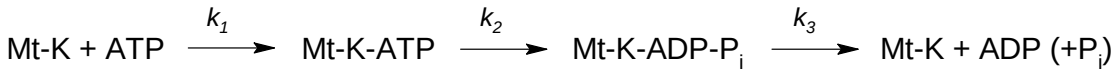

Stopped-Flow Experiments. A KinTek Stopped-Flow apparatus (Model SF-2001, KinTek Corp, Austin, TX) was used for stopped-flow experiments. A mercury-xenon lamp outfitted with a diffraction grating for wavelength selection was used for optical cell illumination. Instrument dead time was between 1.8 and 2.2 milliseconds, and assumed for the purpose of curve fitting to be 2.0 milliseconds. Assays were performed at 35°C in ATPase buffer. All depicted traces represent an average of 10-15 measurements. Indicated reagent concentrations represent concentrations achieved after mixing. All graphs were prepared using GraFit software.

Measurements of Kinesin-Microtubule Association Rates. A direct measurement of the rate at which kinesin binds to microtubules was made by exploiting a change in turbidity that accompanies the association of these two components. Measurements were made in the stopped-flow instrument, in which kinesin (2 μM, as determined by active-site titration) was mixed with microtubules at various concentrations. Turbidity at 340 nm was monitored in real-time using a photodiode detector positioned to receive light transmitted through the optical cell containing the mixed sample. Traces of received light intensity were transformed according to the

relationship $T_t = -\ln(I_t/I_0)$, where T_t is the turbidity at time t, I_t and I_0 represent recorded intensity and reference intensity, respectively. A double-exponential equation $T = A_1 \cdot \exp(-k_1 t) + A_2 \cdot \exp(-k_2 t) + C$ was fit to each trace, and rate parameters describing the fast and slow phases in the binding process were plotted against microtubule concentration. The linear relationship between binding rate and microtubule concentration, fitting the equation $k_{obs} = k_{on}[Mt] + k_{off}$. Graphs were made using GraFit software.

Phosphate Release Kinetics. Phosphate release kinetics were measured in the stopped-flow instrument, using a fluorescent phosphate reporter [166]. The reporter, which exhibits enhanced fluorescence upon binding to phosphate, consists of the A179C mutant of the *E. coli* phosphate binding protein (PBP), covalently modified at the mutated residue by the covalent addition of *N*-[2-(1-maleimidyl)ethyl]-7-diethylaminocoumarin-3-carboxamide (MDCC). Phosphate was removed from reagents using a "phosphate mop", consisting of 0.1 mM 7-methylguanosine and 0.01 units/mL purine nucleoside phosphorylase. An experiment was performed by mixing kinesin-microtubule complex with ATP in the stopped-flow instrument, and measuring the change in fluorescence using an excitation wavelength of 425 nm and a 450 nm cutoff long-wave filter. After-mixing concentrations were 50 nM kinesin, 75 nM microtubules, and 500 μM ATP. MDCC-PBP was present at a concentration of 4 μM. The inclusion of 100 mM KCl, which weakens the interaction between kinesin and microtubules, was tested in order to reduce multiple enzyme turnovers, enabling a better examination of single-turnover phosphate release kinetics. In order to correlate fluorescence with phosphate concentration, a standard curve was constructed, whereby the fluorescence of 4 μM MDCC-PBP in the presence of KH_2PO_4 at concentrations of 0, 0.1, 0.2, 0.3, 0.5,

and 1.0 μM was determined and a linear relationship between fluorescence and phosphate concentration extracted. Correlated fluorescence traces were used to fit the equation $[P_i] = A \cdot \exp(-k_{obs}t) + k_2 t + C$, with k_{obs} representing the rate of phosphate release under the conditions tested.

Measurements of mantATP- and mantADP-Kinesin Association. The rate constants governing the binding of nucleotide to kinesin were estimated using fluorescently labeled ADP and ATP, and rapid mixing in the stopped-flow instrument permitted real-time measurement over millisecond time scales. The kinetics of mant-conjugated nucleotide interaction with kinesin are seen as being an accurate reflection of the kinetics of the unmodified substrate, since values for k_{cat} and K_m with respect to mantATP and *Drosophila* conventional kinesin are similar to those values for ATP [79]. Excitation of a sample at 280 nm, from a source orthogonal to the detection path, permitted indirect excitation of the bound fluorophore by fluorescence resonance transfer. At the wavelength used, energy absorbed by tryptophan and/or tyrosine residues in the protein is emitted as 430-445 nm light by the mant moiety of the bound nucleotide, and in the stopped-flow instrument, was measured using a photomultiplier tube equipped with a 400 nm cutoff long-wave pass filter.

To perform the experiment, kinesin-microtubule complex was preformed, consisting of 2 μM kinesin (determined by active-site titration) and 20 μM microtubules. The complex was then rapidly mixed at 35°C with with mantATP or mantADP, and real-time measurements made of the fluorescence change over the desired time interval. Reactant concentrations are diluted by a factor of two after mixing. Fluorescent data reflecting binding kinetics, expected to follow a pseudo first order kinetic model when substrate concentration exceeds kinesin concentration, was fit to an exponential model

$F = A \cdot \exp(-k_{obs}t) + k_2 t + C$, where k_{obs} is the rate constant governing nucleotide binding. The values of k_2 and C, representing parameters extraneous to nucleotide binding, were not considered in the analysis of these experiments. Values of k_{obs} obtained for multiple nucleotide concentrations were plotted against the independent variable and fit to a hyperbolic model $k_{obs} = k_{max}[mAD(T)P]/(K_d + [mAD(T)P]) + k_{off}$. All graphs were prepared using GraFit software.

Release of mantADP from Kinesin. Experiments measuring rates of dissociation of mantADP, the fluorescently tagged hydrolysis product, were performed in the stopped-flow instrument. Excitation of the fluorophore was direct, performed using 360 nm light, and a decrease in fluorescence accompanying dissociation of mantADP is attributed to the sensitivity of the fluorophore to local hydrophobicity [164]. Kinesin-mantADP complex was formed by mixing kinesin and mantATP, with the nucleotide in twofold excess, and permitting 20 minutes at room temperature for bound and free nucleotide to exchange and hydrolysis to occur. The complex was then rapidly mixed with microtubules plus ATP or ADP in the stopped-flow instrument, and fluorescence change monitored using a photomultiplier tube equipped with a 400 nm cutoff long-wave pass filter.

Experiments were done to measure the dependence of mantADP release rate on varying microtubule, ATP, and ADP concentrations. To study microtubule dependence, kinesin-mantADP complex (after-mixing concentrations of 2 μM kinesin and 4 μM microtubules) were rapidly mixed with microtubules plus 1 mM ATP, with microtubules varied across trials, and fluorescence decay monitored. Fluorescence traces were fit to a double-exponential model of the form $F = A_1 \cdot \exp(-k_1 t) + A_2 \cdot \exp(-k_2 t) + C$, and could typically be resolved into fast and slow decay phases. Decay rates observed at each

microtubule concentration were then plotted against the independent variable, and fit to a linear model of the form $k_{obs} = k_{on}[\mathrm{Mt}] + k_{off}$. The parameters k_{on} and k_{off} describe the binding and dissociation of kinesin and microtubules. Dependence of mantADP dissociation rate on ATP concentration was examined in a similar fashion, with microtubule concentration kept constant at 20 μM, and ATP concentration varied. Each mantADP release event contributes to the overall decrease in fluorescence, and, as depicted in scheme 2.2, the expected sequence of events cannot be easily modeled mathematically. For this reason, traces from these experiments were analyzed by simulation (see next section).

Scheme 2.2: *Release of (mant)ADP by kinesin-microtubule complex after mixing with microtubules and ATP*

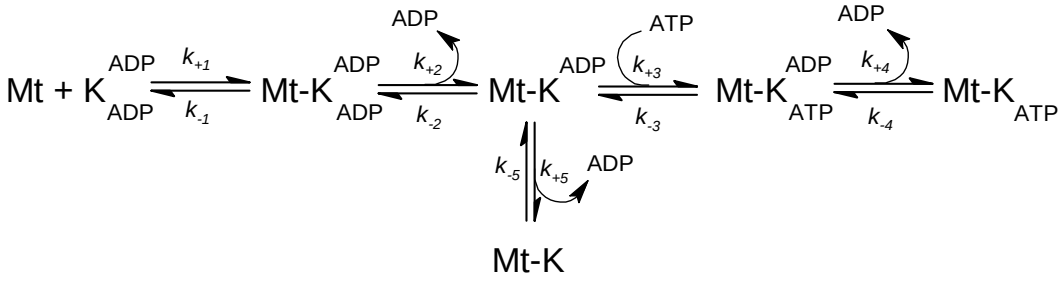

The dependence of mantADP release rate on the concentration of ADP, the product of hydrolysis, was also measured. Kinesin-mantADP complex (1 μM kinesin plus 2 μM mantATP after mixing) was formed and allowed to come to equilibrium. The complex was then mixed with microtubules (20 μM after mixing) in the stopped-flow instrument, and fluorescence monitored as before. Time-dependent fluorescence data were used to obtain a best-fit double exponential curve of the form $F = A_1 \cdot \exp(-k_1 t) + A_2 \cdot \exp(-k_2 t) + C$ by nonlinear regression. One rate parameter was found to be dependent on the concentration of ADP, and this dependence was modeled using a

hyperbolic curve of the form $k_{obs} = k_{max}[ADP]/(K_{D\text{-}ADP} + [ADP] + k_0)$, where k_{max} is the maximum ADP-stimulated release rate of mantADP, $K_{D\text{-}ADP}$ the equilibrium ADP dissociation rate, and k_0 the apparent mantADP dissociation rate in the absence of added nucleotide.

Analysis of Transient State Kinetics. Kinetic data from a time-dependence experiment can often be fit to a mathematical model consisting of exponential and linear phases, representing the solution to a series of ordinary differential equations corresponding to an enzymatic pathway. The mathematical relationship between an observed rate of a reaction and the concentration of an added component can be useful in the construction and evaluation of a kinetic model describing the reaction in question. The simplicity and rapidity of applying these techniques has made curve-fitting a tried and true method. An alternative to curve fitting involves global fitting of computer simulated data, possible using any of a variety of mathematics programs. The KINSIM program [172;173] is a dedicated kinetics simulator, and was used for global fitting of fluorescent data from mantADP release experiments. Data simulation has two advantages over fitting to multiple exponential functions. First, large errors can occur when multiple rate parameters have similar values. Since amplitudes and rate constants float independently during the fitting process, values obtained in a best-fit search may not make sense in the context of the model being applied. A best-fit parameter set for a double or triple exponential curve may be one in which the rate at which one step has occurred has "bled" into the value obtained for the rate of another step, skewing values obtained for the rates and amplitudes of both steps away from their true values. Constraining values to force conformity to the model reduces the flexibility of the fitting process, and in practice does not alleviate the problem. For multi-step pathways, the

number of exponential terms in the fitting equation increases, adding two parameters (amplitude and rate) for each additional step, and permitting additional opportunities for error. Curve fitting loses additional accuracy when the simplifying assumptions required for the validity of the mathematical model no longer apply. When substrate depletion occurs in the course of a reaction, for example, the simplifying assumption that substrate concentration remains constant during the reaction no longer applies, and time-dependent concentration data can no longer be modeled by a simple exponential decay curve. It is for these reasons that we have analyzed kinetic data for reactions following complex pathways using KINSIM-mediated global fitting of simulated data.

To fit data using KINSIM, a model is programmed into the computer. Unlike conventional curve-fitting, KINSIM performs model-dependent fitting, in which each parameter corresponds directly to a rate constant in the pathway. Estimates of each rate constant are entered, as well as the known starting concentrations of each reagent used in the reaction. Rate constants that are known through direct measurements can be held constant, while others may be allowed to float within a range that is defined. The software then performs a simulation of the data using the provided parameters, followed by an iterative search for values for floating parameters that might provide an optimal fit to the provided data. Fitting can be global, in that multiple curves following the same model may be simultaneously fit. The resulting simulations, based on parameters obtained by global fitting of simulated data, seldom fit the real data as well as conventionally fit curves do, since they are constrained by the supplied model. However, each parameter obtained by the former method has direct meaning with regard to the supplied model, and kinetically irrelevant information is absence. For this reason, KINSIM global curve fitting was done to obtain estimates for the parameters of the model depicted in Scheme 2.2. The parameter sets obtained by this method are

admittedly incomplete. Few reverse rates are described, and the validity of the rate constant values is contingent upon that of the underpinning model, which is not established with absolute certainty, and individual steps may in the future be resolved into sub-steps, each with a forward and reverse rate constant.

CHAPTER 3

Analysis of the Wild-type kinesin Construct

INTRODUCTION

The processive, plus-end directed, dimeric kinesins are likely to achieve motility via a hand-over hand mechanism, in which the two microtubule-binding heads of the protein alternate in relative position, advancing the molecule by 8 nm, the distance spanned by one αβ-tubulin dimer with each step [117-120]. This model is supported by structural studies of fixed kinesin-microtubule complexes, x-ray crystallography of monomeric and dimeric kinesin, spectroscopic analysis of kinesin dynamics using fluorescent and spin-label probes, physical measurements of kinesin force-generation using laser-trapping and kinetic analysis of kinesin ATPase activity. Despite extensive analysis by a variety of techniques, however, there remains much disagreement concerning the enzymatic pathway by which processive motility proceeds, and the nature and order of the conformational changes involved are subjects of dispute. Taking advantage of rapid, transient-state kinetic analysis of *Drosophila* conventional kinesin, in which the pre-steady-state processing of ATP and interaction with microtubules by kinesin is examined and rate constants for each discernible step estimated, a detailed model of kinesin motility has emerged [20;74;75;79;93;149;175].

One drawback of using *Drosophila* conventional kinesin is the absence of an x-ray crystal structure for this molecule. Given the potential utility of a crystal structure for structure-function relationship analysis, in which residues appearing in the crystal structure as participating in interactions whose disruption might impede a particular enzymatic step might be targeted for mutagenesis, it is unfortunate that the best-

understood and most thoroughly characterized conventional kinesin has proved refractory to crystallization. The use of crystal structures to identify residues in enzymes where mutations might alter that enzyme's function and provide information relating structure to function has been fruitful in probing the active sites of enzymes such as dihydrofolate reductase [176], carboxypeptidase A [177], aspartate transcarbamoylase [178], just to name a few. In more recent times, site-directed mutagenesis, along with a variety of spectroscopic techniques, has been used to examine the conformational changes that take place during the complex catalytic cycle of dihydrofolate reductase [179]. Clearly, the availability of an x-ray crystal structure is a valuable, perhaps indispensable foundation for structure-function analysis.

The first conventional kinesin crystal structure to become available was that of the rat [54]. This structure, published in late 1997, was that of a truncated version of the protein, lacking the neck domain required for dimerization. A few months hence saw the publication of a crystal structure featuring the dimeric form of the protein [19]. By this time the pre-steady-state kinetics of *Drosophila* conventional kinesin had been thoroughly described using transient-state kinetic methods. The work described in this chapter was undertaken to provide a kinetic characterization of rat brain conventional kinesin, which has been crystallized in its dimeric form and whose structure has been thereby determined.

Previous kinetic studies have led to a model for microtubule-dependent kinesin motility, called the "alternating site mechanism" [93]. This model, outlined in Scheme 3.1, depicts a hand-over-hand movement of the protein, whereby each ATP hydrolysis event results the trailing head of the kinesin dimer advancing towards the microtubule plus end by 16 nm, the distance spanned by two αβ-tubulin dimers. The dimer as a whole advances 8 nm by this action, and the two heads have effectively swapped relative

Scheme 3.1: *Proposed ATP hydrolysis pathway of conventional kinesin associated with microtubule-dependent movement*

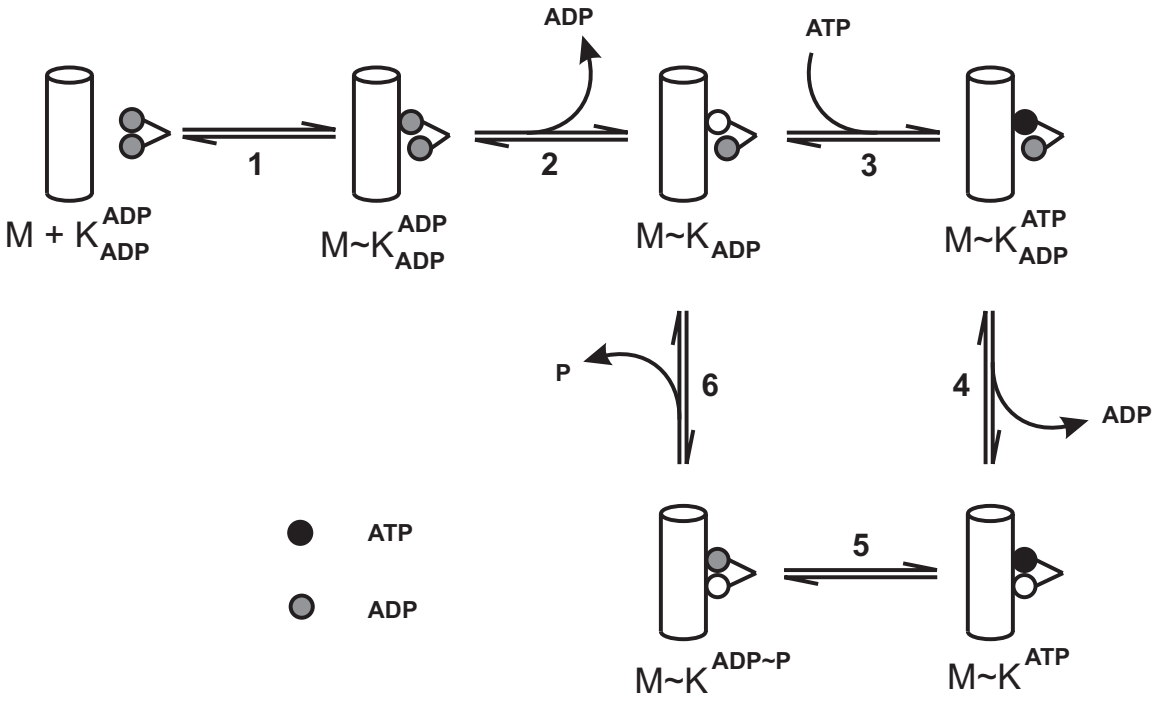

Table 3.1: *Rate constants for Drosophila conventional kinesin K401* [79]

Step	*k*+	*k*-
1	$19.5 \pm 0.7\ \mu M^{-1}s^{-1}$	
2	$306 \pm 25\ s^{-1}$	
3	$2.0 \pm 0.8\ \mu M^{-1}s^{-1}$	$71 \pm 9\ s^{-1}$
4	$300 \pm 100\ s^{-1}$	
5	$100 \pm 30\ s^{-1}$	
6	$50 \pm 8\ s^{-1}$	

positions. Rate constants for each step in this cycle were determined (Table 3.1). To begin a kinetic characterization of rat conventional kinesin, it was first necessary to devise an expression and purification scheme by which the protein in its dimeric form could be acquired. Next, it was deemed prudent to verify the dimeric structure of the purified protein using the method of sedimentation equilibrium analytical ultracentrifugation. The method was used to determine the apparent association constant for a *Drosophila* conventional kinesin dimeric construct of 401 residues in size [21]. The determined value, 2.74×10^7 M^{-1}, suggests that the protein exists in the dimeric state at micromolar concentrations. Finally, the rat conventional kinesin construct was analyzed using transient-state kinetic methods.

RESULTS

Purification of KHC407A. A purification procedure for KHC407A, based on ion-exchange chromatography, was devised. This procedure routinely gave protein whose purity exceeded 98%, as judged by densitometry of stained SDS-PAGE gels. From ~25 grams of cells, 25-150 nmol (1-6 mg) active KHC407A monomer could be purified. Figure 3.1 shows representative gels on which were analyzed fractions from successive BioRex70, Q-sepharose, and S-sepharose columns. Kinesin was capable of binding to both BioRex70 (a cation-exchange resin) and S-sepharose (an anion-exchange resin) under equivalent conditions of ionic strength and pH.

Active-Site Titration. Free kinesin contains associated Mg-ATP bound to the enzyme's active site [170;180]. To determine the concentration of kinesin active sites in a given preparation, the protein was labeled with [α^{32}P]ADP. The concentration of the radiolabeled nucleotide made inaccessible to added phosphocreatine kinase due to its

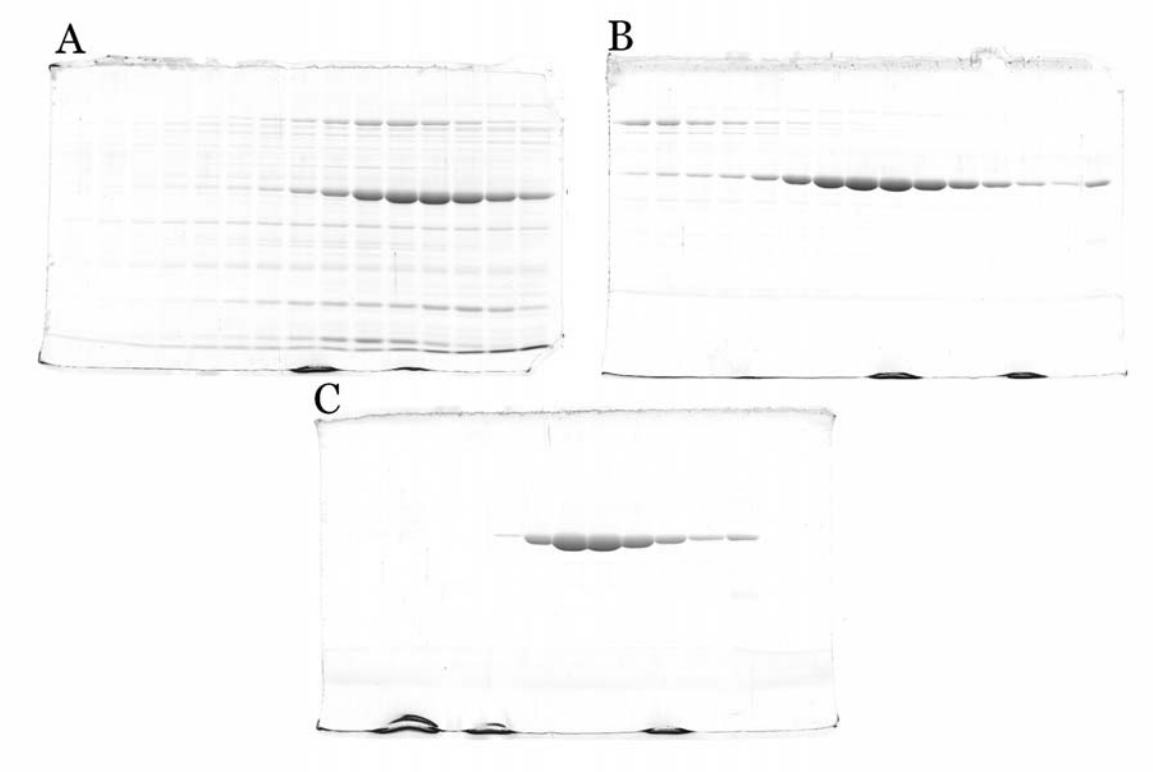

Figure 3.1: *Protein purification.* 8% SDS-polyacrylamide gels showing fractions from BioRex70 (A), Q-sepharose (B), and S-sepharose (C) columns.

association with kinesin was then measured using an ATP regenerating system [170]. When phosphocreatine kinase, phosphocreatine, and cold ATP are added, [α^{32}P]ADP is slowly lost from the kinesin active site, replaced by cold nucleotide, and phosphorylated to [α^{32}P]ATP. The rate at which the process occurs is equal to the dissociation rate of ADP from kinesin, and extrapolation of [α^{32}P]ADP concentration to t = 0 provides an estimate of the concentration of bound [α^{32}P]ADP at the reaction initiation time. In figure 3.2, the results of an active-site determination experiment are shown. The concentration of the kinesin preparation being tested was estimated by spectrophotometry as 56.5 μM. A 1:1 mixture of kinesin and [α^{32}P]ATP at 68.2 μM was prepared and allowed to come to equilibrium. Fitting of the active-site determination data to the single exponential curve $F = A \cdot \exp(-k \cdot t) + C$ yielded a value of 0.286 ± 0.005 for the amplitude A. The figure is dimensionless because it represents a ratio of concentrations. The relationship [kinesin] = ([ATP] $\cdot A$)/(1 – A), providing an estimate of the active site concentration, or the concentration of active kinesin monomer, was evaluated as 27.3 ± 0.5 μM, and this value became the assumed concentration of the preparation in all experiments. Active site concentration decreased by less than 10% after six months at -80°C, and was equally stable after 5 days at 4°C.

The concentration of active sites in this preparation as determined by the assay described above is almost exactly 50% of that determined spectrophotometrically, and this was a consistent phenomenon for every kinesin preparation tested in this manner. It is unlikely that this difference is due to contaminating proteins, given the apparent purity of the preparations as judged by SDS-PAGE, although the presence of small molecular weight peptides with high optical density at 280 nm has not been ruled out. Alternatively, it is possible that the exchangeability of ADP from the two binding sites in

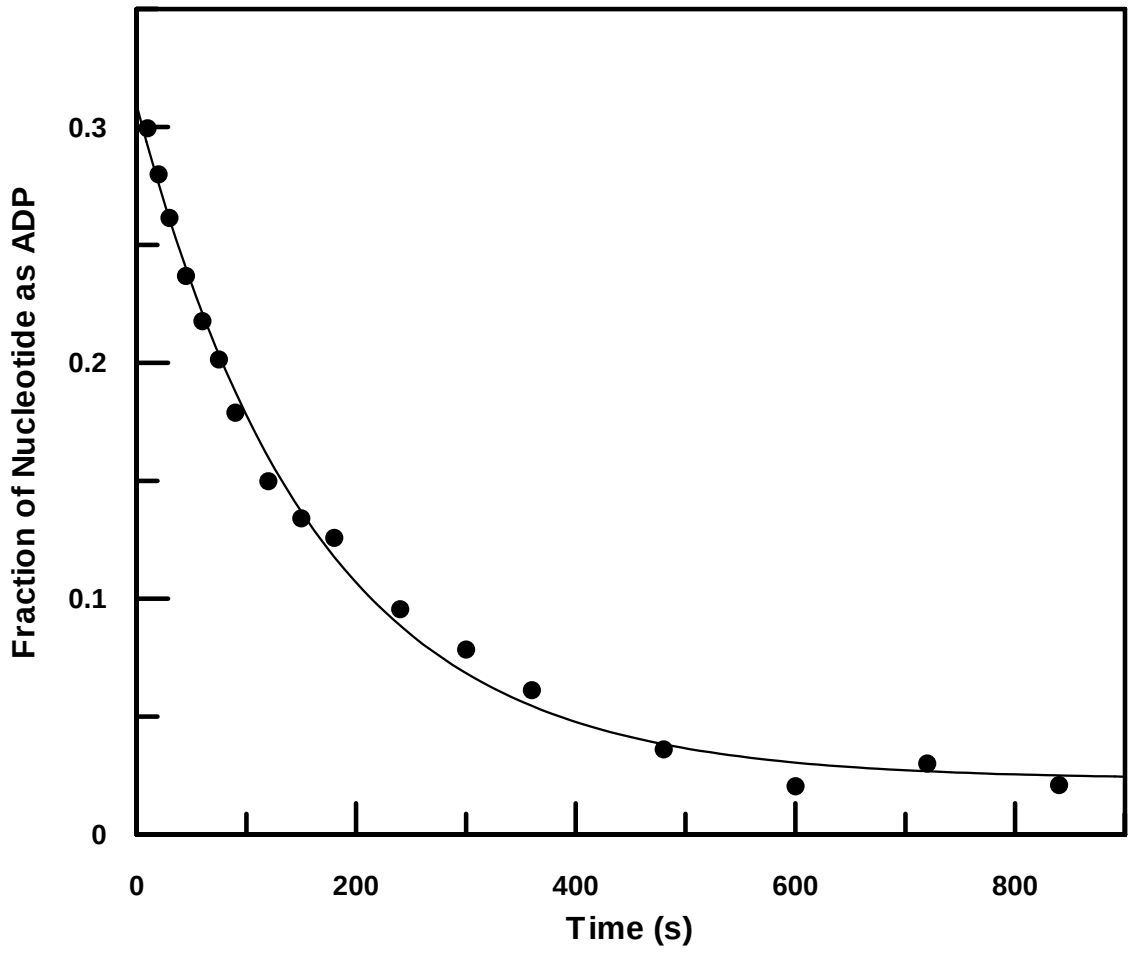

Figure 3.2: *Active-site titration of KHC407A.* KHC407A-[α^{32}P]ADP complex (28.3 μM kinesin, 34.1 μM [α^{32}P]ADP) was rapidly mixed with phosphocreatine kinase (0.3 mg/mL), phosphocreatine (4 mM), and Mg-ATP (5 mM) in ATPase buffer. The ratio of [α^{32}P]ADP to total labeled nucleotide is plotted against reaction time, as well as a best-fit single exponential curve $F = A \cdot \exp(-k \cdot t) + C$. Parameter values obtained from the fitting were A: 0.286 ± 0.005, k: 0.0062 ± 0.0003 s^{-1}, C: 0.023 ± 0.004. An active-site concentration of 27.3 ± 0.5 μM was estimated, based on values for A and the concentration [α^{32}P]ATP used in the initial labeling, according to the relationship [kinesin] = ([ATP] $\cdot A$)/(1 – A).

each kinesin dimer is asymmetric, with one nucleotide-binding site releasing ADP at a slower rate than the other; this possibility, if true, might render the initial labeling reaction 50% efficient, resulting in an underestimate of the true active-site concentration. A third possibility is that the method used in the preparation of the protein consistently produces a protein with 50% activity, in which case a formal possibility exists that the kinesin preparations obtained by this method consist of a population of fully active dimers, fully inactive dimers, and heterodimers of active and inactive subunits.

The rate of ADP release from the kinesin dimer is $0.0062 \pm 0.0003\ s^{-1}$, as determined in this assay. The kinesin labeling reaction that begins the active-site determination assay is predicated on a slow, microtubule-independent ATPase activity of kinesin, which permits the exchange and hydrolysis of [α^{32}P]ATP. Such an activity has been previously reported for native kinesin and truncated constructs [92;170;181-184]. ADP release is the rate limiting step in the ATPase reaction when microtubules are absent.

Sedimentation Equilibrium Analysis of KHC407A. To verify the dimeric structure of KHC407A, analytical ultracentrifugation using the sedimentation equilibrium protocol was used. In a thorough analysis of truncated *Drosophila* conventional kinesin constructs, it was found that a 366-residue N-terminal fragment of the protein does not self-associate in solution, whereas a 401-residue fragment does so tightly, with an association constant of $2.74 \times 10^7\ M^{-1}$. Thus, it has been shown that the domain necessary for self-association is between residues 367 and 401 in this protein. Given the structural and sequence similarities between *Drosophila* and rat conventional kinesins, it is likely that the 407-residue N-terminal fragment of rat conventional kinesin will possess the equivalent domain. Nevertheless, to provide a rigorous dismissal of the possibility

that KHC407A fails to self-associate at the concentrations used in kinetic experiments, the oligomerization of the expressed protein was examined.

The sedimentation of KHC407A at equilibrium was examined by examining the optical profiles of solutions of the protein at nine concentrations. The concentrations tested were 44, 154, 264, 374, 484, 594, 704, 814, and 924 nM. After 20 hours of centrifugation at 13,000 rpm at 24°C, sedimentation was judged to have achieved equilibrium. Figure 3.3A shows the optical profiles of the nine samples after equilibrium. Each data set was translated along the y-axis so as to set to zero the extrapolated absorbance at each sample's meniscus. The superimposed curves represent that expected from a best-fit monomer-dimer association model, whose single equilibrium association constant K_2 was determined by global fitting of all nine data sets by nonlinear regression. A value for K_2 of 2.15×10^7 M^{-1} with a 95% confidence interval (± 2 S.D.) between 9.25×10^6 and 5.70×10^7 M^{-1} was determined by NONLIN. Attempts to fit to monomer-dimer-trimer or monomer-dimer-tetramer models failed to yield converging values for K_3 or K_4, respectively. These results suggest that the KHC407A dimer has a dissociation equilibrium constant of 46 nM, similar to the value of 36.5 nM found for the 401 residue long N-terminal truncation of its *Drosophila* counterpart [21].

Steady-State ATPase Activity. A measurement of the steady-state activity of KHC407A, including determinations of values of k_{cat} and $K_{m\text{-}ATP}$, was made. The ATPase reaction catalyzed by kinesin requires substrate and microtubules, the latter of which is assumed to remain chemically unmodified by the enzyme. The concentrations of both influence the rate of catalysis. The value of $K_{0.5,\ Mt}$, the concentration of microtubules required for half-maximal ATPase activity by kinesin at near-saturating ATP concentration, was evaluated at 1 μM for the dimeric 401-residue N-terminal truncation

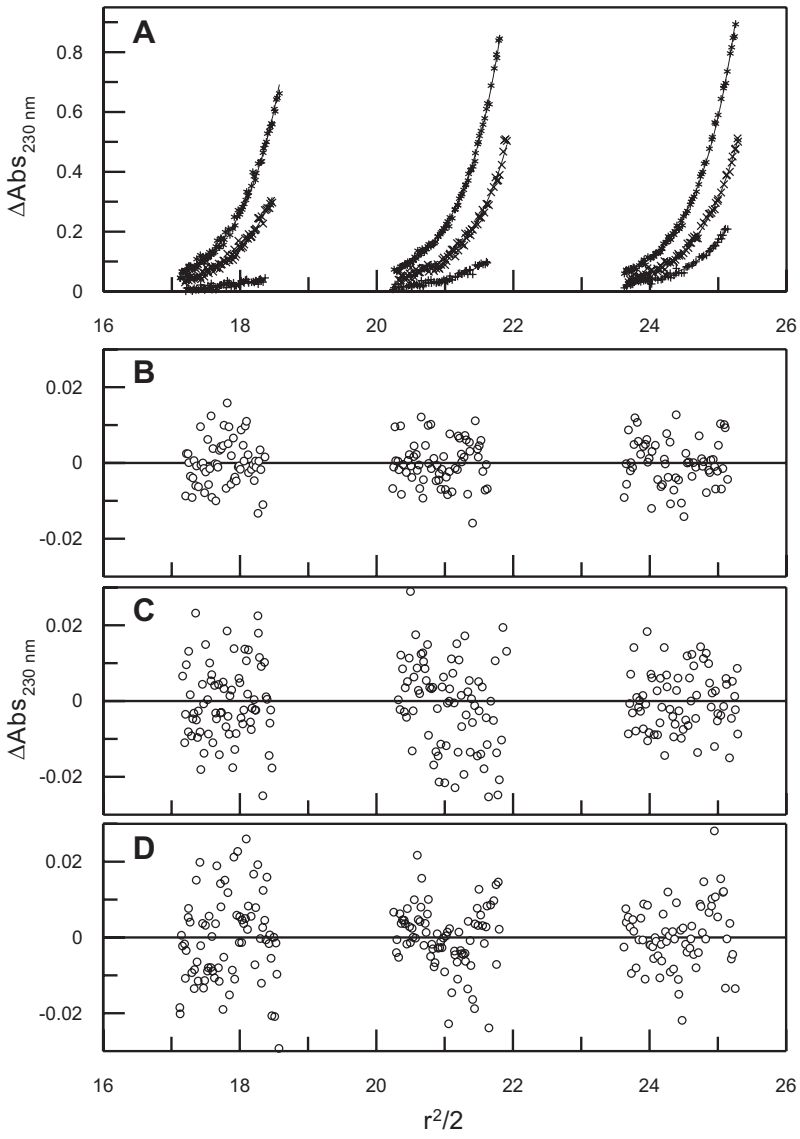

Figure 3.3: *Sedimentation equilibrium analysis of KHC407A*. KHC407A was analyzed by analytical ultracentrifugation using the sedimentation equilibrium protocol. Rotor speed (AnTi60) was 13,000 rpm, run time 20 hours, run temperature 24°C. Enzyme concentrations, according to active site titration, were 44, 154, 264, 374, 484, 594, 704, 814, and 924 nM. **Panel A**: Optical profiles at 230 nm of protein samples at equilibrium, taken at 0.003 cm resolution (×) and curves representing a global fitting of data using NONLIN to a monomer-dimer model (solid curves). Global fitting indicated a value for K_2, the dimer association equilibrium constant, of 2.15×10^7 M^{-1} (9.25×10^6, 5.70×10^7). Values in parentheses are the 95% confidence interval calculated by NONLIN. **Panels B-D:** Residuals for each of the nine samples.

of *Drosophila* conventional kinesin [75]. To measure k_{cat} of KHC407A, the concentration of microtubules used was 60 μM, exceeding $K_{0.5,\ Mt}$ by a factor of 60, and judged to be at near-saturation. ATPase rates for 5 nM KHC407A (active site) against ATP at concentrations ranging from 1 to 200 μM were determined and plotted. Figure 3.4 shows the data for KHC407A plotted along with a best-fit hyperbola of the form $k_{obs} = k_{cat}[ATP]/(K_{m\text{-}ATP} + [ATP]) + C$. The enzyme hydrolyzes its substrate with a k_{cat} of $40 \pm 1\ s^{-1}$ and a $K_{m\text{-}ATP}$ of 54 ± 5 μM. The value for k_{cat} is extracted from the data with no assumptions made concerning mechanism. If ATP hydrolysis by the kinesin dimer occurs by an alternating site mechanism, then only one subunit of the dimer is actively releasing product at any given time, and the actual value of k_{cat} doubles to $80 \pm 2\ s^{-1}$. These values contrast somewhat with those found for the *Drosophila* dimeric 401-residue N-terminal truncation, which gave values for k_{cat} at $20\ s^{-1}$ and $K_{m\text{-}ATP}$ at 62 μM. It appears from this data that KHC407A has a maximum hydrolysis rate that is approximately four times that of its *Drosophila* counterpart. Finally, the apparent second-order rate constant (the lower limit for the true rate constant) for substrate binding can be estimated by $k_{cat}/K_{m\text{-}ATP}$, or $1.5 \pm 0.1\ \mu M^{-1}s^{-1}$. Further experiments that seek to refine this figure are described below.

Binding of mantATP to KHC407A. In order to obtain an estimate of the rate constant governing the apparent second-order binding of ATP to KHC407A, a fluorescent ATP analog was used in a rapid mixing experiment, in which kinesin-microtubule complex was mixed with mantATP in the stopped-flow instrument. Excitation was at 280 nm and fluorescence detected by a photomultiplier tube fitted with a 400 nm cutoff long-wave pass filter. Fluorescence resonance energy transfer (FRET) between optically excited tryptophans in the protein and the *N*-methylanthraniloyl moiety

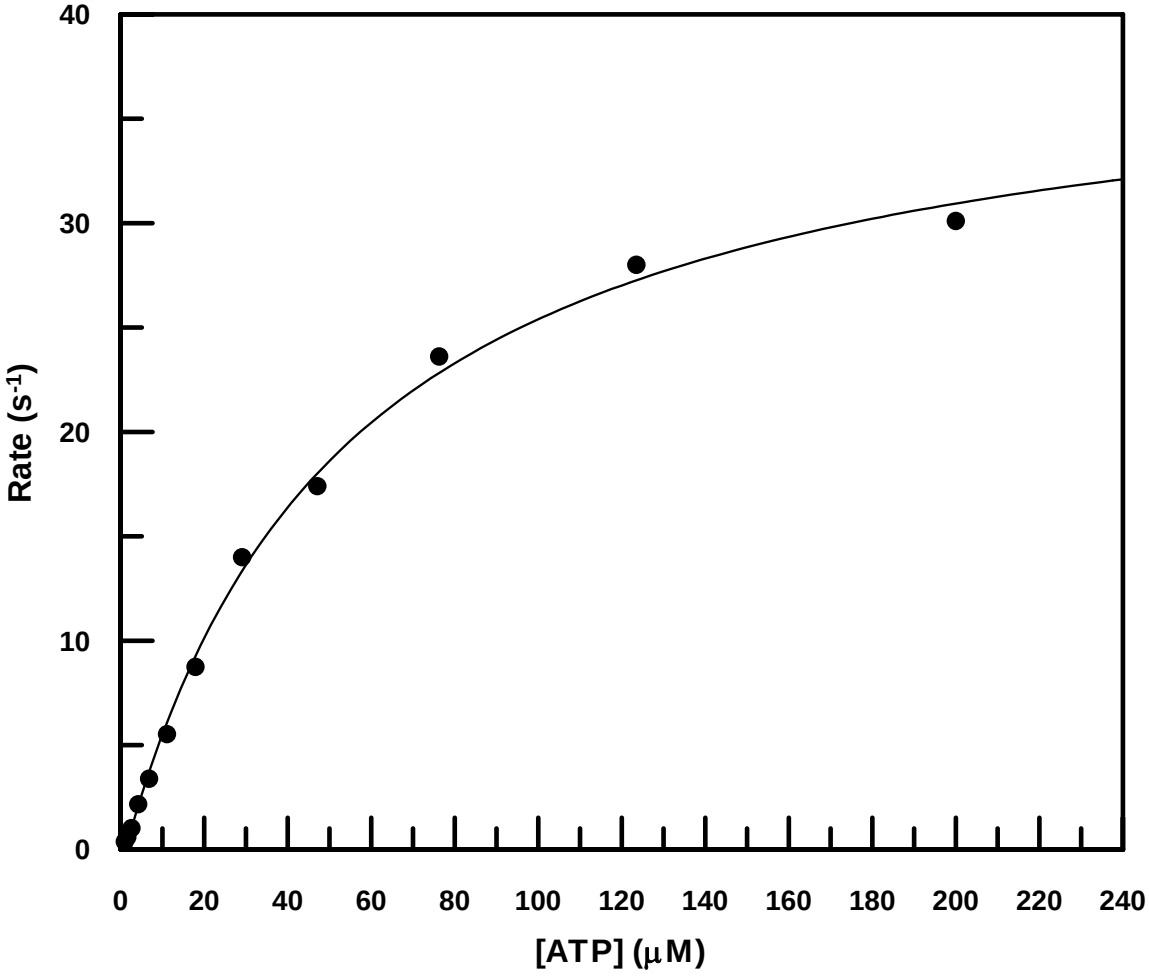

Figure 3.4: *Steady-state ATP hydrolysis by KHC407A in the presence of microtubules.* Hydrolysis rates of [α^{32}P]ATP by KHC407A were determined at substrate concentrations of 1 to 200 μM. 5 nM KHC407 and 60 μM microtubules were incubated with labeled substrate, and a time course created. Products were separated by thin-layer chromatography, visualized, and the hydrolysis rates extracted from the results by curve fitting. The observed relationship between hydrolysis rate and substrate concentration, once plotted, was used to generate a best-fit curve $k_{obs} = k_{cat}[ATP]/(K_{m\text{-}ATP} + [ATP]) + C$, whose parameters yield estimates of k_{cat} and $K_{m\text{-}ATP}$. From the data and subsequent curve fitting, $k_{cat} = 40.3 \pm 1.1\ s^{-1}$ and $K_{m\text{-}ATP} = 53.6 \pm 4.8$ μM.

of mantATP, and the detection of fluorescence by the stopped flow instrument provides a means by which the binding rate can be measured after mixing. Although the experiment measures the binding kinetics of a substrate analog rather than those of the substrate itself, the results are considered an accurate reflection of the behavior of the enzyme towards its natural substrate because k_{cat} and k_m for the fluorescent analog are within two times the corresponding values for ATP [79]. After-mixing reagent concentrations were 2 μM KHC407A (active-site), 10 μM microtubules, and mantATP at concentrations from 5-100 μM. Figure 3.5A shows a representative trace in which the concentration of mantATP was 50 μM. Because the background fluorescence in each experiment varied with the concentration of the fluorophore, the range of detection was adjusted in each case to permit a linear response, and for this reason, the amplitudes of the traces do not allow for convergence of the signals to a common maximum. Hence, a meaningful composite plot displaying all traces is not shown. A binding rate k_{obs} was extracted from each trace by fitting a curve of the form $F = A \cdot \exp(-k_{obs}t) + k_2 t + C$ to the data by nonlinear regression. The linear constant k_2 never exceeded 0.8 s^{-1} for the data examined, and its significance is not apparent.

In figure 3.5B values of k_{obs} determined for different concentrations of mantATP are plotted against the dependent variable. A best-fit hyperbola of the form $k_{obs} = k_{max}[mATP]/(K_d + [mATP]) + k_{off}$ was generated from the data in order to extract kinetic parameters for the binding reaction. The rate constant for nonproductive ATP dissociation (k_{off}), restricted to a positive value in order for it to be kinetically meaningful, could not be accurately determined by this experiment, and was set to zero. Its magnitude can be considered to be either negligible in comparison to k_{max}, or else an unknown parameter. The maximum achievable binding rate, to which k_{obs} converges as

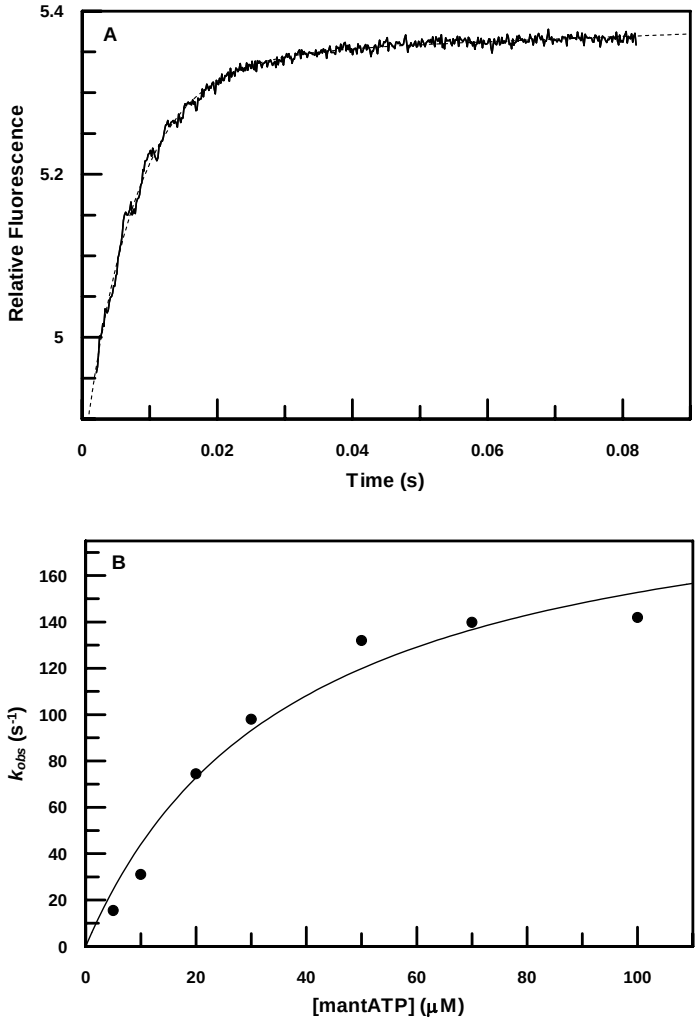

Figure 3.5: *Pre-steady-state binding of mantATP to KHC407A-microtubule complex.* **A:** A representative trace of fluorescence change incurred by KHC407A-microtubule complex upon rapid mixing with mantATP. Concentrations after mixing were 2 μM kinesin, 10 μM microtubules, and 50 μM mantATP. The dashed line indicates a best-fit curve $F = A \cdot \exp(-k_{obs}t) + k_2t + C$. Similar curves were generated for mantATP concentrations of 5, 10, 20, 30, 50, 70, and 100 μM mantATP. **B:** Values for k_{obs} obtained from fluorescence traces at each mantATP concentration are plotted against the independent variable. The solid curve represents the best-fit hyperbola $k_{obs} = k_{max}[mATP]/(K_d + [mATP])$ determined by nonlinear regression. Convergence of parameters provide estimates of k_{max} at 210 ± 25 s^{-1} and K_d at 38 ± 10 μM. The ratio k_{max}/K_d provides a lower limit to the apparent second-order rate constant for mantATP binding to the complex, and is 5.6 ± 1.7 $\mu M^{-1}s^{-1}$.

the concentration of mantATP increases (k_{max}), was evaluated at 210 ± 25 s^{-1}. Finally, the parameter K_d converged to 38 ± 10 μM.

The asymptotic convergence of k_{obs} to a maximum value suggests that the observed fluorescence change does not come about as a direct result of mantATP binding, but is instead the manifestation of a subsequent step, occurring at a rate of 210 s^{-1}, independent of mantATP concentration. Scheme 3.2 represents a simplified model in which enzyme and substrate combine to form a "collision complex", which subsequently undergoes a conformational change accompanied by an increase in fluorescence. The existence of such a complex, though not certain, is supported by evidence from kinetic and structural studies, which suggested the possibility of two distinguishable sequential kinesin-ATP complexes [75;183;185]. The conformational change may, for example, bring an aromatic residue, excitable at 280 nm, to within a distance from the recently bound fluorophore sufficient to permit fluorescence resonance energy transfer and the consequent radiation of fluorescent energy, or may otherwise alter the local environment of the bound mantATP to reduce fluorescence quenching by the solvent.

Scheme 3.2: *Proposed ATP-kinesin binding pathway, in which fluorescence change accompanies internal rearrangement*

$$E + ATP \underset{k_{-1}}{\overset{k_{+1}}{\rightleftharpoons}} E\text{-}ATP \xrightarrow{k_{+2}} E\text{-}^{*}ATP$$

Two interpretations of this data are proposed. ATP may bind rapidly to the enzyme, with a rate governed by k_{+1} as indicated in scheme 3.2. The initial slope of the

fitted curve in figure 3.5B, where the concentration of mantATP approaches zero, approximates the value of k_{+1}, and is equal to k_{max}/K_d, or 5.6 ± 1.7 $\mu M^{-1}s^{-1}$. Thus, this interpretation provides an estimate of 5.6 ± 1.7 $\mu M^{-1}s^{-1}$ for the apparent (measurable) rate constant governing ATP binding to kinesin. Alternatively, mantATP and kinesin may bind reversibly, coming to rapid equilibrium with a dissociation constant of 37.7 μM. The absence of a lag in the fluorescence traces at low mantATP concentrations supports the conclusion that the binding step is in rapid equilibrium, and is followed by a rate limiting isomerization step (k_2).

Pre-Steady-State Kinetics of ATP Hydrolysis. When the kinesin-microtubule complex is mixed with ATP, the kinetics of product formation are initially determined by the rate constants governing substrate binding, dissociation, and the conformational rearrangements within the enzyme that result in the cleavage of the targeted phosphate bond. These events constitute "single-turnover" hydrolysis. Each subsequent turnover requires the release of the hydrolysis products of the previous one, and cannot occur with a rate exceeding that of the rate-limiting step. To examine the enzymatic behavior of kinesin prior to product release, a rapid quench experiment was performed, whereby KHC407A-microtubule complex was rapidly mixed with [α^{32}P]ATP, incubated for a predetermined period, and then quenched with acid. This experiment resembles that which was done to determine steady-state activity, except that a rapid-quench instrument, capable of limiting the incubation period to intervals as short as 5 milliseconds, was utilized. In this way it was possible to examine the kinetics of ATP hydrolysis prior to product release.

Kinesin-microtubule complex was mixed with [α^{32}P]ATP in the quench-flow instrument such that after-mixing concentrations were 2.18 μM KHC407A, 10 μM

microtubules, and 100 μM [α^{32}P]ATP. Reaction times were varied from 5 to 200 milliseconds. Figure 3.6 plots the concentration of detected [α^{32}P]ADP versus time. The data are fit best to a linear model (dashed line) with slope and y-intercept determined at $75 \pm 2\ \mu M^{-1}s^{-1}$ and $1.8 \pm 0.2\ \mu M$, respectively. This reaction appears to have a steady-state rate of $34 \pm 2\ s^{-1}$, equal to the hydrolysis rate divided by the enzyme concentration. This value, short of k_{cat} ($40 \pm 1\ s^{-1}$) for the reaction by ~14%, reflects the sub-saturating concentration of labeled ATP used in this experiment (100 mM), and is consistent with the results of steady-state determination. There is no easily distinguishable burst phase that is expected from data gathered from a rapid quench experiment. The rapid evolution of product, followed by descent into steady-state hydrolysis is expected to generate data conforming to a burst equation $[ADP] = A \cdot \exp(-k_{obs}t) + k_{ss}t + C$. The apparent linear relationship suggests that the burst phase occurred too rapidly to be detected by the procedure used, and was essentially finished before the collection of initial data at 5 milliseconds.

To illustrate the expected burst kinetics of KHC407A, given rate constants measured directly, the reaction was simulated using KINSIM software, programmed with the reaction mechanism outlined in scheme 3.3.

Scheme 3.3: *ATP hydrolysis by preformed kinesin-microtubule complex*

$$\text{Mt-K + ATP} \xrightarrow{k_1} \text{Mt-K-ATP} \xrightarrow{k_2} \text{Mt-K-ADP-P}_i \xrightarrow{k_3} \text{Mt-K + ADP (+P}_i\text{)}$$

Of the three rate constants required for the simulation, only k_1 has been estimated directly, by measuring the binding rates of the fluorescent ATP analog mantATP in a stopped-flow experiment. The apparent second-order rate constant for ATP binding to

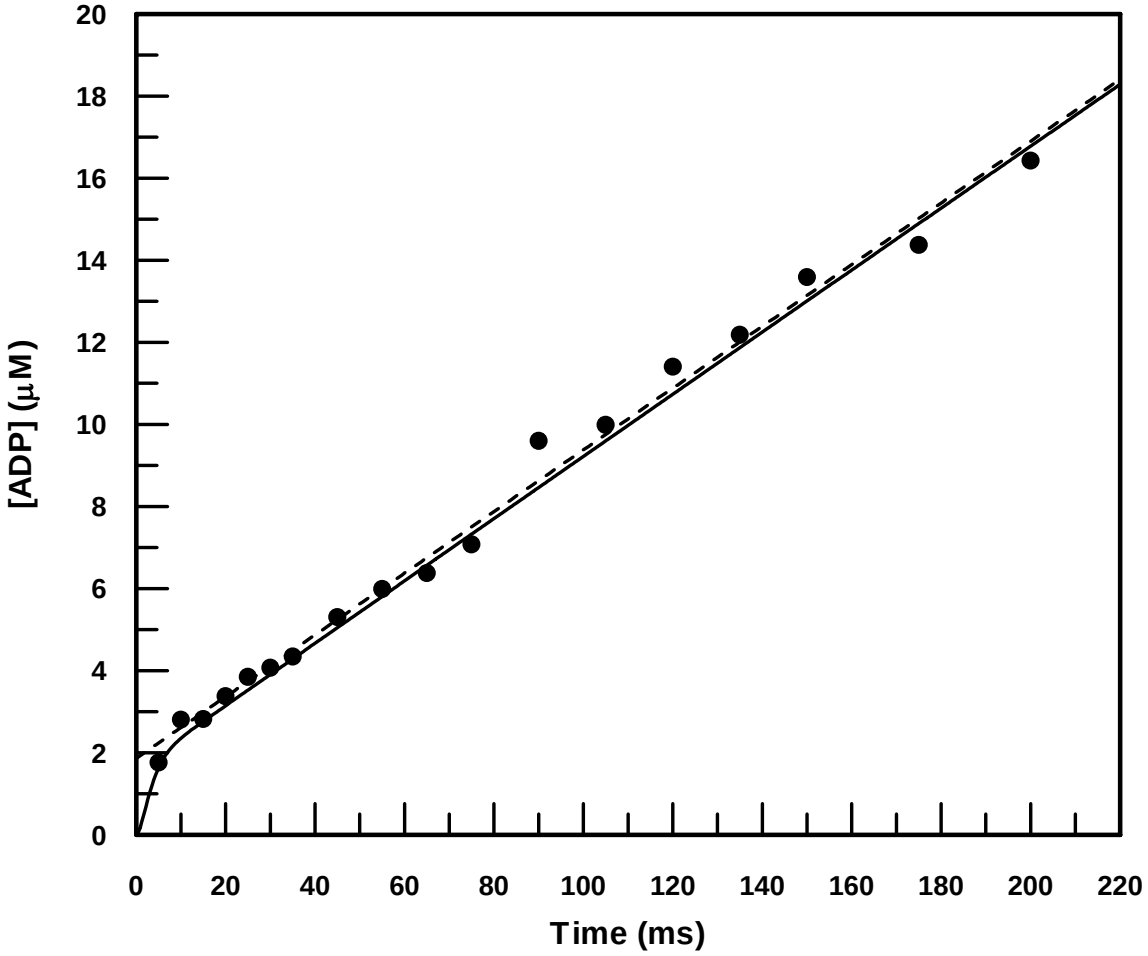

Figure 3.6: *Pre-steady state hydrolysis of ATP by KHC407A.* Microtubule-dependent ADP formation by KHC407A was monitored in the quench-flow instrument. KHC407A-microtubule complex was rapidly mixed with [α^{32}P]ATP (post-mixing concentrations 2.18 μM KHC407A, 10 μM microtubules, and 100 μM [α^{32}P]ATP) and [α^{32}P]ADP formation examined by TLC. A linear fit (dashed line) was generated from the data (circles), estimating the hydrolysis rate at 34.5 ± 1.7 s^{-1} and the burst amplitude at 0.85 ± 0.07. A KINSIM simulation using the reaction of scheme 3.3 (solid line) suggests values for kinetic parameters k_2 (ATP hydrolysis) at 523 ± 58 s^{-1}, and k_3 (ADP release) at 43.6 ± 2.9 s^{-1}. The rate of ATP binding was set at 5.6 $\mu M^{-1}s^{-1}$ based on results from mantATP binding experiments.

kinesin-microtubule complex was estimated at $5.6 \pm 1.7\ \mu M^{-1}s^{-1}$, so a value of $5.6\ \mu M^{-1}s^{-1}$ was used in the simulation. The accuracy of this value depends on assumptions described in the previous section, and the validity of the simulation presented here will be examined in light of additional results later in this section. The rate constants k_2 and k_3, representing the rate constants governing substrate hydrolysis and ADP release, respectively, were determined indirectly using an estimate of the burst amplitude of the quench flow data and the value of k_{cat}, determined directly by steady-state kinetics. The burst amplitude (0.85 ± 0.07), a dimensionless number, is inferred defined by the y-intercept of the linear extrapolation of the data divided by the active-site concentration of the enzyme in the reaction; this relationship is best appreciated by comparing the linear fit (dashed line) to the simulation results (solid line) in figure 3.6. Thus, k_2 and k_3 can be calculated by solving the simultaneous relationships $A = [k_2/(k_2 + k_3)]^2$ and $k_{cat} = k_2k_3/(k_2 + k_3)$, with known amplitude A and steady-state rate constant k_{cat}. This operation predicts a value of $520 \pm 60\ s^{-1}$ for k_2, the rate constant governing ATP hydrolysis, and $44 \pm 3\ s^{-1}$ for k_3, governing ADP release.

Figure 3.6 shows the data, the linear fit to the data (dashed line), and the simulated data (solid line). It is important to note that values obtained for k_2 and k_3 describe the hydrolysis of ATP and release of ADP, respectively, according upon the model described in scheme 3.3. The simplified scheme correlates data to behavior expected from an enzyme with a single active site and no intervening steps that might be invisible to the assay. If kinesin hydrolyzes ATP using an alternating site mechanism as has been proposed [79;92;93], then the hydrolysis of [α^{32}P]ATP by the active site to which it has bound will not immediately follow the binding step, but will be delayed until the prescribed conformational changes occur within the other subunit of the kinesin dimer. Similarly, the alternating site model suggests that the release of product from one

site may occur only after prerequisite rearrangements occur at the other. For this reason, values of k_2 and k_3 describe what are likely to be composite reactions that incorporate more than one distinguishable step. The absence of a visible burst phase suggests that hydrolysis occurs at a rate too fast to measure using this assay.

Phosphate Release Kinetics. The pre-steady-state kinetics of phosphate release by KHC407A were studied using a fluorescent phosphate sensor. The sensor consists of a mutant *E. coli* phosphate binding protein into which has been introduced the mutation A179C, which provides a single cysteine near the phosphate binding site of the protein [166]. When a fluorescent probe (MDCC) is covalently attached via C179, the resulting protein (MDCC-PBP) exhibits a five-fold increase in fluorescence upon binding to inorganic phosphate. The interaction is tight (K_d = 0.1 μM) and rapid ($k = 1.36 \times 10^2$ $\mu M^{-1} s^{-1}$). A "phosphate mop", consisting of 7-methylguanosine and purine nucleoside phosphorylase (PNPase), sequesters free phosphate as ribose-1-phosphate, and is used to remove phosphate from reagents prior to mixing. This reaction has a K_{eq} of >100, so the concentration of phosphate can be reduced to less than 0.1 μM, and by limiting PNPase concentration, the rate of the sequestration can be reduced so as to be negligible over the time scale during which phosphate release from kinesin is observed. Fluorescence data from phosphate release experiments were correlated with phosphate concentration according to a standard curve, generated by measuring the fluorescence of the phosphate sensor in the presence of known concentrations of KH_2PO_4.

Figure 3.7 plots the release of phosphate from KHC407A-microtubule complex after rapid mixing with ATP. Post-mixing component concentrations were 0.05 μM kinesin, 0.075 μM microtubules, and 500 μM ATP. A concentration of kinesin-microtubule complex was selected that would release phosphate at a rate slower than that

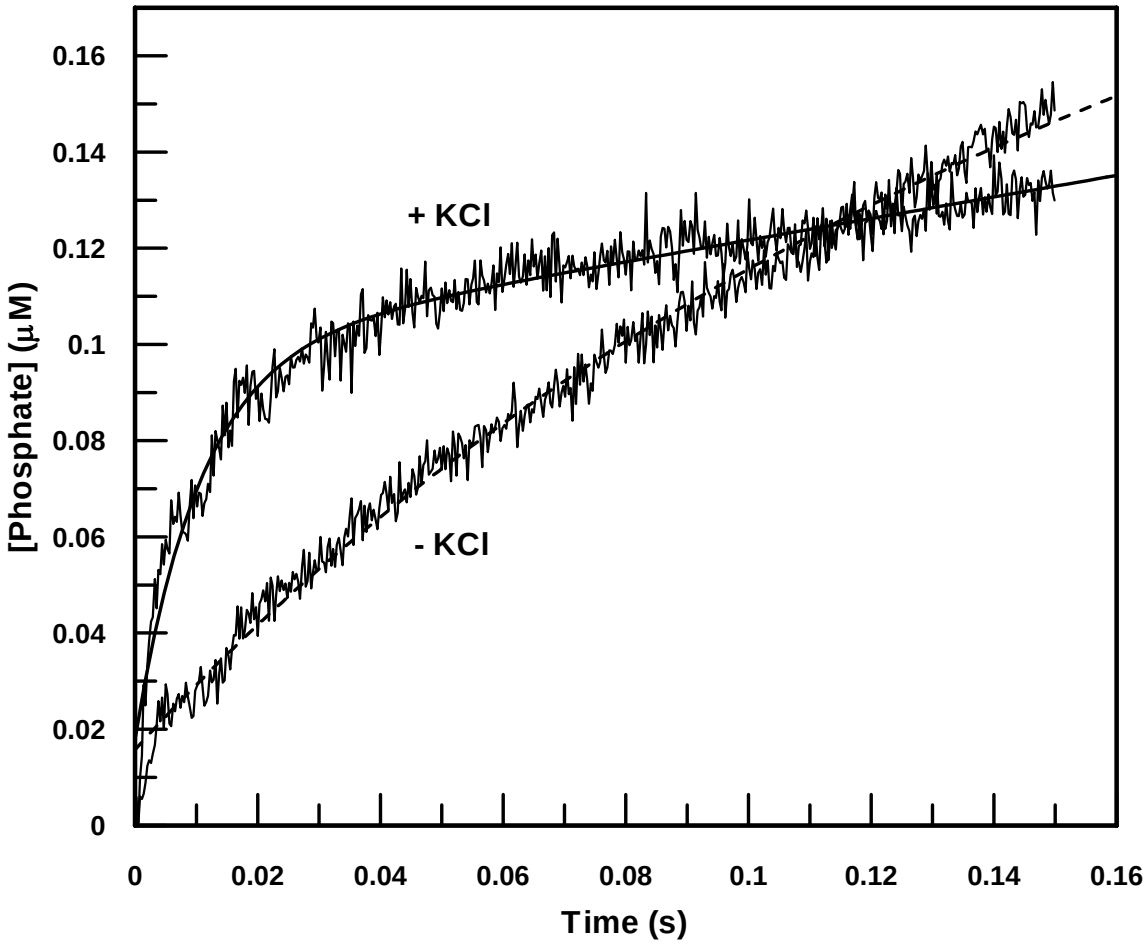

Figure 3.7: *Pre-steady-state phosphate release kinetics of KHC407A.* Kinesin-microtubule complex (0.05 μM kinesin, 0.075 μM microtubules) was mixed with ATP (500 μM) in the stopped-flow instrument in the presence of MDCC-PBP (4 μM) and a "phosphate mop" (1 unit/mL PNPase, 0.1 mM 7-methylguanosine). Where indicated, 100 mM KCl was included. All concentrations are post-mixing. Fluorescence change was converted to phosphate concentration based on a standard curve. Fitting to a burst equation by nonlinear regression generated the solid and dashed curves representing experiments performed with and without KCl, respectively. At high salt, k_{obs} = 93.5 ± 3.6 s^{-1}, and the burst amplitude predicts a turnover number of 0.8 per dimer before dissociation from microtubules.

with which MDCC-PBP binds phosphate. Additionally, at low concentrations, kinesin becomes more predisposed to dissociate from microtubules after one hydrolysis event. The 50 nm KHC407A concentration used in these experiments was only marginally higher than the dissociation constant of the dimer (46 nM) predicted from sedimentation equilibrium experiments, and nothing is known about the dissociation kinetics of the dimer in the presence of microtubules. Nevertheless, the kinetic data from this experiment is viewed as providing a reasonable estimate of the rate of phosphate release from the complex upon rapid mixing with ATP.

Two traces are plotted in figure 3.7, and both are shown with fitted burst curves of the form $[P_i] = A \cdot \exp(-k_{obs}t) + k_2 t + C$. The experiment was performed in ATPase buffer, with and without 100 mM KCl. The purpose of the added salt was to destabilize the kinesin-microtubule interaction, so as to promote dissociation after a single turnover. In this way, the measured rate of phosphate release might more closely represent the rate of phosphate release after the hydrolysis of a single ATP molecule. Curve fitting was performed with each parameter permitted to float. The dashed line fits the trace obtained in the absence of KCl, and the solid line in the presence of the salt. The parameters extracted from the fittings are summarized in table 3.2. In the presence of KCl, the time-dependence of phosphate release has the appearance of a single-turnover event, with distinct exponential and linear phases. The amplitude of the exponential phase is 0.081 ± 0.002 μM, or 1.6 per active site, or 0.8 per dimer. This suggests that a single turnover event was measured in this experiment. In the absence of KCl there are no distinct phases, and phosphate release is continuous during the time interval examined. This suggests that multiple hydrolysis per kinesin generated the phosphate detected during this experiment. The burst rate (k_{obs}) in the presence of KCl was 93.5 ± 3.6 s^{-1},

which provides an estimate of the apparent first-order rate constant governing phosphate release from KHC407A subsequent to ATP binding.

Table 3.2: *Parameters from curves fit to KCH407A phosphate release data*

Parameter	+ KCl	- KCl
Amplitude	-0.081 ± 0.002 μM	-0.125 ± 0.004 μM
k_{obs} (exp.)	93.5 ± 3.6 s^{-1}	9.2 ± 0.3 s^{-1}
k_2 (linear)	0.22 ± 0.01 $\mu M^{-1}s^{-1}$	0.25 ± 0.02 $\mu M^{-1}s^{-1}$

Pre-Steady-State Binding of KHC407A to Microtubules. Kinesin-microtubule association is the first step in microtubule-dependent kinesin motility. It is well established that conventional kinesin motility is processive, meaning that the motor takes multiple steps along its microtubule track before dissociating [74-76]. Two methods were employed to examine the kinetics of kinesin binding to microtubules. Using the first method, binding is measured directly by exploiting the change in turbidity that accompanies kinesin-microtubule association. In the second method, which will be described in the next section, the release of mantADP from kinesin upon binding to microtubules serves as a reporter for the initial association reaction.

KHC407A (2 μM post-mixing) was rapidly mixed with microtubules at concentrations between 5 and 15 μM (after mixing) in the stopped-flow apparatus in the absence of nucleotide, and the intensity of 340 nm light transmitted through the mixture was monitored. From intensity traces were extracted time-dependent turbidity functions. Figure 3.8A shows a trace for 2 μM KHC407A rapidly mixed with 5 μM microtubules. The dashed line represents a fitted double exponential curve of the form

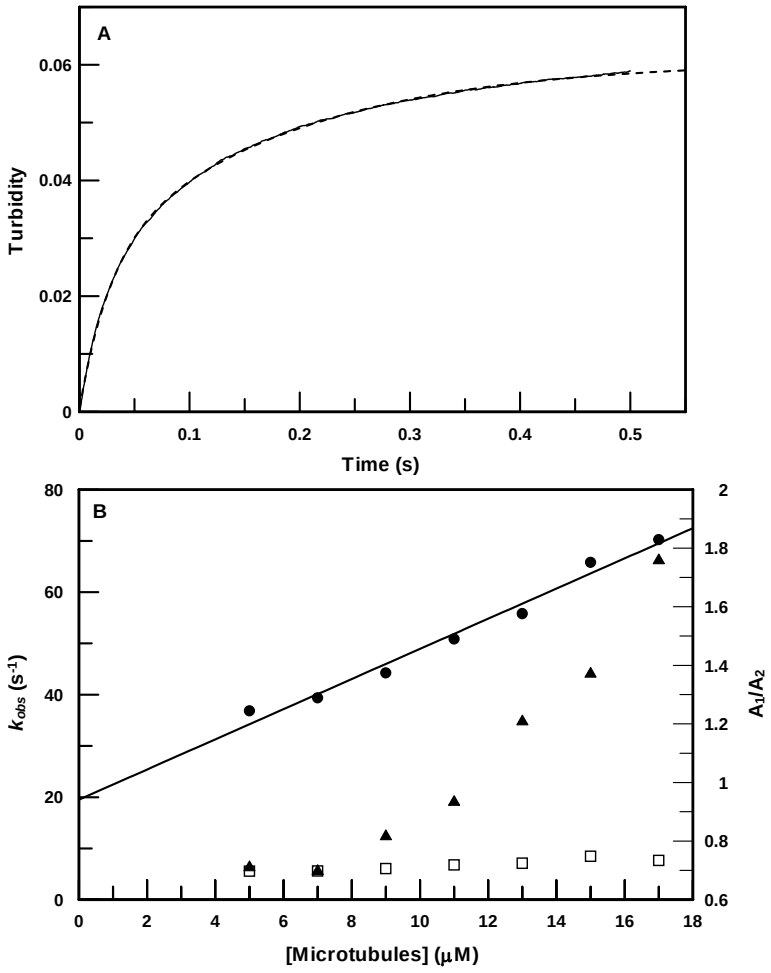

Figure 3.8: *Pre-steady-state binding of KHC407A to microtubules*. **A:** Representative turbidity trace at 340 nm illumination of kinesin and microtubules after mixing (2 μM kinesin, 5 μM microtubules, post-mixing). The dashed line represents a best-fit double exponential curve $T = A_1 \cdot \exp(-k_1 t) + A_2 \cdot \exp(-k_2 t) + C$, whose parameters A_1, A_2, k_1, k_2, and C were determined by nonlinear regression. Similar traces were recorded for microtubule concentrations of 5, 7, 9, 11, 13, 15, and 17 μM microtubules, each of which were fit by double exponential models. **B:** Both fast (circles) and slow (squares) rates were plotted against microtubule concentrations. The ratios of the amplitudes (fast-phase amplitude/slow-phase amplitude) are also shown (triangles). Fast rates were fit by linear regression, whose gradient of 2.9 ± 0.2 $\mu M^{-1}s^{-1}$ estimates the second-order rate constant for kinesin-microtubule association. A y-intercept at 19 ± 2.2 s^{-1} is the apparent rate constant for dissociation of the complex.

$T = A_1 \cdot \exp(-k_1 t) + A_2 \cdot \exp(-k_2 t) + C$. A similar analysis was performed on each turbidity trace in the microtubule concentration dependence series. For each microtubule concentration, a fast and slow phase was identified based on the relative magnitudes of k_1 and k_2, and these rates plotted against microtubule concentration, as depicted in figure 3.8B.

The rates of both fast (circles) and slow (squares) phases show a linear response to microtubule concentration; however, only the fast phase appears to be dependent on the variable. The slope of a linear fit to the fast phase data ($2.9 \pm 0.2\ \mu M^{-1}s^{-1}$) provides an estimate of the apparent second-order binding rate constant for KHC407A-microtubule association, while the y-intercept ($19 \pm 2.2\ s^{-1}$) estimates the rate constant governing dissociation. A dissociation equilibrium constant K_d of $6.7 \pm 0.9\ \mu M$ is indicated from these two measurements. The significance of the slow-phase data is not immediately clear. If the measured rates of the slow phase are relevant to the kinetics of kinesin-microtubule interaction, their independence from microtubule concentration suggests that they describe a process that is most likely first-order with respect to kinesin, the reaction component that is held constant at 2 μM throughout the series of experiments. For this reason, the fast-phase rates are considered as indicating a second-order binding process, while the slow-phase rates indicate an unknown first-order process.

The amplitudes of both phases were comparable at each microtubule concentration tested. The ratio of A_1 to A_2 for each concentration is plotted in figure 3.8B (triangles). The value of this ratio varies from 0.7 to 1.7, although the significance of the upward trend is unknown, perhaps an artifact of curve fitting; as k_1 increases relative to k_2, it acquires a greater single-exponential character over the examined time interval as the fast-phase signal overshadows that of the slow phase. If the ratio of amplitudes is actually constant (which is not determinable from the data), it would suggest that the two

phases represent two reactions in series: a fast, microtubule-dependent reaction (most likely the second-order association), followed by a slower, microtubule-independent reaction of the kinesin-microtubule complex (i.e. a conformational change).

Microtubule-dependence of mantADP Release from KHC407A. In the absence of microtubules, conventional kinesin contains one ADP bound in each of its active sites [180]. Upon binding to microtubules, the kinesin dimer will release both ADP molecules in succession [79;92;93]. The rate at which the fluorescent analog mantADP is released from KHC407A upon binding to microtubules in the presence of a near-saturating concentration of ATP was examined using the stopped-flow apparatus. A kinesin-mantADP complex was formed by mixing the two components to concentrations of 4 μM KHC407A (active site) and 8 μM mantATP. The mixture was allowed to come to equilibrium for 20 minutes, during which time bound ADP was presumably released from the kinesin active sites and replaced by mantATP. The mantATP is then hydrolyzed, yielding the mantADP complex. Active-site titration suggested an ADP release rate of ~0.006 s^{-1} in the absence of microtubules, which is likely to be the rate-limiting step in microtubule-independent ATP hydrolysis. 30 minutes were provided for complete mantADP hydrolysis, and complex formation.

KHC407A-mantADP complex was rapidly mixed with microtubules at concentrations from 8 to 80 μM (after mixing) in the stopped-flow instrument, and fluorescence monitored using an excitation wavelength of 360 nm, which provides direct excitation of the fluorophore. Fluorescence output was monitored through a 400 nm cutoff long-wave pass filter. Figure 3.9A shows a representative trace of time-dependent fluorescent decay after mixing 2 μM KHC407A-mantADP complex and 18 μM microtubules plus 1 mM ATP. In this and all other traces in this series of experiments,

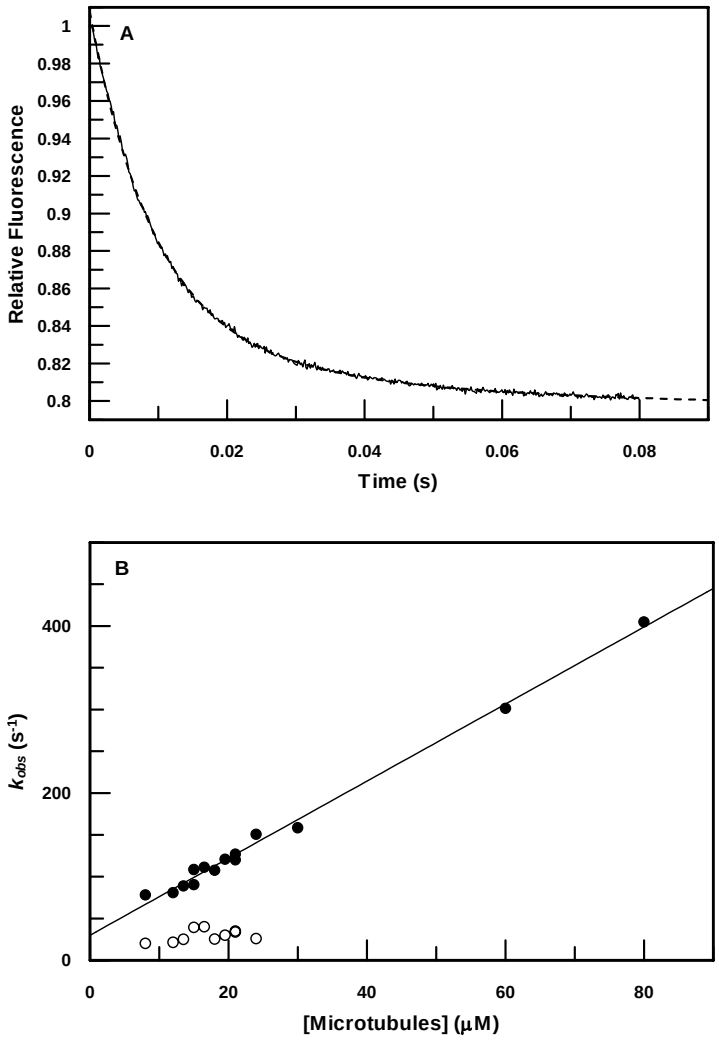

Figure 3.9: *Microtubule dependence of mantADP release from KHC407A*. **A:** Representative trace of fluorescence decay resulting from rapid mixing of kinesin-mantADP complex with microtubules and ATP. Post-mixing concentrations were 2 μM kinesin, 4 μM mantADP, 18 μM microtubules, and 1 mM ATP. A best-fit double exponential curve $F = A_1 \cdot \exp(-k_1 t) + A_2 \cdot \exp(-k_2 t) + C$ (dashed) was determined by nonlinear regression. Parameters A_1, A_2, k_1, k_2, and C were determined for microtubule concentrations at 8, 12, 13.5, 15, 16.5, 18, 19.5, 21, and 24 μM. At 30, 60, and 80 μM, model fitting was best achieved using a single exponential model. **B:** Fast- (filled circles) and slow- (open circles) phase rates are plotted against microtubule concentration, and fast-phase rates were fit by linear regression. The gradient of the linear fit, $4.6 \pm 0.1\ \mu M^{-1}s^{-1}$, predicts the second order rate constant for microtubule-kinesin association, while a y-intercept of $30 \pm 3.3\ s^{-1}$ is the apparent rate constant for dissociation.

the fluorescence intensity function was scaled to make the initial intensity equal to one. A double exponential curve $F = A_1 \cdot \exp(-k_1 t) + A_2 \cdot \exp(-k_2 t) + C$ was fit to each trace by nonlinear regression. For the representative curve in figure 3.9A, $k_1 = 108.2\ s^{-1}$, $k_2 = 26.7\ s^{-1}$, and amplitudes A_1 and A_2 were 1.17 and 0.26, respectively. Like the turbidity data described in the previous section, the fluorescence traces from this experiment were best fit to a double exponential rather than a single; however, the amplitudes of the two phases were not comparable, with those of the slow phase being typically less than 40% of the corresponding fast-phase amplitudes. Curve fitting to fluorescence data at the highest microtubule concentrations only converged to single exponential models.

Fast- and slow-phase rates (filled and empty circles, respectively) are plotted in figure 3.9B, as well as a linear fit to the fast-phase rates. In this experiment, the fast-phase rates are considered to represent the release of both mantADP molecules from the dimer. The release of the first mantADP molecule is likely to occur immediately after kinesin-microtubule binding, with a minimum of intervening steps (see scheme 3.1). A second mantADP release event is though to take place only after ATP has bound to the newly vacated nucleotide-binding site and a rearrangement has taken place within the dimer structure. Since a kinetic analysis of mantATP binding to KHC407A-microtubule complex suggests that ATP binds with a k_{max} of ~210 s^{-1} at near-saturating concentrations (see figure 5), it is likely that the second mantADP molecule is released after only a brief (no less than ~5 millisecond) interval. Furthermore, there is no reason to expect that the release rates of mantADP from each nucleotide binding site of the dimer are released with significantly divergent rate constants; for the dimeric *Drosophila* kinesin truncation K401, primary and secondary (ATP-dependent) ADP release events take place with rate constants of ~300 s^{-1} each [79].

The initial gradient of the fast-phase data reveals the apparent second order rate constant for KHC407A binding to microtubules, while the y-intercept estimates the dissociation rate constant. Curve fitting by nonlinear regression sets these values at $4.6 \pm 0.1\ \mu M^{-1}s^{-1}$ and $30 \pm 3.3\ s^{-1}$, respectively. These values are in reasonable agreement with the corresponding rate constants obtained more directly by turbidity analysis ($2.9 \pm 0.2\ \mu M^{-1}s^{-1}$ for binding, $19.5 \pm 2.2\ s^{-1}$ for release), and cover a larger range of microtubule concentrations. Interestingly, despite the differences between the results obtained using turbidity and mantADP release methods, the equilibrium dissociation constants suggested by each experiment are nearly identical, $6.5 \pm 0.7\ \mu M$ indicated by the mantADP dissociation reaction, and $6.6 \pm 0.9\ \mu M$ by the turbidity assay. That the k_{obs} versus microtubule concentration data are fit best to a linear model suggests that the initial binding event remains the rate-limiting step in the mantADP release reaction at all microtubule concentrations tested. Hence, the rate constant governing mantADP release, although of indeterminate value, is certainly much larger than $400\ s^{1}$, the observed rate of mantADP dissociation at 80 μM microtubules. In the section following this one, an attempt at a more accurate determination of this rate constant is described.

Values for the slow phase rates are difficult to interpret, but the small amplitudes of the slow phase rates relative to those of the fast phase rates suggest that they do not reflect a process that has the same stoichiometry as that which was responsible for fast signal decay. The rates of the slow phase are almost invariant with microtubule concentration. For these reasons, no model was fit to these data, and no interpretation made, although their values are plotted in figure 3.9B (empty circles).

ATP-dependence of mantADP Release from KHC407A. In the alternating-site model of conventional kinesin motility, two ADP release events are predicted to occur

after the kinesin binds to microtubules [79;92;93]. In the experiments described previously, it was shown that at least one of these release events occurs at a rate that is dependent on microtubule concentration. In the experiment described in this section, the ATP dependence of mantADP release is examined. KHC407A-mantADP complex was formed by mixing the two components to concentrations of 2 μM enzyme (by active-site titration) and 4 μM mantATP, and allowing the enzyme-substrate mixture to come to equilibrium. The complex was then rapidly mixed with microtubules (20 μM) plus nucleotide (ATP at 5, 10, 25, and 50 μM, or ADP at 10 μM) in the stopped-flow instrument, and the fluorescence of the mixture monitored. Direct excitation of the fluorophore was accomplished using light at 360 nm, and the fluorescence output was measured through a 400 nm cutoff long-wave pass filter.

The data from this experiment formed a family of curves displayed in figure 3.10. The effect of ATP is apparent, as higher concentrations result in progressively more rapid decay. The upper trace represents the release of the fluorescent product in the presence of 10 μM ADP, while each additional trace from top to bottom was generated using the next ATP concentration in the series. Each trace was normalized to its initial signal intensity, and shifted along the x-axis to account for an instrument dead time of 2.0 milliseconds, and these operations are expected to affect neither apparent rate constants nor phase amplitude ratios.

Two regimes are immediately visible in each of the ATP traces. The initial decay phases seen in these traces are consistent with the prediction that mantADP dissociation from the nucleotide-binding pocket is accompanied by a loss of fluorescence due to quenching. There is visible in each trace, however, a subsequent reversal in the predicted decay, beginning at ~0.5 seconds after mixing. This behavior was not seen in similar studies performed using the *Drosophila* K401 dimeric N-terminal truncation, which

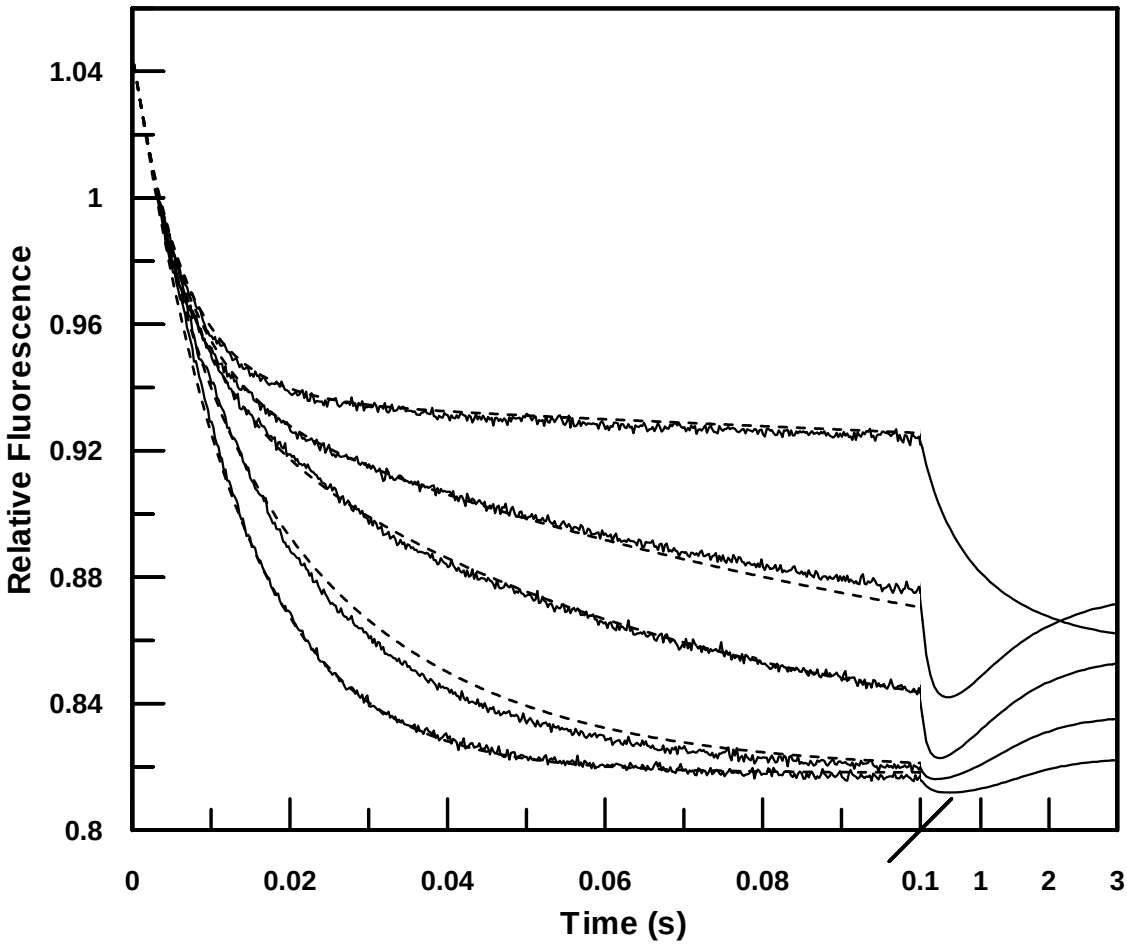

Figure 3.10: *Pre-steady-state mantADP release from KHC407A.* KHC407A-mantADP complex (1 μM enzyme active site, 2 μM mantADP) was rapidly mixed with microtubules (20 μM) plus ADP (10 μM), or ATP (5, 10, 25, and 50 μM), and fluorescence decay monitored. Concentrations are post-mixing. Solid lines represent normalized fluorescence data. Dashed lines are kinetic simulations of the reaction, based on a reaction depicted in scheme 3.4, rate constants in table 3.3, and initial reagent concentrations used in the experiments.

generated a family of traces converging to a common minimum within 1 second of mixing [93]. Thus, the observations made using KHC407A suggest a qualitative difference in the way in which the two enzymes interact with and process nucleotide.

Because of the complexity of the reaction that is proposed to take place in these experiments, curve fitting by nonlinear regression was not used. Instead, the reaction summarized in scheme 3.4 was used in a KINSIM simulation. Using this software, a given reaction can be simulated according to a set of differential equations defining the reaction, a set of initial reagent concentrations, a set of rate constants, and a set of output parameters correlating product formation with fluorescence. As subsets of rate constants and output parameters are varied, a systematic search for values generating simulated curves with smallest deviation from the observed data is made. In this way, values can be assigned to rate constants that yield a best global fit to the data. In figure 3.10, dashed lines represent simulated data based on reaction scheme 3.4 and rate constants summarized in table 3.3.

Estimates for the rate constants governing KHC407A-microtubule association and dissociation, as well as ATP-KHC407A association, obtained from experiments described in previous sections, were used as initial values for the KINSIM simulations described here, leaving the remainder to float. As successive fittings improved, these values were permitted to float as well, until a stable set of rate constants were obtained. Note that the rate constants for initial KHC407A-microtubule association (k_{+1}) and dissociation (k_{-1}) have been previously investigated directly by turbidity measurements, and indirectly by mantADP dissociation measurements. The value determined here, 7.8 $\mu M^{-1}s^{-1}$, is ~1.7 times that made from mantADP dissociation experiments, and ~2.7 times that from turbidity measurements, and can be considered an upper limit to the range of estimates for this parameter. The estimate for the dissociation rate constant for this

Scheme 3.4: *Release of (mant)ADP by kinesin-microtubule complex after mixing with microtubules and ATP*

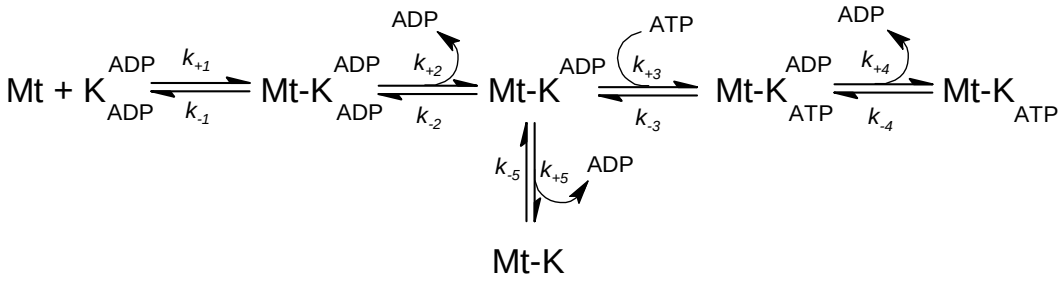

Table 3.3: *Rate constants for ATP hydrolysis and ADP release by KHC407A.* Rate constants were determined by global fitting to data shown in figure 3.10 using reaction in scheme 3.4

Step	***k*+**	***k*-**
1	7.8 $\mu M^{-1}s^{-1}$	9.3 s^{-1}
2	>3000 s^{-1}	42.9 $\mu M^{-1}s^{-1}$
3	1.7 $\mu M^{-1}s^{-1}$	18.4 s^{-1}
4	>3000 s^{-1}	33.2 $\mu M^{-1}s^{-1}$
5	1 s^{-1}	-

process, 9.3 s^{-1}, is one-half and one-third that of the corresponding values determined by turbidity and mantADP dissociation, respectively. The ATP binding rate constant determined here, 1.7 $\mu M^{-1}s^{-1}$, is less than one-third that of the mantATP binding rate constant, 5.6 ± 1.7 $\mu M^{-1}s^{-1}$, determined previously. Lastly, an off-rate constant for ATP (k_{-3}) was undeterminable using the mantATP binding assay, but is estimated at 18.4 s^{-1} by global fitting.

The most striking results of this experiment are the predicted rate constants for mantADP dissociation. A value of 3000 s^{-1} for both k_{+2} and k_{+4} were required for the fit seen in figure 3.10, although no improvement occurred by elevating them. These large values are consistent with the results of an experiment described previously, in which mantADP release from KHC407A after rapid mixing with microtubules at varying concentrations was examined (figure 3.9B). In that experiment, k_{obs} for mantADP release had a linear dependence on microtubule concentration up to 80 μM, at which point it had a value of over 400 s^{-1}. No rate-limiting step was apparent within this range. The results presented here confirm that the rate-limiting step may exceed 400 s^{-1} by at least an order of magnitude. This was not the case for the *Drosophila* K401 N-terminal truncation of conventional kinesin, which released mantADP with rate constants of ~300 s^{-1} [93].

Additionally, the reaction pathway for KHC407A simulation required the introduction of a third mantADP release step (step 6), occurring with a rate constant k_{+6} of ~1 s^{-1}. This step was necessary to account for the slow decay of the 10 μM ADP (0 μM ATP) curve after its initial rapid decay ending at ~0.02 seconds. In the absence of ATP, it was expected that each KHC407A dimer would release only one mantADP molecule after its interaction with microtubules, the second release event being ATP-dependent. Step 6, therefore, represents a nucleotide-independent release of the second bound mantADP. The shape of the 10 μM ADP cuve may also be explained, perhaps

more convincingly, as being an ADP-dependent mantADP release event, whereby ADP binds to the vacant nucleotide-binding pocket subsequent to the initial mantADP departure event, and drives the release of the second mantADP at a rate of ~1 s^{-1}. The latter mechanism proved too difficult to model.

ADP-dependence of mantADP Release from KHC407A. The ATP-indpependent release of mantADP observed in the experiment described in the previous section prompted an investigation of the ability of ADP to stimulate mantADP release. KHC407A-mantADP complex was prepared by mixing the enzyme with mantATP, and 20 minutes allowed for equilibrium to be reached. The complex was then mixed in the stopped-flow instrument with microtubules plus ADP. Post mixing concentrations were 1 μM KHC407A (active site), 2 μM mantADP, 20 μM microtubules, and ADP at concentrations at 5, 10, 20, 50, and 250 μM. Figure 3.11A shows the family of fluorescence traces from this experiment, each normalized to its initial intensity. Note that the bottom curve, with the steepest rate of descent, represents the rate of ATP-stimulated mantADP release, having been generated by mixing KHC407A-mantADP with 20 μM microtubules plus 250 μM ATP. This curve does not contribute to the calculation of an ADP binding rate constant.

A double exponential curve of the form $F = A_1 \cdot \exp(-k_1 t) + A_2 \cdot \exp(-k_2 t) + C$ was fit to each curve, revealing two phases in each mantADP release profile. A set of fast phase rates was interpreted as representing an initial release of mantADP immediately following microtubule binding. Slow phase rates indicate the ADP sensitivity of the second mantADP release event. These rates are plotted in figure 3.11B. The relationship fits a hyperbola $k_{obs} = k_{max}[ADP]/(K_{d\text{-}ADP} + [ADP]) + k_{off}$, whose parameters were determined by nonlinear regression. The initial gradient of the curve, equal to

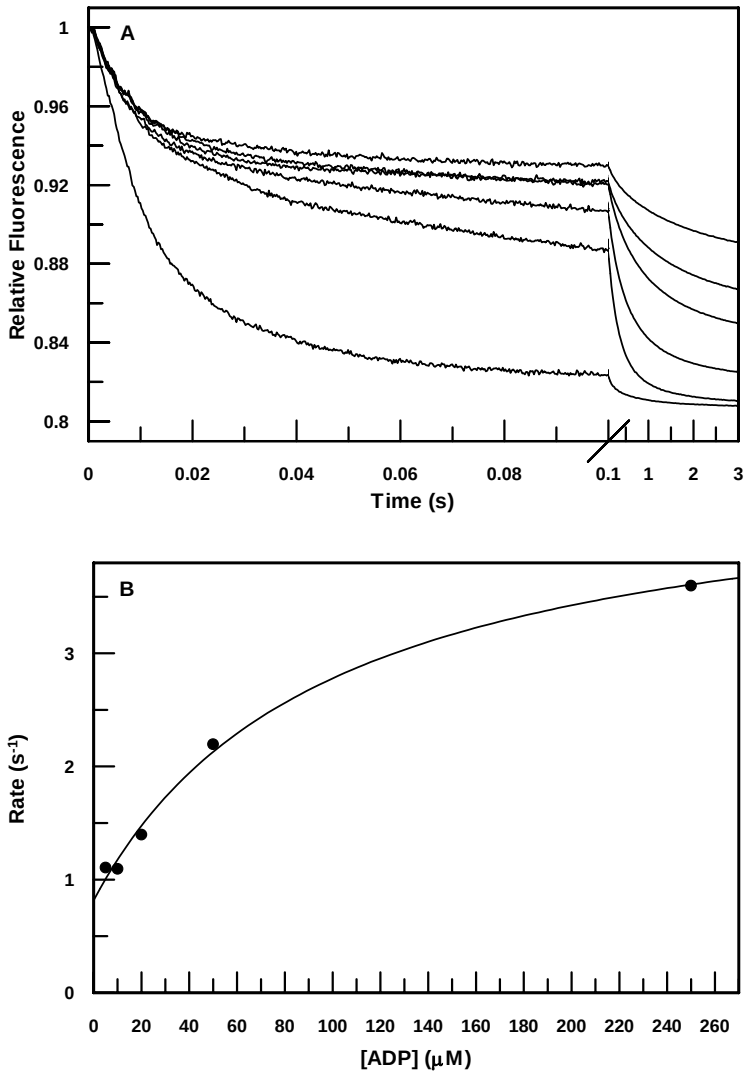

Figure 3.11: *ADP-dependence of mantADP release from KHC407A*. **A**: The set of fluorescence traces resulting from the rapid mixing of kinesin-mantADP complex with microtubules plus ADP. Post-mixing concentrations were 1 μM kinesin, 2 μM mantADP, 20 μM microtubules, and ADP at concentrations of 5, 10, 20, 50 and 250 μM, or ATP at 250 μM (top curve to bottom). Curves were fit to double exponential models ($F = A_1 \cdot \exp(-k_1 t) + A_2 \cdot \exp(-k_2 t) + C$) by nonlinear regression (fit curves not shown), generating a set of parameters A_1, A_2, k_1, k_2, and C for each. **B**: Fast-phase rates are plotted against ADP concentration, with a best-fit hyperbola of the form $k_{obs} = k_{max}[ADP]/(K_{d\text{-}ADP} + [ADP]) + k_{off}$. The parameters obtained by nonlinear regression estimate of k_{max} at 3.9 ± 0.3 s^{-1}, $K_{d\text{-}ADP}$ at 98 ± 31 μM, and k_{off} at 0.8 ± 0.1 s^{-1}. The ratio $k_{max}/K_{d\text{-}ADP}$ (0.04 ± 0.01 $\mu M^{-1}s^{-1}$) estimates the apparent second order rate constant for ADP binding to the stalled KHC407A-microtubule complex.

$k_{max}/K_{D\text{-}ADP}$, provides an estimate of the apparent second order rate constant governing ADP binding to the stalled KHC407A-microtubule complex in the absence of ATP. From the data, this rate constant is 0.04 ± 0.01 $\mu M^{-1}s^{-1}$. The rate constant for mantADP dissociation in the absence of added nucleotide, k_{off}, is 0.8 ± 0.1 s^{-1}. It can be concluded from this analysis, therefore, that the slow phase of mantADP release from KHC407A bound to microtubules in the absence of ATP consists of two components: one that is nucleotide-independent, occurring with a rate constant of ~0.8 s^{-1}, and one that can be stimulated ~5-fold to 3.9 ± 0.3 s^{-1} (the value of k_{max}) by weak ADP binding.

Binding of mantADP to KHC407A. In figure 3.10, which depicts the release of mantADP from KHC407A upon binding to microtubules plus ATP, there is an apparent reversal in the fluorescence decay that accompanies ATP depletion. The most straightforward explanation for this behavior maintains that mantADP rebinds to the active site of the enzyme as ATP becomes depleted. Simple competition by mantADP for vacant binding sites seems insufficient to explain the reversal in fluorescence decay, however, since the behavior implies a shift in binding equilibrium, which is difficult to explain. To further examine the interaction between mantADP and KHC407A, stopped-flow experiments were performed.

KHC407A-microtubule complex was formed, and rapidly mixed with mantADP at various concentrations in the stopped-flow instrument. After-mixing concentrations were 1 μM KHC407A, 10 μM microtubules, and mantADP at 5, 10, 15, 20, 25, 30 and 35 μM. As in mantATP binding experiments, optical excitation was at 280 nm, which excites tryptophan residues within the protein, and emission detected by a photomultiplier tube fitted with a 400 nm long pass filter. Fluorescence resonance energy transfer (FRET) between optically excited tryptophans in the protein and the *N*-

methylanthraniloyl moiety of mantATP, and the detection of fluorescence by the stopped flow instrument provides a means by which the binding rate can be measured after mixing. Figure 3.12A shows a representative trace, in which the mantADP concentration was 5 μM. This and each trace was used to generate a best-fit curve of the form $F = A \cdot \exp(-k_{obs}t) + k_2 t + C$. This equation provided a consistently better fit than did a simple exponential, as the second rate k_2 was necessary to account for a drift in the fluorescence signal that invariably accompanied the exponential phase. For the curve in figure 3.12A, k_1 was 0.940 ± 0.006 s^{-1} and k_2 was 0.0146 ± 0.0004 s^{-1}. Figure 3.12B shows observed rates of the exponential phases plotted against mantADP concentration. The data were evaluated as being better fit by a hyperbolic than a linear model. The equation $k_{obs} = k_{max}[mADP]/(K_d + [mADP]) + k_{off}$ was used to fit the data by nonlinear regression. From the fitting, $k_{max} = 6.1 \pm 0.9$ s^{-1}, $K_d = 81.1 \pm 18.8$ μM, and $k_{off} = 0.58 \pm 0.04$ s^{-1}.

The value of k_{max} was not closely approached by the data and is therefore of questionable validity. However, a value of 0.08 ± 0.02 $\mu M^{-1}s^{-1}$ for the apparent second order rate constant governing binding of mantADP to KHC407 in the absence of added nucleotide is indicated, calculated as the ratio of k_{max}/K_d. Based on this value and that of the off rate k_{off}, the equilibrium dissociation constant can be estimated at 7.7 ± 2.1 μM. This analysis shows that mantADP can bind weakly to the kinesin nucleotide-binding pocket, but sheds no additional information on the unexpected reversal of the fluorescence decay seen in mantADP dissociation experiments.

DISCUSSION

The kinetics of the dimeric rat conventional kinesin N-terminal truncation KHC407A have been investigated in the experiments described in this section.

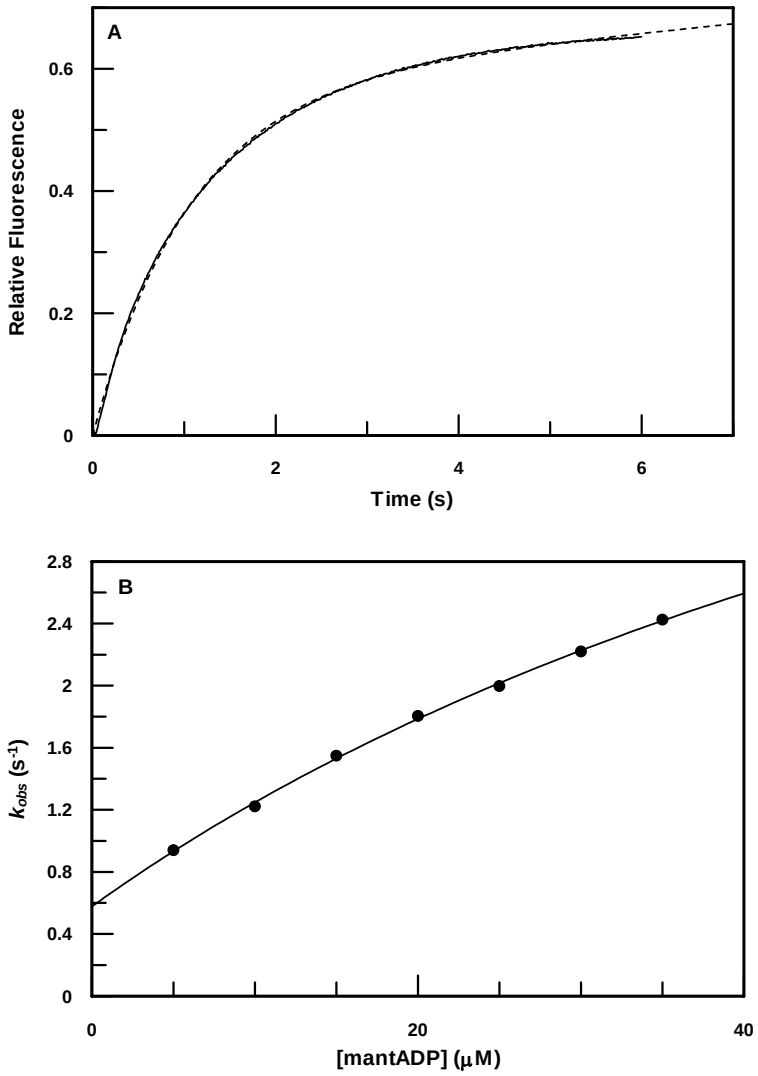

Figure 3.12: *Binding of mantADP to KHC407-microtubule complex.* **A:** Representative trace (solid line) of fluorescence change observed when kinesin-microtubule complex was rapidly mixed with mantADP (1 μM kinesin, 10 μM microtubules, and 5 μM mantADP, post-mixing). The trace is fit by a single exponential model containing a linear term ($F = A \cdot \exp(-k_{obs}t) + k_2t + C$) by nonlinear regression (solid line). Similar traces were obtained at mantADP concentrations of 5, 10, 15, 20, 25, 30, and 35 μM. **B:** Rates obtained by nonlinear regression of fluorescence trace data to an exponential model are plotted against mantADP concentration. The data are fit to the hyperbolic model $k_{obs} = k_{max}[mADP]/(K_d + [mADP]) + k_{off}$ by nonlinear regression. Curve fitting yielded values of k_{max} at 6.1 ± 0.9 s^{-1}, K_d at 81.1 ± 18.8 μM, and k_{off} at 0.58 ± 0.04 s^{-1}.

Sedimentation equilibrium analysis showed that the protein exists primarily as a dimer at low concentration, with a dissociation equilibrium constant of 46 nm (figure 3.3). Therefore, for most of the experiments described in this section, in which kinesin is used at micromolar concentrations, the motor most likely exists as a dimer in solution. Furthermore, the KHC407A dimer is of comparable stability as its *Drosophila* counterpart of similar length [21].

The interaction between KHC407A and microtubules were investigated using three methods. A rapid mixing experiment was performed in which the two components were mixed in the absence of ATP and turbidity change was measured (figure 3.8). The results of this experiment suggest a rate constant of $2.9 \pm 0.2\ \mu M^{-1}s^{-1}$ for KHC407A-microtubule binding (k_{+1}), and $2.9 \pm 0.2\ \mu M^{-1}s^{-1}$ for dissociation (k_{-1}). Using mantADP release as a reporter event for the initial KHC407A-microtubule association reaction, values of $4.6 \pm 0.1\ \mu M^{-1}s^{-1}$ and $29.8 \pm 3.3\ s^{-1}$ were obtained for these two rate constants. This experiment, unlike the turbidity measurement, was performed in the presence of ATP, although it is not clear why this should affect the apparent binding and dissociation rate constants describing kinesin-microtubule interaction. Finally, an experiment was performed in which the release of mantADP from KHC407A was monitored after rapid mixing of the enzyme-mantADP complex with microtubules plus varying amounts of ATP, and simulated curves yielding estimates for the rate constants involved were fit to the acquired data. This experiment estimated k_{+1} at $7.8\ \mu M^{-1}s^{-1}$ and k_{-1} at $9.3\ s^{-1}$. Taken together, the experiments can be considered to describe upper and lower limits for estimate for the two rate constants in question.

Likewise, two estimates have been made for the rate constants ATP binding. The first comes from stopped-flow measurements on mantATP binding to KHC407A-microtubule complex (figure 3.5B), while the second from the global fitting of simulated

curves to mantADP release traces (figure 3.10). Its prediction of a value of 5.6 ± 1.7 $\mu M^{-1}s^{-1}$ for the binding rate constant k_{+3} is contingent upon the assumption that binding is irreversible. That the off-rate for the reaction was too small to measure by this method supports the assumption. Secondly, the results of global fitting to mantADP dissociation data of KINSIM-simulated data estimated k_{+3} at 1.7 $\mu M^{-1}s^{-1}$ and k_{-3} at 18.4 s^{-1}. Thus, although the reaction is unlikely to be completely irreversible, the value of k_{+3} obtained under that assumption may indeed be valid.

The most striking finding from this set of experiments is the speed of mantADP release. Analysis of the dependence of mantADP release on microtubule concentration in a stopped-flow mixing experiment (figure 3.9B) revealed that this step was not rate limiting at the highest microtubule concentration tested, at which k_{obs} was over 400 s^{-1}. Varying ATP concentration in a stopped-flow mantADP release experiment (figure 3.10) produced fluorescence traces which, when globally fit by kinetic simulation, revealed values for two mantADP release rate constants in excess of 3000 s^{-1}. This was unexpected, since the corresponding rate constants for the *Drosophila* counterpart has been measured at only 300 s^{-1} [79]. It seems to be of little advantage for rat kinesin to have accelerated product release to this extent, given that k_{cat} differs between the two enzymes by only a factor of two (20 s^{-1} for *Drosophila*, 40 s^{-1} for rat). The significance of this difference, if any, remains unresolved.

The rate at which KHC407A hydrolyzes ATP was too rapid to measure by quench flow analysis (figure 3.6), since the burst phase of ADP production was too brief to be resolved. Analysis of the data by simulation suggested an apparent ATPase rate constant of 523 ± 58 s^{-1}. This value is only slightly less than the rate at which 100 μM ATP binds to kinesin, given the binding rate constant of 5.6 $\mu M^{-1}s^{-1}$ used in the simulation, suggesting that under the conditions used in the quench flow experiment, ATP binding

was the rate limiting step. It is impossible, therefore, to assign a value to the rate constant governing ATP hydrolysis, other than to concede that it is too large to measure with this technique. Likewise, analysis of the data suggests an apparent rate constant for ADP release of 43.6 ± 2.9 s^{-1}, two orders of magnitude lower than that governing mantADP release. This low value reflects steps intervening ATP binding and ADP release. One way to overcome this limitation would be to perform the mixing experiment with a high concentration of [α^{32}P]ATP; however, since interpretation of the data from this experiment depends on the accuracy with which the fraction of [α^{32}P]ATP hydrolyzed to the diphosphate is measured, data becomes progressively inaccurate with increasing [α^{32}P]ATP concentration.

The rate of phosphate release by KHC407A-microtubule complex can be predicted using parameters measured in the experiments discussed thus far. ATP appears to bind with a k_{max} of 210 s^{-1}, as estimated by mantATP binding experiments. ADP release is predicted to occur rapidly, with a rate constant of >3000 s^{-1}, predicted by fitting of computer simulations to mantADP release data. ATP hydrolysis is likewise predicted to be rapid, although no estimate of its rate constant can be made at this time. Finally, k_{cat} of microtubule-dependent ATP hydrolysis by KHC407 is 40 s^{-1}. Given a postulated pathway in which ATP binding is followed by ATP hydrolysis and ADP release, both of which occur rapidly, phosphate release is predicted to be the rate limiting step, with a rate constant of about 50 s^{-1}. A measurement of the rate at which phosphate was released from KHC407A-microtubule complex gave a release rate of 94 s^{-1}. Whatever the true phosphate release rate constant, this step is most likely the rate-limiting step of the kinesin motility cycle, as it is in the case of the *Drosophila* counterpart, which releases inorganic phosphate with a rate constant of 50 s^{-1}.

The interaction between the kinesin ADP was investigated in two ways. The ability of ADP to stimulate mantADP release from KHC407A-mantADP complex in the presence of microtubules was measured in a stopped-flow experiment, as well as the binding rate of mantADP to KHC407A-microtubule complex. The interaction studied here is not believed to be important in the motility cycle of the motor, although it may be relevant to the unexpected reversal in the fluorescence decay observed at ~0.5 seconds in the release of mantADP from KHC407A-microtubule complex (figure 3.10). The fluorescent nucleotide diphosphate binds weakly (K_d = 7.7 μM) and slowly (k_{on} = 0.08 $\mu M^{-1}s^{-1}$), and ADP interacts with similar kinetics. Although, as suspected, mantADP can bind the active site of kinesin, the mechanism by which the reversal in fluorescence decay occurs remains unclear.

By these studies, a kinetic picture of kinesin emerges, and serves as a standard with which mutant kinesins can be compared. Some aspects of the motility cycle remain uncertain. The reaction depicted in scheme 3.1 maintains the existence of a "captive head" intermediate, in which kinesin is bound via only one head, the other poised to vault over its companion and seek the next binding site on the microtubule surface. It is not known whether this represents a true distinguishable intermediate, or whether the trailing head detaches from its binding site and seeks the next in one concerted movement. Likewise, the identity of the force-generating step is not known; the release of inorganic phosphate, being the rate-limiting step, is an attractive candidate. It cannot be said for certain whether phosphate release precedes, is concurrent with, or follows the conformational change in the dimer that advances the motor. Despite these uncertainties, the model serves as a useful guideline for understanding the motility of kinesin.

CHAPTER 4

Analysis of the N256K Mutant

INTRODUCTION

Conventional kinesin is a microtubule-dependent molecular motor responsible for anterograde movement of vesicles and organelles in axons [15;16]. This protein is one of at least 144 known motor proteins comprising the kinesin superfamily, a group that shares both structural and functional characteristics [1;4]. The kinesins are ATPases, and conventional kinesin has been shown to exhibit movement along its microtubule track that is tightly coupled with ATP hydrolysis [114;115]. Optical trapping experiments on conventional kinesin at low mechanical load have shown that the motor takes one 8 nm step along a microtubule for every ATP it hydrolyzes, the step size being sufficient to span the distance between two binding sites on the microtubule surface [112;113]. Conventional kinesin is a processive motor; once bound to a microtubule, it may take 10-100 steps without dissociating [74-76].

An understanding of the mechanism by which conventional kinesin utilizes the energy released by ATP hydrolysis to perform mechanical work begins with that of the sequential conformational changes that occur in the protein structure during motility, as well as the structural elements and domains involved in those changes. To this end, a catalog of structure-function relationships implicated in kinesin-microtubule interaction, nucleotide binding, and energy transduction, has been compiled. The microtubule binding surface of the motor domain has been identified by examination of mutants [132]. The nucleotide binding pocket, visible in the crystal structure [19], contains a γ-

phosphate sensor apparatus, consisting of four domains that are conserved throughout the kinesin superfamily [67;133;138;186].

Two of these domains, switch I and II (residues 199-204 and 232-237, respectively, in rat conventional kinesin), appear to undergo specific translational and rotational movements relative to surrounding structures in response to changes in the phosphorylation state of the nucleotide bound in the active site. Additionally, a switch I arginine (R204) and switch II glutamic acid (E237) are likely to participate in the formation of a salt bridge only when the bound nucleotide is in the diphosphate state. These two structures may serve to communicate nucleotide phosphorylation state from the active site to other domains elsewhere in the protein.

A mutation that appeared to decouple nucleotide phosphorylation state and microtubule binding was identified in the minus-end directed kinesin-like protein Kar3 [62;187]. The mutant, Kar3-N650K, binds and hydrolyzes ATP with activity similar to that of wild-type, but unlike wild-type, microtubule binding does not stimulate ATP hydrolysis by the mutant. Similarly, the mutant binds tightly to microtubules in both the presence and absence of nucleotide, whereas microtubule affinity of the wild-type is decreased 10-fold by added nucleotide. Thus, although the decoupled Kar3 mutant binds to microtubules and is capable of binding to and hydrolyzing ATP, it does not exhibit wild-type nucleotide-dependent behavior.

The Kar3 residue whose mutation creates the decoupled phenotype is implicated in neither nucleotide or microtubule interaction. It resides ~15 residues N-terminal to switch II, and ~17 Å from the β-phosphate of the bound ADP in the crystal Kar3 crystal structure [64]. Kar3 N650 is part of helix α4 (the relay helix), a structure containing residues that in conventional kinesin participate in microtubule binding, although the residue corresponding to Kar3 N650 in the latter protein can be mutated to alanine

without disturbing the interaction [132]. In myosin, the relay helix undergoes a piston-like translation along its axis in response to alternate phosphorylation states of the bound nucleotide, and is thought to act as a mechanical transmitter of conformational state information between the nucleotide- and actin-binding sites [69;142;143], and helix α4 is likely to serve an analogous function in kinesin. In crystal structures of monomeric Kif1A in ADP and ATP-like states, helix α4 appears to accommodate the ADP state by translating along its axis, underging a ~20° rotation, and recruiting ~10 residues from loop L11, immediately N-terminal to it [67].

Alignment of the Kar3 and rat conventional kinesin sequences identifies the residue N256 in the latter sequence as corresponding to Kar3 N650. In the crystal structure of rat conventional kinesin [19], the position of N256 defines the boundary between helix α4 and loop L11. The loop is disordered, and it is not resolved in the crystal structure. The experiments described in this section were undertaken to examine the effects of the N256K mutation on dimeric rat conventional kinesin. One question that was addressed initially was that of whether the mutation would yield effects in rat kinesin similar to those seen in Kar3. This was not certain, given the differences between the structures of the two proteins, as well as the mechanisms by which they move upon microtubules. Conventional kinesin functions as a processive dimer whose motility is directed towards the plus end of the microtubule, most likely using a "hand-over-hand" alternating site mechanism for motility, whereby the motor maintains an attachment to its microtubule track via one catalytic core domain while the other seeks its next binding site along the microtubule surface [117-120]. Kar3, by contrast, functions as a monomer, is nonprocessive, and moves towards the minus end of the microtubule.

The kinetics of mantADP release from Kar3 N650K and its Ncd counterpart, Ncd N600K, were examined [62]. Ncd, like Kar3, is a minus-end directed microtubule motor;

it differs from Kar3 in that it is dimeric and nonprocessive. It was found that upon mixing with microtubules plus ATP, neither mutant exhibited a release of mantADP that was significantly accelerated over that of wild type. The experiments described in this section were undertaken in order to form a more complete picture of the effects of the mutation introduced into rat conventional kinesin.

RESULTS

Active-Site Titration of KHC407A N256K. The concentration of each preparation of KHC407A N256K was determined by active-site titration. For this assay to succeed, it must be possible to label the protein with [α^{32}P]ADP, the success of which requires an active site capable of binding the nucleotide in the absence of microtubules, which is the case for the wild-type enzyme. This was found to be the case for the mutant protein as well. The assay measures the extent of [α^{32}P]ADP release from the labeled protein as a function of time. Upon initiation of the assay, an ATP regenerating system composed of phosphocreatine kinase and phosphocreatine converts released [α^{32}P]ADP to the triphosphate form, and the ratio of diphosphate to triphosphate can be measured as a function of time [170]. The presence of unlabeled ATP prevents rebinding of [α^{32}P]ATP to kinesin, and permits the measurement of the rate of ADP dissociation, while extrapolation of the data to t = 0 permits an estimation of the concentration of bound [α^{32}P]ADP before reaction initiation. This concentration is considered to be equal to the active site concentration in the kinesin preparation. Figure 4.1 shows the results of an active-site titration of a preparation of KHC407A N256K, with a single exponential curve $F = A \cdot \exp(-k \cdot t) + C$ fit to the data by nonlinear regression.

The value k, the rate constant by which [α^{32}P]ADP dissociates from the protein, is over twice that of the wild type (0.014 vs. 0.0062 s^{-1}). Since the residue at position 256

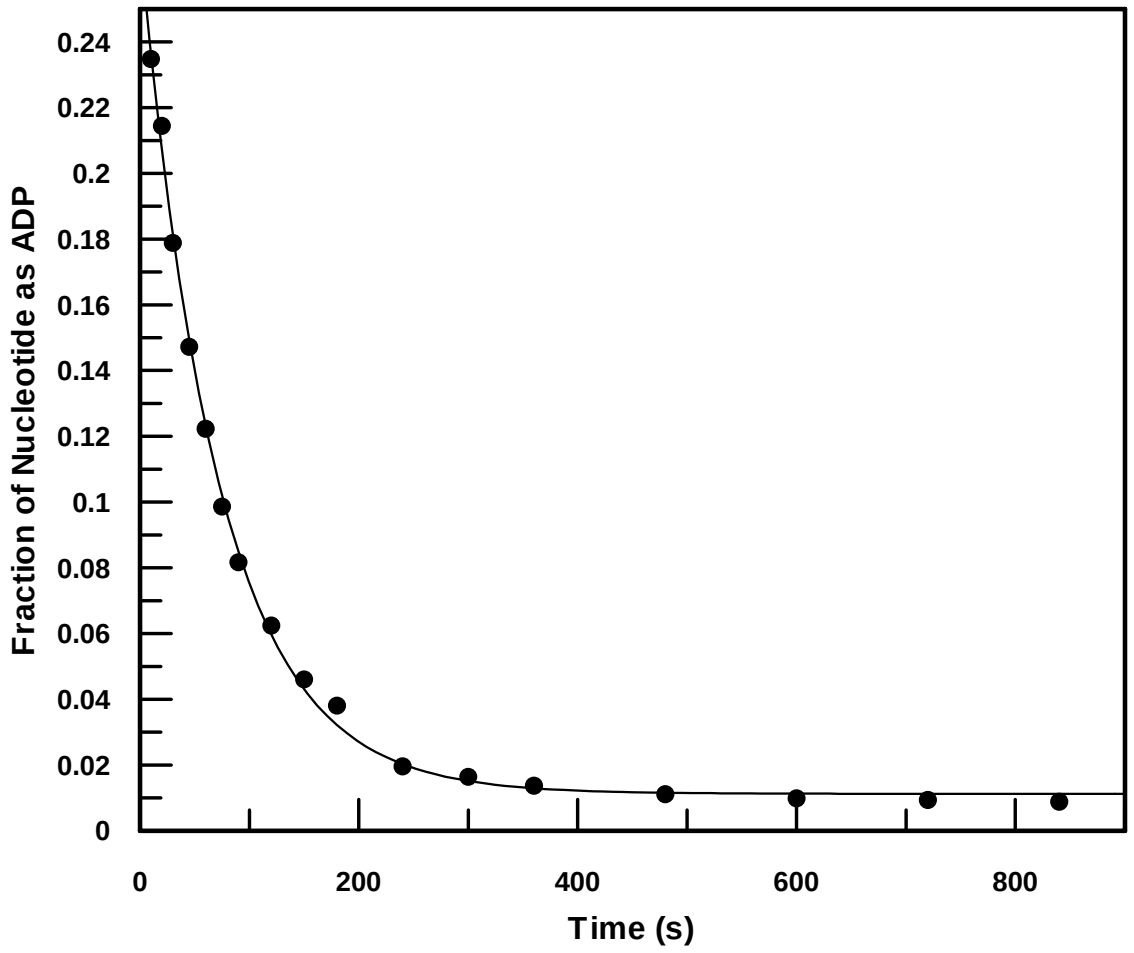

Figure 4.1: *Active-site titration of KHC407A N256K.* Kinesin-[α^{32}P]ADP complex (16.5 μM kinesin, 21.7 μM [α^{32}P]ADP) was rapidly mixed with phosphocreatine kinase (0.3 mg/mL), phosphocreatine (4 mM), and Mg-ATP (5 mM) in ATPase buffer. The ratio of [α^{32}P]ADP to total labeled nucleotide is plotted against reaction time, as well as a best-fit single exponential curve $F = A \cdot \exp(-k \cdot t) + C$. Parameter values obtained from the fitting were A: 0.260 ± 0.003, k: 0.014 ± 0.001 s^{-1}, C: 0.011 ± 0.001. An active-site concentration of 15.1 ± 0.2 μM was estimated, based on values for A and the concentration [α^{32}P]ATP used in the initial labeling, according to the relationship [kinesin] = ([ATP] $\cdot A$)/(1 – A).

makes no contact with the bound nucleotide, it is unlikely to directly affect the binding affinity of the enzyme for ADP. The mutation probably affects the conformation of the protein in such a way as to indirectly weaken the interactions between binding site residues and the bound nucleotide.

Steady-state Kinetics of KHC407A-N256K. The Kar3 N650K mutant was reported to posses no microtubule stimulated ATP activity above that observed in the absence of microtubules [62]. To quantify this qualitative assessment of steady-state ATP hydrolysis, a rigorous evaluation of KHC407A-N256K steady-state kinetics in the presence of microtubules was undertaken in the present study. The assay measured the rate of [α^{32}P]ATP hydrolysis by the enzyme as a function of [α^{32}P]ATP concentration in the presence of 60 μM microtubules. Though not tested for KHC407A-N256K, this concentration of microtubules was considered to be in excess of the $K_{0.5,\ Mt}$ of the dimeric *Drosophila* kinesin N-terminal truncation K401 by a factor of 60 [75], and therefore likely to represent a microtubule concentration at near saturation. In figure 4.2, values of observed hydrolysis rate are plotted against ATP concentration. A fitting of a hyperbolic model to the data provides estimates of the kinetic parameters k_{cat} and $K_{m\text{-}ATP}$, which are 0.33 ± 0.02 s^{-1} and 13.8 ± 3.4 μM, respectively. The ATPase activity of KHC407A-N256K is stimulated by microtubules. Although not measured directly, the k_{cat} of this enzyme in the absence of microtubules cannot exceed (and is likely to approach) 0.014 s^{-1}, the rate of ADP release from KHC407A-N256K as determined by active-site titration. Thus, the presence of excess microtubules stimulates the ATPase activity of the mutant by ~20-fold, contrasting with a >6000-fold stimulation afforded to the wild-type motor.

$K_{m\text{-}ATP}$ is reduced in the mutant (53.6 ± 4.8 μM for KHC407A), although the significance of this with respect to the overall kinetic mechanism of the enzyme is not

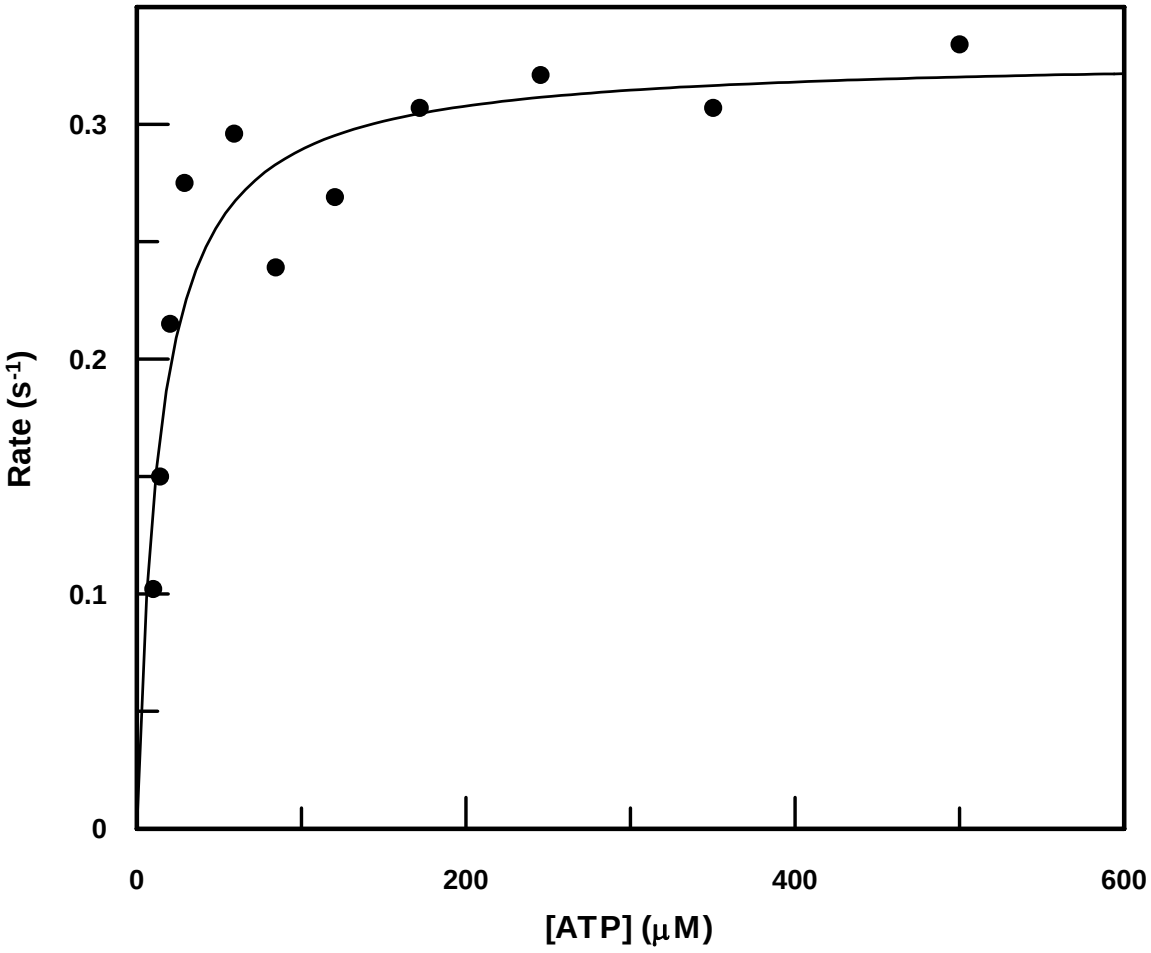

Figure 4.2: *Steady-state ATP hydrolysis by KHC407A-N256K in the presence of microtubules.* Hydrolysis rates of [α^{32}P]ATP by KHC407A were determined at substrate concentrations of 10 to 500 μM. 5 nM KHC407 and 60 μM microtubules were incubated with labeled substrate, and a time course created. Products were separated by thin-layer chromatography, visualized, and the hydrolysis rates extracted from the results by curve fitting. The observed relationship between hydrolysis rate and substrate concentration, once plotted, was used to generate a best-fit curve $k_{obs} = k_{cat}[ATP]/(K_{m\text{-}ATP} + [ATP]) + C$, whose parameters yield estimates of k_{cat} and $K_{m\text{-}ATP}$. From the data and subsequent curve fitting, $k_{cat} = 0.33 \pm 0.02$ s^{-1} and $K_{m\text{-}ATP} = 13.8 \pm 3.4$ μM.

immediately apparent. However, the apparent second-order rate constant (the lower limit for the true rate constant) for substrate binding, estimated by $k_{cat}/K_{m\text{-}ATP}$, is 0.024 ± 0.006 $\mu M^{-1}s^{-1}$, is lower than the corresponding figure for the wild type (0.75 ± 0.07 $\mu M^{-1}s^{-1}$) by a factor of 30. This ratio measures the specificity of the enzyme; it is less than the true substrate binding constant by a factor equal to the probability that the enzyme-substrate complex will proceed forward before dissociating. Hence, from measurements of steady-state hydrolysis rates of the mutant and wild-type kinesins, it is apparent that nonproductive substrate binding occurs in the former with a frequency 30 times that for the latter. This estimate was refined using mantATP association and mantADP dissociation stopped-flow experiments described in the following sections.

Binding of mantATP to KHC407A-N256K. The binding rate of the fluorescent ATP analog mantATP to the mutant kinesin was examined in a stopped-flow experiment. As in previously described experiments with the wild-type enzyme, the association kinetics measured using the fluorescent nucleotide are considered to reflect those of the natural substrate. The concentration of fluorescent nucleotide was varied in a stopped-flow experiment, in which nucleotide was rapidly mixed with kinesin-microtubule complex. Optical excitement at 280 nm resulted in fluorescence of bound nucleotide due to fluorescence resonance energy transfer from protein tryptophans to the *N*-methylanthraniloyl moiety of mantATP. Figure 4.3A shows a representative trace for the fluorescence change resulting from mixing components to final concentrations of 2 μM KHC407A-N256K, 10 μM microtubules, and 20 μM mantATP. A best-fit curve of the form $F = A \cdot \exp(-k_{obs}t) + k_2 t + C$ was generated for the fluorescence data by nonlinear regression, yielding a value of 105 ± 1 s^{-1} for k_{obs} and 0.04 ± 0.02 s^{-1} for k_2. The linear phase of the curve, defined by k_2, does not correspond to any component of the predicted

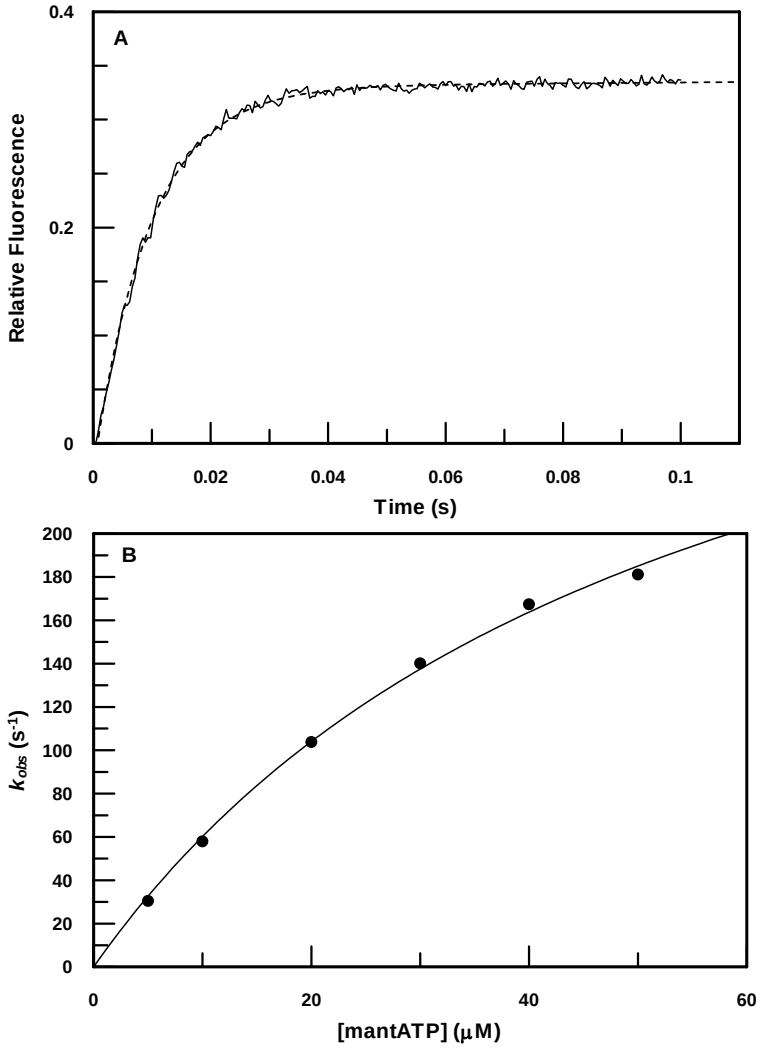

Figure 4.3: *Pre-steady-state binding of mantATP to KHC407A-N256K-microtubule complex.* **A:** A representative trace of fluorescence change incurred by KHC407A-microtubule complex upon rapid mixing with mantATP. Concentrations after mixing were 2 μM kinesin, 10 μM microtubules, and 20 μM mantATP. The dashed line indicates a best-fit curve $F = A \cdot \exp(-k_{obs}t) + k_2t + C$. Similar curves were generated for mantATP concentrations of 5, 10, 20, 30, 40, and 50 μM mantATP. **B:** Values for k_{obs} obtained from fluorescence traces at each mantATP concentration are plotted against the independent variable. The solid curve represents the best-fit hyperbola $k_{obs} = k_{max}[mATP]/(K_d + [mATP])$ determined by nonlinear regression. Convergence of parameters provide estimates of k_{max} at 385 ± 25 s^{-1} and K_d at 54 ± 6 μM. The ratio k_{max}/K_d provides a lower limit to the apparent second-order rate constant for mantATP binding to the complex, and is 7 ± 1 $\mu M^{-1}s^{-1}$.

binding mechanism, and may represent an optical effect that is independent of substrate binding.

Figure 4.3B shows the values for k_{obs} determined at mantATP concentrations from 5 to 50 μM. The dependence on substrate concentration, although nearly linear, was best fit to a hyperbolic model $k_{obs} = k_{max}[mATP]/(K_d + [mATP]) + k_{off}$, suggesting saturation kinetics. The apparent dissociation constant K_d for the binding reaction was 54 ± 6 μM, and k_{max} was 385 ± 28 s^{-1}. The y-intercept was not permitted to float, but instead was fixed at zero in order to maintain for it a kinetically valid non-negative value, and for this reason, k_{off} cannot be estimated from these data.

The highest tested concentration of mantATP was 50 μM; higher concentrations resulted in traces that were progressively noisier and of unacceptable quality. Hence, mantATP concentrations significantly above the value of K_d were not tested, and the value of k_{max} to which the data converges may not be reliable. Nevertheless, the ratio of k_{max}/K_d provides the initial slope of the fitted curve, an estimate of the apparent second-order rate constant for mantATP binding to the enzyme. This ratio is 7 ± 1 $\mu M^{-1}s^{-1}$, similar to the corresponding value of 6 ± 2 $\mu M^{-1}s^{-1}$ for the wild-type enzyme. Both estimates rely on the assumption of negligible dissociation rates of mantATP subsequent to binding, and are lower limits to the true association rate constants.

Microtubule-dependence of mantADP Release from KHC407A-N256K. Wild-type kinesin retains ADP, and the motor releases its bound nucleotide upon binding to microtubules [170;180]. The pre-steady-state rate at which nucleotide release from KHC407A-N256K occurs was measured by exploiting the fluorescence change incurred by the nucleotide analog mantADP upon dissociation. The apparent dissociation rate was shown to be dependent on both microtubule and ATP concentration [79;93]. In this

section are described measurements of the microtubule concentration dependence of mantADP dissociation from KHC407A-N256K, and extraction of rate constants governing the binding and dissociation of the motor and microtubules.

Kinesin-mantADP complex was formed and rapidly mixed with microtubules plus ATP in the stopped-flow instrument. Figure 4.4A shows the decay in the fluorescence of the mixture of components to concentrations of 2 μM kinesin, 4 μM mantADP, 20 μM microtubules and 1 mM ATP. A double-exponential curve taking the form $F = A_1 \cdot \exp(-k_1 t) + A_2 \cdot \exp(-k_2 t) + C$ was fit to the data, yielding two rates, 1.123 ± 0.004 s^{-1} and 0.239 ± 0.002 s^{-1}. The two apparent decay modes were of unequal amplitude, that of the fast phase being 3 times that of the slow (0.15:0.05). Measurements of fluorescence decay for mixing experiments at microtubule concentrations from 5 to 25 μM and curve fitting produced a set of fast and slow phase rates for each microtubule concentration, and figure 4.4B shows rates for both phases plotted against the independent variable. Fast phase data were best fit to a hyperbola of the form $k_{obs} = k_{max}[Mt]/(K_{50\text{-}Mt} + [Mt]) + k_{off}$. The rate constant for dissociation, k_{off} was assumed to be negligible, and set to zero.

The mutation has impaired apparent mantADP release as well as microtubule-kinesin association. The wild-type enzyme released the fluorescent product at rates that showed a linear dependence on microtubule concentration up to 80 μM microtubules, and no value of k_{max} could be discerned. Additional mantADP release measurements along with global fitting of computer simulated kinetic data suggested that the rate constants governing mantADP release exceeded 3000 s^{-1}. By contrast, the release of mantADP from the N256K mutant has an apparent k_{max} of 1.22 ± 0.01 s^{-1}. This value exceeds k_{cat} by a factor of ~3.5. This contrasts with the corresponding value for the wild-type enzyme, >75 times that of wild-type k_{cat}. The concentration of microtubules required for

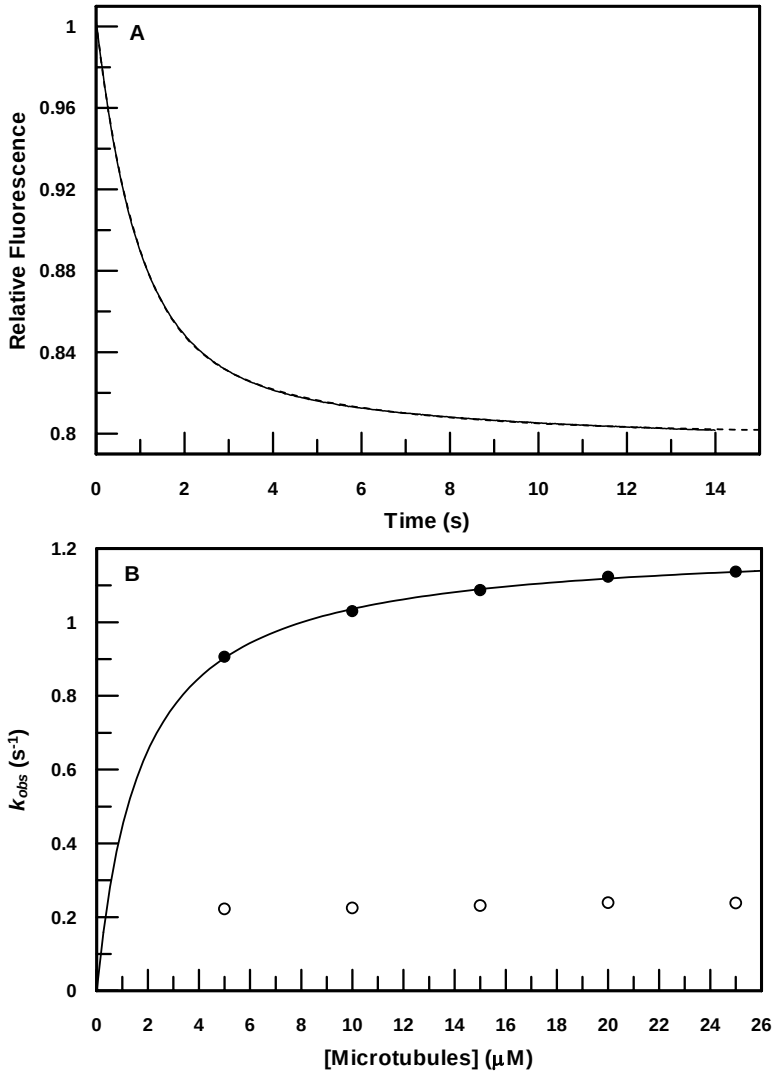

Figure 4.4: *Microtubule-dependent release of mantADP from KHC407A-N256K.* **A:** Representative trace of fluorescence decay resulting from rapid mixing of kinesin-mantADP complex with microtubules and ATP. Post-mixing concentrations were 2 μM kinesin, 4 μM mantADP, 20 μM microtubules, and 1 mM ATP. A best-fit double exponential curve $F = A_1 \cdot \exp(-k_1 t) + A_2 \cdot \exp(-k_2 t) + C$ (dashed) was determined by nonlinear regression. Parameters A_1, A_2, k_1, k_2, and C were determined for microtubule concentrations at 5, 10, 15, 20 and 25 μM. **B:** Fast- (filled circles) and slow- (open circles) phase rates are plotted against microtubule concentration, and fast-phase rates were fit by linear regression. Curve fitting using a hyperbolic model $k_{obs} = k_{max}[Mt]/(K_{50\text{-}Mt} + [Mt])$ by nonlinear regression yielded values for k_{max} of 1.22 ± 0.01 s^{-1} and $K_{50\text{-}Mt}$ of 1.73 ± 0.06 μM. The ratio $k_{max}/K_{50\text{-}Mt}$ provides a minimum estimate of the second order rate constant for the binding of KHC407A-N256K to microtubules at 0.70 ± 0.03 $\mu M^{-1}s^{-1}$.

a half-maximal mantADP release rate is given by $K_{50\text{-}Mt}$, which is equal to 1.73 ± 0.06 μM, and the ratio $k_{max}/K_{50\text{-}Mt}$ serves as a minimum estimate of the second order rate constant for the binding of KHC407A-N256K to microtubules. This ratio, the gradient of the initial portion of the curve where microtubule concentration is small, is 0.70 ± 0.03 $\mu M^{-1}s^{-1}$.

Pre-steady-state Binding of KHC407A-N256K to Microtubules. Kinesin-microtubule association is the first step in the motility of a processive motor, and is followed by multiple force-generating cycles. Examination of mantADP dissociation from KHC407A-N256K upon binding to microtubules provided an estimate of the lower limit of the motor-microtubule association rate constant. The experiments described here were performed in order to obtain a direct measurement of the association rate constant by exploiting a turbidity change that accompanies the reaction. Microtubules and KHC407A-N256K were mixed in the stopped-flow instrument to concentrations of 11 and 2 μM respectively, and the transmission of light at 340 nm was monitored. Figure 4.5A shows the unfolding of turbidity with time. A best-fit double exponential model of the form $T = A_1 \cdot \exp(-k_1 t) + A_2 \cdot \exp(-k_2 t) + C$ generated by nonlinear regression (dashed line) superimposes on the collected data. Both fast- and slow-phase rates were determined by the fit as 50.9 ± 0.3 s^{-1} and 6.77 ± 0.03 s^{-1}. The amplitudes were similar (0.034 and 0.036). For fitting of turbidity trace data, single exponential models with and without linear terms, as well as a double exponential model were attempted. The use of the double exponential can be justified over that of the single not only in its superior fit to individual traces, but in the closeness of fit for compiled fast-phase rate data for 6 microtubule concentrations to a linear model seen in figure 4.5B.

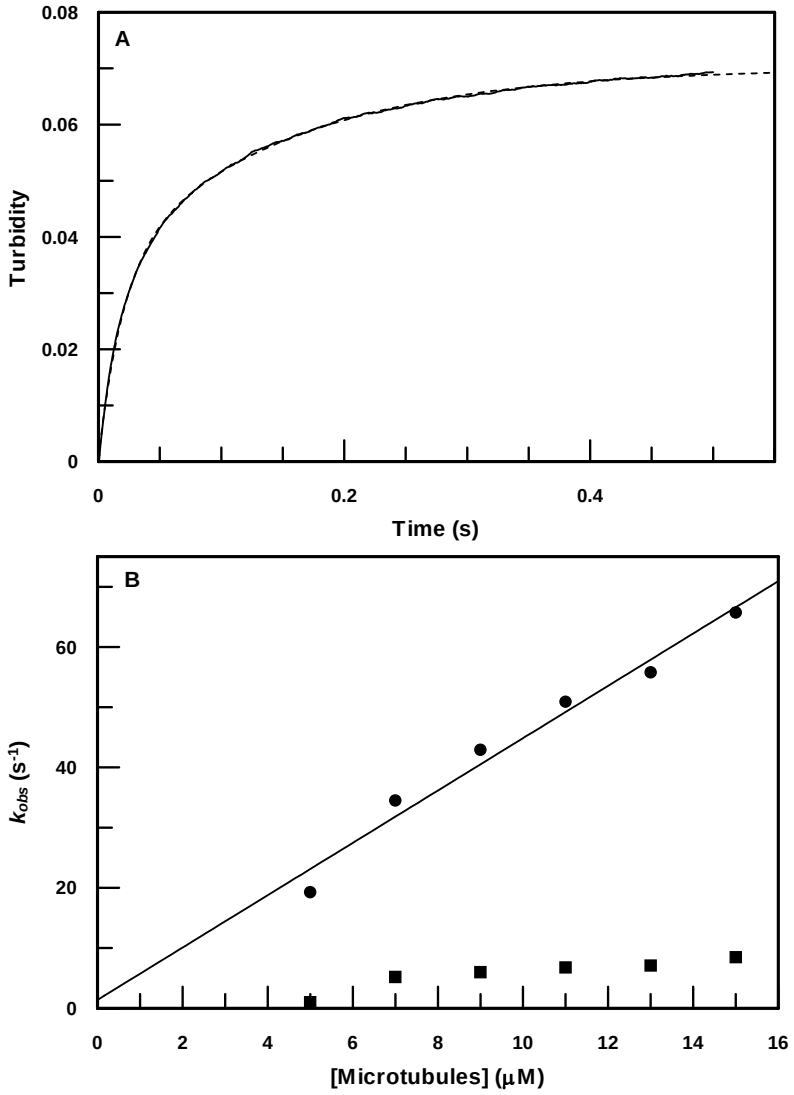

Figure 4.5: *Pre-steady-state binding of KHC407A-N256K to microtubules*. **A:** Representative turbidity trace at 340 nm illumination of kinesin and microtubules after mixing (2 μM kinesin, 11 μM microtubules, post-mixing). The dashed line represents a best-fit double exponential curve $T = A_1 \cdot \exp(-k_1 t) + A_2 \cdot \exp(-k_2 t) + C$, whose parameters A_1, A_2, k_1, k_2, and C were determined by nonlinear regression. Similar traces were recorded for microtubule concentrations of 5, 7, 9, 11, 13, and 15 μM microtubules, each of which were fit by double exponential models. **B:** Both fast (circles) and slow (squares) rates were plotted against microtubule concentrations. Fast rates were fit by linear regression, whose gradient of $4.3 \pm 0.4\ \mu M^{-1}s^{-1}$ estimates the second-order rate constant for kinesin-microtubule association. A y-intercept at $1.4 \pm 0.4\ s^{-1}$ is the apparent rate constant for dissociation of the complex.

In figure 4.5B, fast-phase (circles) and slow-phase (squares) rates were plotted against microtubule concentration. The gradient of a linear fit to the fast-phase data estimates of the apparent second order rate constant for KHC407A-N256K binding to microtubules at 4.3 ± 0.4 $\mu M^{-1}s^{-1}$. This value is similar to that determined for the wild-type KHC407A, 2.9 $\mu M^{-1}s^{-1}$, described in the previous chapter, and it is apparent that the N256K mutation does little to impair microtubule association. One possible difference between the two is in the apparent dissociation rate constants, equal to the y-intercepts of the graphs. The fast-phase data for the mutant has a y-intercept close to the origin, and linear regression places it at 1.4 ± 0.4 s^{-1}. The wild-type enzyme, by contrast, has an apparent dissociation rate constant of 20 s^{-1}. The kinesin-microtubule complex in the absence of nucleotide appears to be stabilized by the N256K mutation, which decreases K_d from 6.7 ± 0.9 μM (wild-type) to 0.3 ± 0.1 μM. This contrasts with what was reported for the Kar3 N650K, which bound as tightly to microtubules in the absence of nucleotide as did the wild-type motor.

The slow-phase rate data plotted in figure 4.5B are of uncertain significance, and no mathematical model has been fit to them. Each slow phase rate is between one-seventh and one-eighth that of its corresponding fast phase rate. Their amplitudes are consistently similar to those of the fast phase data, which may suggest that the observed rates are kinetically relevant; each fast-phase event appears to be accompanied by one occurring with a slower rate. Turbidity data collected from the wild-type motor was also best fit by a double exponential curve, although the relative amplitudes of the two rates observed at each microtubule concentration were more variable, strongly suggesting that no linkage exists between the two processes that generated them.

The apparent rate constant governing the association between the mutant kinesin and microtubules determined by the method of turbidity analysis differs from the

corresponding figure extracted from mantADP release data described in the previous section (4.3 vs 0.7 $\mu M^{-1}s^{-1}$). In the mantADP release experiment, additional data describing k_{obs} at low microtubule concentration might have helped resolve the initial slope of the graph in figure 4.4B. Such data points could not be obtained, since meaningful data could only be obtained when microtubules were in excess of kinesin. An attempt was made to constrain the initial slope of the graph in figure 4.4B to 4.3 $\mu M^{-1}s^{-1}$, but this produces an unsatisfactory fit.

ATP-dependence of mantADP Release from KHC407A-N256K. In the alternating-site model of conventional kinesin motility, two ADP release events are predicted to occur after the kinesin binds to microtubules [79;92;93]. Results of experiments performed with the KHC407A motor as well as the *Drosophila* 401 residue N-terminal truncation suggest that motor-microtubule interaction is immediately followed by the release of one bound ADP molecule, and that the release of the second is dependent on the presence of ATP. KHC407A-mantADP complex exhibited a rapid release of its bound nucleotides upon being mixed with microtubules and ATP, with rate constants in excess of 3000 s^{-1}. In the experiments described here, KHC407A-N256K containing bound mantADP was mixed in the stopped-flow apparatus with microtubules plus ATP at varying concentrations. These experiments are expected to reveal two fluorescence decay modes; one whose rate is dependent on microtubule concentration and independent of ATP, and the other whose rate reflects the release of a second bound nucleotide subsequent to ATP binding. This is reflected in the kinetic model shown in scheme 4.1. Kinesin-mantADP complex (1.25 μM kinesin, 2.5 μM mantADP) mixed with microtubules (16 μM) plus ADP (5 μM) or ATP (25, 50, 100, and 250 μM) produced the fluorescence traces shown in figure 4.6.

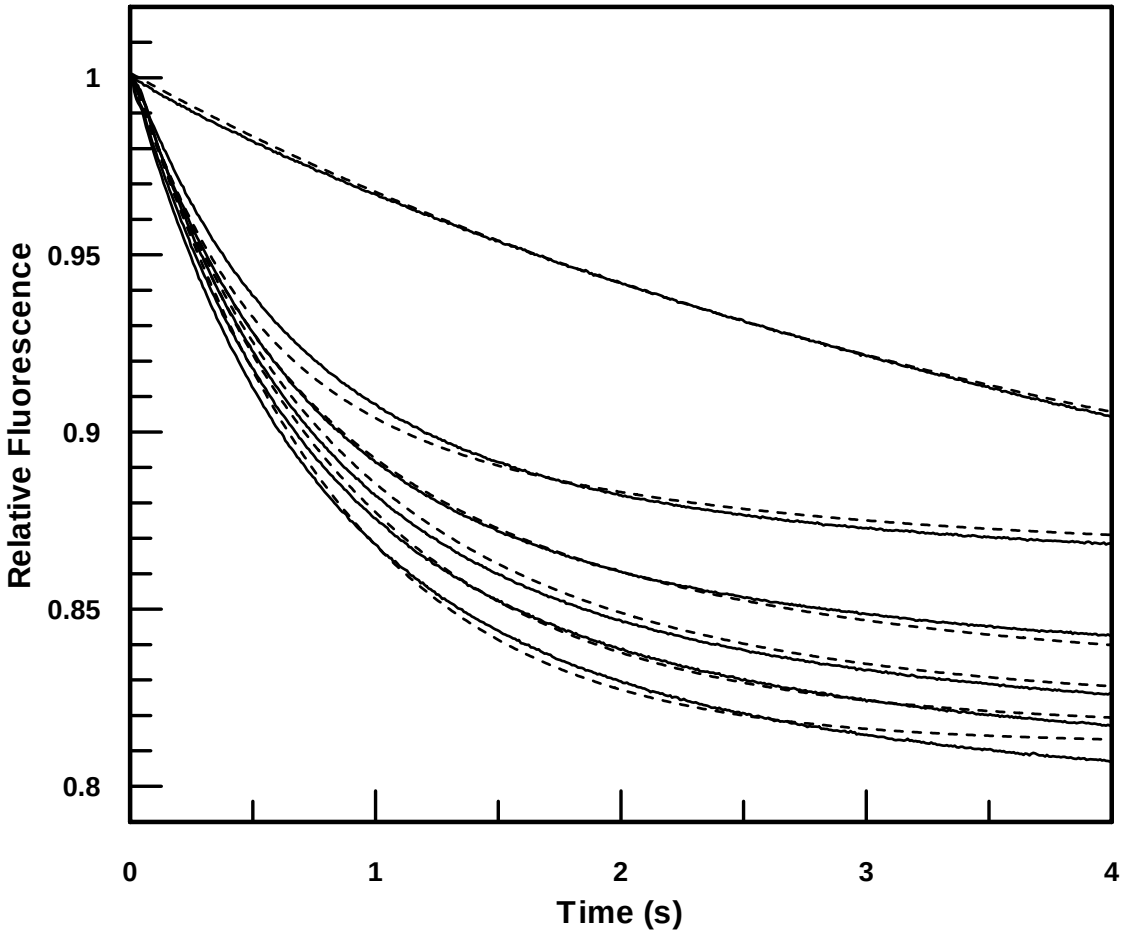

Figure 4.6: *Pre-steady-state mantADP release from KHC407A-N256K.* KHC407A-N256K-mantADP complex (1.25 μM enzyme active site, 2.5 μM mantADP) was rapidly mixed with microtubules (16 μM) plus ADP (10 μM), or ATP (25, 50, 100, and 250 μM). The upper trace represents KHC407A-N256K-mantADP mixed with 500 μM ATP in the absence of microtubules. Concentrations are post-mixing. Solid lines represent normalized fluorescence data. Dashed lines are kinetic simulations of the reaction, based on a reaction depicted in scheme 4.1, rate constants in table 4.1, and initial reagent concentrations used in the experiments.

The effect of ATP on the release of mantADP is apparent, as higher concentrations result in progressively more rapid signal. The upper trace represents the release of the fluorescent product from the kinesin-mantADP complex after rapid mixing with ATP in the absence of microtubules, while each additional trace from top to bottom was generated using the next ATP concentration in the series. Each trace was normalized to its initial signal intensity, and shifted along the x-axis to account for an instrument dead time of 2.0 milliseconds, and these operations are expected to affect neither apparent rate constants nor phase amplitude ratios.

The fluorescence decay data shown in figure 4.6 (solid lines) have several features that are distinct from the corresponding data for the wild-type enzyme shown in figure 3.10. First, data for mantADP dissociation in the absence of microtubules was included in figure 4.6 (upper trace) in order to accommodate the microtubule-independent release of the nucleotide that might take place during the lengthier period of fluorescence decay. This effect was not due to photobleaching, since its decay rate was independent of incident light intensity, and physical interruption of the light source during data collection had no effect on the extent of decay (data not shown). Instead, this represents mantADP release from the KHC407A-N256K dimer in the absence of microtubules. A single exponential curve fit to this data had a rate constant of $0.097 \pm 0.001\ s^{-1}$. This is substantially faster than the rate of [α^{32}P]ADP release ($0.014\ s^{-1}$) determined by the active site titration assay (figure 4.1). This may be attributable to the difference in release rates from the protein of ADP and mantADP.

The N256K data does not show the same reversal of fluorescence decay that is apparent for the wild type ~0.5 seconds after mixing (fgure 3.10). It is possible that a similar reversal might have been observed in the N256K data had collection continued long enough. The reversal apparent in figure 3.10 was attributed to rebinding of

mantADP subsequent to ATP depletion, and this effect may be less pronounced in the mutant.

A fitting of simulated data was performed using KINSIM, and a set of best-fit simulations is depicted in figure 4.6 (dashed lines). Scheme 4.1 shows part of the reaction used to generate the simulated data, and rate constants in table 4.1 provided a best fit to the data. Also shown in table 4.1 are the rate constants obtained by global fitting for the KHC407A wild-type enzyme. The fit using the reaction in scheme 4.1 was improved by adding two microtubule-independent mantADP release steps (not shown), which permitted the release of both bound mantADP molecules from free kinesin in succession. Both rate constants converged to ~0.1 s^{-1} in the fitting procedure, and are represented by the entry for step 6 in table 4.1.

Comparison between the rate constants estimated for KHC407A-N256K and the wild-type enzyme suggest that the primary effect of the N256K mutation is to reduce the apparent rate constant governing the release of the hydrolyzed nucleotide. This effect is consistent with the effect of the Kar3 N650K mutation, which caused no defect in the affinity of the motor for microtubules, save that of its modulation by ATP binding. The rate constant governing microtubule association (step 1) appears unchanged in the fitting, as does the rate constant for the dissociation reaction. The association rate constant determined by turbidity measurements was similar, at 4.3 $\mu M^{-1}s^{-1}$. Similarly, ATP binding to both the mutant and wild-type enzymes appears to obey similar kinetics (step 3). Examination of mantATP binding to the mutant provides a rate constant of 7 $\mu M^{-1}s^{-1}$, 4 times faster than that determined in the simulation described here. This may be an effect of the different binding kinetics of the two substrates, or of the different analytical techniques used in the experiments.

Scheme 4.1: *Release of (mant)ADP by kinesin-microtubule complex after mixing with microtubules and ATP*

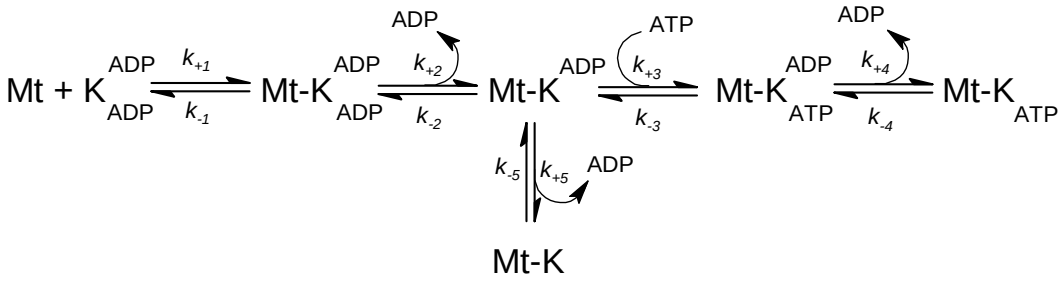

Table 4.1: *Rate constants for ATP hydrolysis and ADP release by KHC407A-N256K and wild type.* Rate constants for the N256K mutant were determined by global fitting to data shown in figure 4.6 using reaction in scheme 4.1. Step 6 represents the microtubule independent release of mantADP from free kinesin, not depicted in scheme 4.1

	KHC407A-N256K		**KHC407A Wt**	
Step	***k*+**	***k*-**	***k*+**	***k*-**
1	6.1 $\mu M^{-1}s^{-1}$	7.0 s^{-1}	7.8 $\mu M^{-1}s^{-1}$	9.3 s^{-1}
2	2.3 s^{-1}	-	>3000 s^{-1}	42.9 $\mu M^{-1}s^{-1}$
3	0.8 $\mu M^{-1}s^{-1}$	100 s^{-1}	1.7 $\mu M^{-1}s^{-1}$	18.4 s^{-1}
4	1.8 s^{-1}	-	>3000 s^{-1}	33.2 $\mu M^{-1}s^{-1}$
5	0.4 s^{-1}	-	1 s^{-1}	-
6	1 s^{-1}	-	-	-

DISCUSSION

The kinetics of ATP hydrolysis and microtubule binding by the N256K mutant of KHC407A have been examined. The data collected suggest that the primary defect caused by the mutation is in the release of the hydrolyzed nucleotide product, stimulated by microtubule binding. The fluorescence change observed due to the release of mantADP from the mutant motor upon binding to microtubules plus varying concentrations of ATP were consistent with a model in which the rate constant governing mantADP release had been diminished ~1,500-fold compared with that of the wild-type enzyme (table 4.1). ATP binding is likely to be unaffected, as indicated by the results of mantATP binding experiments, as is microtubule binding, as judged by the results of turbidity analysis. These results are consistent with those obtained for the N650K mutant of the minus-end directed motor Kar3 [62].

Residue N650 of Kar3 falls within the α4 helix of the motor [64]. The corresponding residue in the *Drosophila* Ncd motor, N600, appears to fall within loop L-11, just N-terminal to the α4 helix. In the crystal structure of the dimeric rat conventional kinesin, N256 is at the N-terminus of α4, and defines the boundary between the helix and a disordered loop [19]. The α4-L-11 domain appears to play a significant role in the communication of nucleotide phosphorylation state to other domains within the motor, for example, the microtubule-binding region. Evidence for such a role for helix α4 is strongest in the crystal structures of myosin, crystallized in ADP, ATP-like, and nucleotide-free states [69;142;143]. Finally, crystal structures of Kif1 in the ADP and ATP-like states suggest that hydrolysis of ATP is accompanied by a recruitment by helix α4 of ~10 residues from loop L11 [67]. Residue N256 in rat conventional kinesin is solvent-exposed. The replacement of asparagine by lysine introduces a basic side-chain

in lieu of a neutral hydrophilic one. It is unclear from the crystal structure what, if any, salt bridges that lysine may participate in at this position. Nevertheless, it is clear from the results of these experiments that the N256K mutation in rat conventional kinesin has a similar effect on the kinetics of the motor as does the N650K mutation in Kar3 and N600K in Ncd.

The results of this set of experiments suggest that the affinity for bound nucleotide by the active site is modulated by events occurring elsewhere in the motor mechanism. ATP binding affinity of the nucleotide binding site is unaffected by the N256K mutation, and proceeds with wild-type kinetics (step 3, scheme 4.2). Similarly, kinesin-microtubule affinity appears to be unaffected (step 1). The slow release of the hydrolysis product ADP by the mutant motor suggests that a mechanism for toggling the active site between "high affinity" and "low affinity" states has been impaired by the N256K mutation, such that bound nucleotide is released slowly regardless of whether it is in the triphosphate or diphosphate state. Scheme 4.2 illustrates a model in which the release of ADP from each motor domain immediately follows the attachment of that domain to the microtubule track. Thus, although only the second ADP release (step 4) is dependent on ATP binding, both presumably require communication between the microtubule binding domain and the nucleotide binding site, and the mechanical coupling between the two is a candidate for that which is directly impaired by the N256K mutation. It is not known what effect the mutation has on the rate constant for ATP hydrolysis (step 5), although any impairment in this step would not affect these conclusions.

Scheme 4.2: *Proposed ATP hydrolysis pathway of conventional kinesin associated with microtubule-dependent movement*

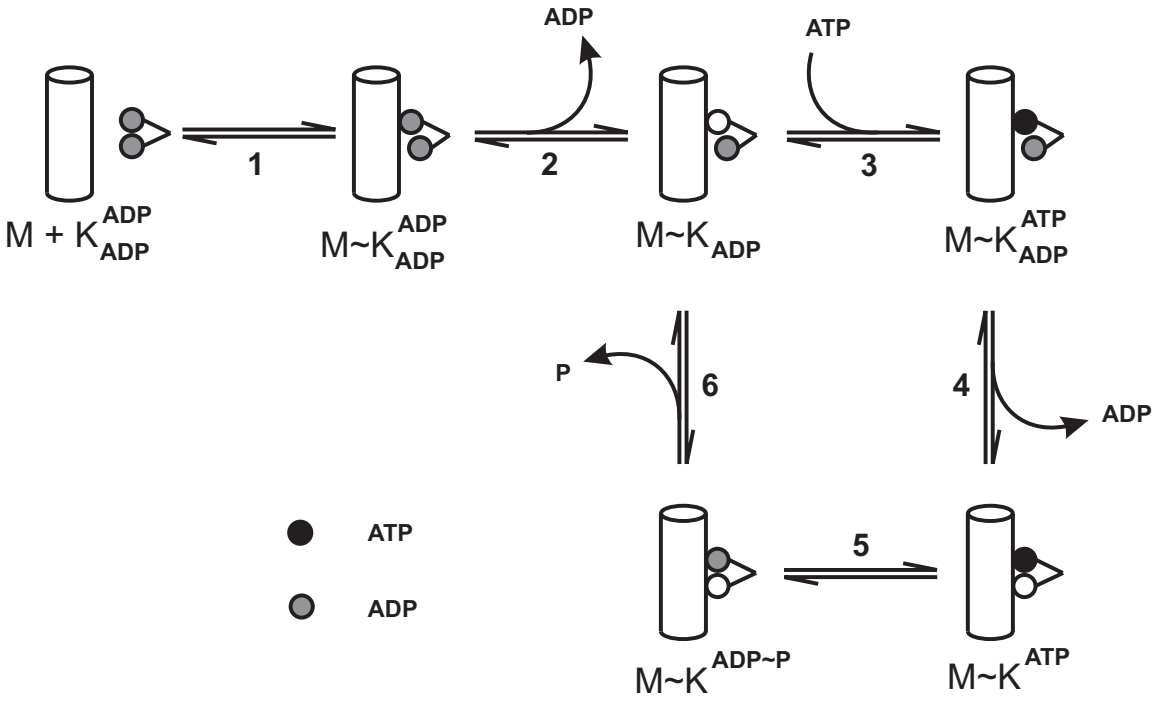

CHAPTER 5

Analysis of Switch I and II Mutants

INTRODUCTION

Conventional kinesin is a microtubule motor responsible for the anterograde transport of vesicles and organelles in neurons [15;16]. The ATPase activity of the motor is tightly coupled with movement, with the motor taking one 8 nm step along the microtubule for each ATP hydrolyzed [112-115]. A prevailing model describing the mechanism by which kinesin and other motor proteins achieve motility is one in which ATP binding and/or hydrolysis induces conformational changes in the protein that produce strain. Strain is relieved by subsequent conformational changes resulting in force production, which is amplified to generate a large conformational change, resulting in overall displacement of the motor along its filament [138]. The motor domain of kinesin may adopt distinct conformations that are dependent on the phosphorylation state of the nucleotide bound in its active site. Crystal structures of kinesins, as well as structurally related domains of myosin and G-proteins reveal distinct conformational states dependent on whether the active sites are occupied by ADP or an ATP analog [47;67;138;140;186], and ERP spectroscopy of spin-labeled motors supports a multiple-state hypothesis [188;189].

Crystal structures of myosin reveal three conformational states, classified as "detached" (ADP-bound), "rigor" (ATP-bound), and "near-rigor (nucleotide-free)" [141-145]. The structures show large-scale structural differences, most notably in the position of the lever arm, consistent with the delivery of a power stroke, by which the motor is able to translocate along an actin filament. Examination of myosin and kinesin crystal

structures suggests the existence of a phosphate sensor apparatus in the motor domains of kinesin and myosin, also conserved among the G-proteins. The structures participate in a switch mechanism, able to adopt two conformations depending on what, if any, nucleotide occupies the binding site. In rat conventional kinesin, switch I (residues 199-204) has the sequence NEHSSR, and switch II (residues 232-237) has the sequence DLAGSE. A third motif, the P-loop, stabilizes the α- and β-phosphates of the bound nucleotide. In myosin, a salt bridge between the conserved switch I arginine and switch II glutamate appears in the ATP-like state, in co-crystals of myosin and ATP analogs [142;143]. In the nucleotide-free and ADP-states the salt bridge is broken [68;147]. Furthermore, the nucleotide binding pockets of myosin, EF-Tu, and $p21^{ras}$ appear to undergo a conformational change in response to ATP hydrolysis that moves the conserved switch II glycine towards the conserved P-loop glycine, the ADP state is considered "open" while the ATP state is "closed", since the binding pocket appears to contract around the bound nucleotide in the closed state [133].

Rat conventional kinesin has been crystallized in the ADP state only [19], and among the structures of all kinesin-like proteins, little evidence of a two-state phosphate sensor switching mechanism can be found despite the presence of the conserved switch I and switch II sequences. The conformation of the switch domains in the ADP form of dimeric rat conventional kinesin resembles that of the myosin closed state, visible in co-crystals of myosin and ATP analogs. A salt bridge between arg204 and E237 is visible in the kinesin-ADP crystal. The conformations of the nucleotide binding pockets of the two subunits of the dimer show subtle differences. Specifically, in one subunit, a hydrogen bond appears to form between arg204 and glu200. The fact that this interaction is visible at all suggests that it may be of some importance to the mechanism of kinesin. It is

possible that the side chain of arg204 toggles between hydrogen bond interactions with glu200 on switch I and glu237 on switch II.

Analyses of kinesins containing salt-bridge mutations reveal defects in steady-state k_{cat} [66;189;190]. A *Drosophila* switch I R210A mutant was found to be defective not only in ATP hydrolysis, but microtubule detachment as well, with ATP binding and microtubule association unaffected [190]. The R210K mutant is similarly impaired in ATPase function, but microtubule detachment is restored [191]. Several studies of kinesin and myosin active sites have suggested that the salt bridge formed between switch I and switch II residues is critical in stabilizing a water molecule required in the catalysis of the ATPase reaction [134;192-194].

The experiments described in this section concern 4 mutations engineered into the phosphate sensor apparatus of KHC407A. The mutations E200A and E200D were intended to disrupt any possible electrostatic interaction between switch I glutamate 200 and switch II arginine 204. The E200D mutation deletes a methylene group from the acidic residue, but preserves the overall charge distribution of the system, whereas E200A removes the acidic residue altogether. A similar rationale was used in selecting the E237A and E237D mutations. It is important to note that only glu237, a well-conserved residue, corresponds to that residue in the myosin motor domain that forms a salt bridge with the switch II arginine; glu200 is not part of the canonical switch I sequence.

RESULTS

Active-Site Titration of KHC407A Mutants. The concentration of each preparation of KHC407A N256K was determined by active-site titration. For this assay to succeed, it must be possible to label the protein with [α^{32}P]ADP, the success of which

requires an active site capable of binding the nucleotide in the absence of microtubules, which is the case for the wild-type enzyme. The assay measures the extent of [α^{32}P]ADP release from the labeled protein as a function of time. Upon initiation of the assay, an ATP regenerating system composed of phosphocreatine kinase and phosphocreatine converts released [α^{32}P]ADP to the triphosphate form, and the ratio of diphosphate to triphosphate can be measured as a function of time [170]. The presence of unlabeled ATP prevents rebinding of [α^{32}P]ATP to kinesin, and permits the measurement of the rate of ADP dissociation, while extrapolation of the data to t = 0 permits an estimation of the concentration of bound [α^{32}P]ADP before reaction initiation. This concentration is considered to be equal to the active site concentration in the kinesin preparation.

For the mutants E200A, E200D, and E237D, an active site was discernable using the method described above. Rate constants governing ADP release in the absence of microtubules for these three mutants were accelerated compared to that of the wild type kinesin (0.0062 ± 0.0003 s^{-1}): 0.0096 ± 0.0001 s^{-1} for E200D, 0.010 ± 0.0005 s^{-1} for E200A, and 0.013 ± 0.003 s^{-1} for E237D. A similar effect was observed for the N256K mutation, which have an ADP release rate constant of 0.014 s^{-1}. The E237A mutant was unusual in that it could not be labeled with [α^{32}P]ADP, and no estimation of active-site concentration was possible using this method. This result suggested that the E237A mutation may have rendered the active site of KHC407A incapable of binding nucleotide, however, this was contradicted by subsequent experiments in which complexes between mantADP and the mutant kinesin were formed. Alternatively, the mutation may make the nucleotide-kinesin complex dissociate faster than the assay can resolve, in which case the dissociation rate constant for the complex may be substantially elevated over that of the wild-type protein.

Steady-state ATPase Activity of Kinesin Mutants. The mutant derivatives of KHC407A suffered various degrees of impairment in microtubule-stimulated ATPase activity. The initial ATP hydrolysis rates of wild-type KHC407A and the four mutants were measured in the presence of 80 μM microtubules and 1 mM ATP. Figure 5.1 compares k_{cat} values for each. The k_{cat} value for wild-type determined in this experiment is 61.8 s^{-1}, ~50% higher than that described in chapter 3. Nevertheless, it is apparent that ATP hydrolysis activity is more sensitive to mutations at residue E237 than at E200. This was expected, since the conserved E237 residue is thought to play a direct role in catalysis. The conservative replacement of this residue with an aspartate results in a >10-fold decrease in ATPase activity, while the elimination of the functional group by alanine substitution reduces ATPase activity to below the detection limits of this assay. By contrast, the two substitutions at E200 tested had mild effects on ATPase activity, and little difference between E200A and E200D were apparent in this assay.

Binding of mantATP to KHC407A-E200D and –E237D. In order to obtain an estimate of the rate constant governing the apparent second-order binding of ATP to KHC407A, a fluorescent ATP analog was used in a rapid mixing experiment, in which kinesin-microtubule complex was mixed with mantATP in the stopped-flow instrument. Excitation was at 280 nm and fluorescence detected by a photomultiplier tube fitted with a 400 nm cutoff long-wave pass filter. Fluorescence resonance energy transfer (FRET) between optically excited tryptophans in the protein and the *N*-methylanthraniloyl moiety of mantATP, and the detection of fluorescence by the stopped flow instrument provides a means by which the binding rate can be measured after mixing. Although the experiment measures the binding kinetics of a substrate analog rather than those of the substrate

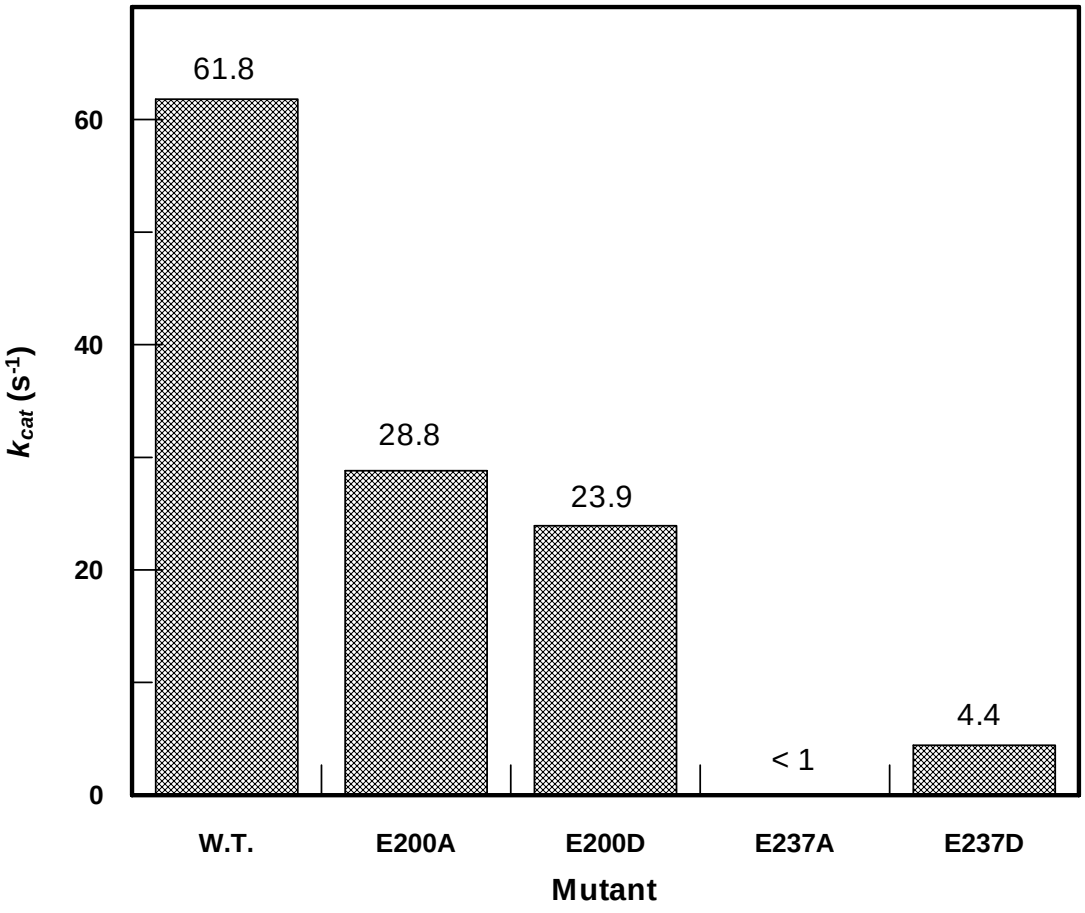

Figure 5.1: *Steady-state activities of KHC407A mutants.* Initial rate of [α^{32}P]ATP hydrolysis was determined for each kinesin variant. Initial concentrations were 0.05 μM kinesin, 1 mM [α^{32}P]ATP, and 80 μM microtubules. Acid-quenched reactions were analyzed for progress of hydrolysis, and product formation expressed as a function of reaction time.

itself, the results are considered an accurate reflection of the behavior of the enzyme towards its natural substrate [79].

After-mixing concentrations were 10 μM microtubules, 2 μM kinesin (either KHC407A-E200D or –E237D) and mantATP at varying concentrations. To traces at each substrate concentration were fit an equation containing exponential and linear terms $F = A \cdot \exp(-k_{obs}t) + k_2 t + C$. Values for k_{obs} are plotted against mantATP concentration in figure 5.2. A best-fit hyperbola of the form $k_{obs} = k_{max}[mATP]/(K_d + [mATP]) + k_{off}$ was generated to the data by nonlinear regression, and the data set is plotted in figure 5.2 along with the fit curve. The value of k_{off} was set to zero in order to maintain a non-negative value. Its true value is likely to be small in comparison with k_{max}.

Like the wild-type construct KHC407A, the E200D mutant shows mantATP binding kinetics that are saturated at increasing concentrations of the nucleotide. The observed binding rate converges to 190 s^{-1}, the value of k_{max}. The parameter for the wild type is nearly identical at 210 s^{-1}, within fitting error. The apparent K_d for the mutant is 18 ± 3 μM, smaller by half than the K_d for the wild-type construct, 37.7 ± 10.6 μM. In a rapid-binding model, in which mantATP binding is rapid and reversible, the apparent second order rate constant governing mantATP binding to the protein can be estimated by the ratio k_{max}/K_d, which in this case is 11 ± 2 $\mu M^{-1}s^{-1}$. For the wild-type enzyme, this rate constant is 5.6 $\mu M^{-1}s^{-1}$. Thus, it is apparent that the binding of mantATP to the E200D mutant follows similar kinetics as does the binding of mantATP to the wild-type enzyme.

Figure 5.3 shows the relationship between k_{obs} and mantATP concentration for the E237D mutant. The mutation causes an increase in k_{max} to almost two-fold over that of the wild-type motor. It has been discussed previously (chapter 3) that k_{max} may represent a rate-limiting step, possibly a conformational change immediately following the

formation of a kinesin-ATP "collision complex" [75;183;185]. Scheme 5.1 outlines a model for the fluorescence change

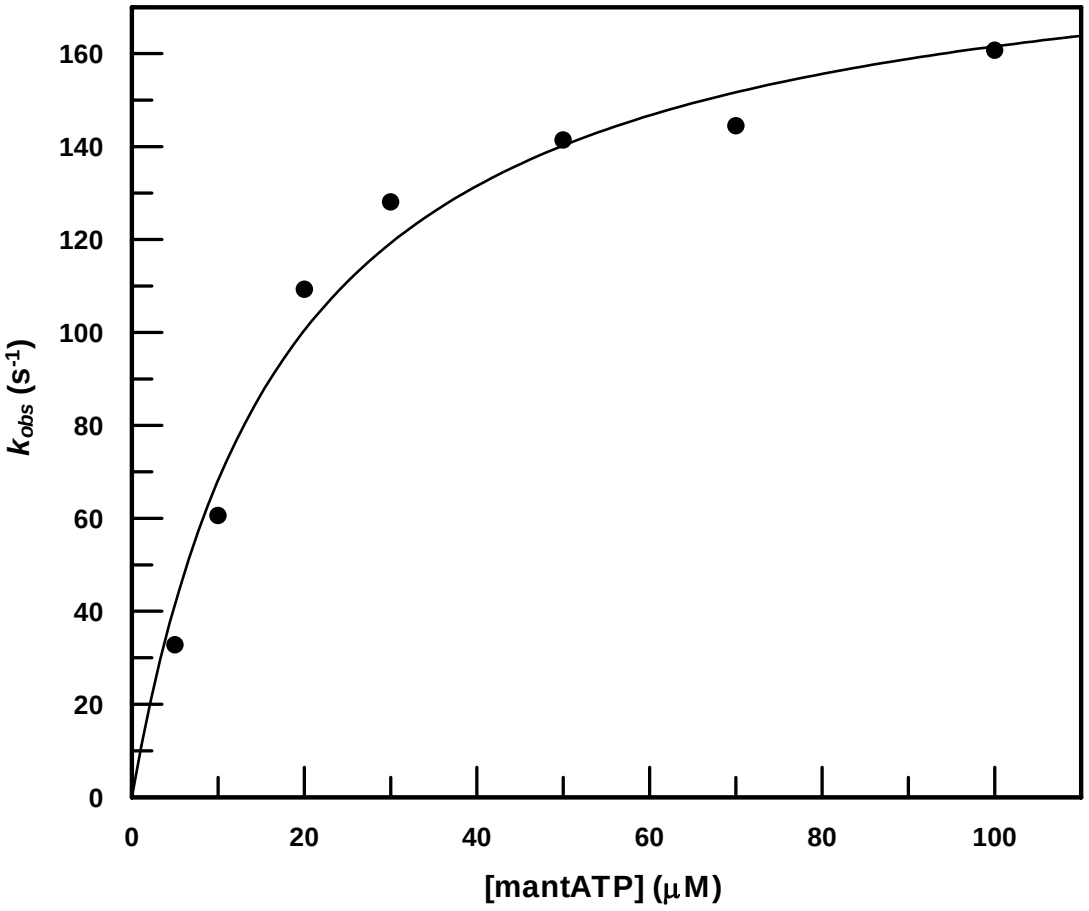

Figure 5.2: *Pre-steady-state mantATP binding to KHC407A-E200D.* 10 μM tubulin and 2 μM KHC407A-E200D were rapidly mixed in the stopped-flow instrument with mantATP at varying concentrations. Traces for each concentration were fit with $F = A \cdot \exp(-k_{obs}t) + k_2 t + C$, and values for k_{obs} plotted against mantATP concentration. The dependence was then fit to a hyperbola $k_{obs} = k_{max}[mATP]/(K_d + [mATP])$ by nonlinear regression. Parameter values obtained by fitting were $k_{max} = 190 \pm 10\ s^{-1}$ and $K_d = 18 \pm 3$ μM.

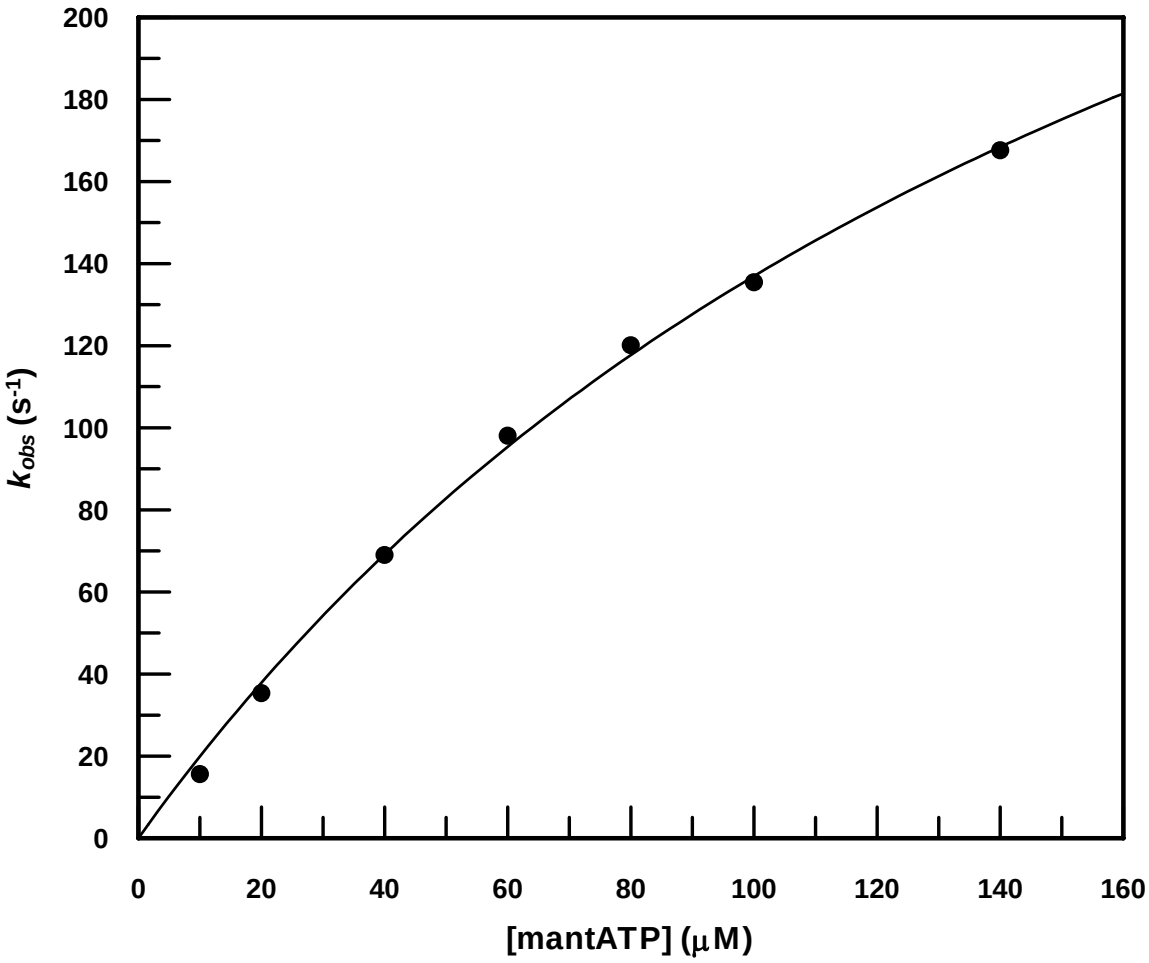

Figure 5.3: *Pre-steady-state mantATP binding to KHC407A-E237D.* 10 μM tubulin and 2 μM KHC407A-E200D were rapidly mixed in the stopped-flow instrument with mantATP at varying concentrations. Traces for each concentration were fit with $F = A \cdot \exp(-k_{obs}t) + k_2 t + C$, and values for k_{obs} plotted against mantATP concentration. The dependence was then fit to a hyperbola $k_{obs} = k_{max}[mATP]/(K_d + [mATP])$ by nonlinear regression. Parameter values obtained by fitting were $k_{max} = 400 \pm 30\ s^{-1}$ and $K_d = 190 \pm 20$ μM.

observed in kinesin upon binding to mantATP, where E*-ATP represents that conformational state observable due to its enhanced fluorescence. The E237D mutation has accelerated this first order process over what is seen in the wild-type enzyme, but the relevance of this is not immediately apparent, nor is it clear that the conformational change that converts the collision complex to one of enhanced fluorescence is relevant to the function of the enzyme. Finally, the apparent second order rate constant for mantATP binding to E237D, equal to k_{max}/K_d, provides a minimum estimate of the true rate constant for this process. This rate constant is 2.1 ± 0.3 $\mu M^{-1}s^{-1}$, not significantly diminished from that determined for the wild-type enzyme, 5.6 $\mu M^{-1}s^{-1}$.

Scheme 5.1: Proposed ATP-kinesin binding pathway, in which fluorescence change accompanies internal rearrangement

Microtubule dependence of mantADP Release from KHC407A-E200D and E237D. In the absence of microtubules, conventional kinesin contains one ADP bound in each of its active sites [180]. Upon binding to microtubules, the kinesin dimer will release both ADP molecules in succession [79;92;93]. The rate at which the fluorescent analog mantADP is released from KHC407A upon binding to microtubules in the presence of a near-saturating concentration of ATP was examined using the stopped-flow apparatus. Kinesin-mantADP complex was formed and rapidly mixed in the stopped-flow instrument with microtubules at concentrations from 10 to 120 μM. Fluorescence

decay accompanied the release of the nucleotide from its binding site. For each trace, a double exponential curve $F = A_1 \cdot \exp(-k_1 t) + A_2 \cdot \exp(-k_2 t) + C$ was generated by nonlinear regression, and two decay rates k_1 and k_2 extracted.

Figure 5.4 shows the fast-phase rates plotted against microtubule concentration for the E200D mutant. The data fit to a hyperbola $k_{obs} = k_{max}[Mt]/(K_{50\text{-}Mt} + [Mt]) + k_{off}$ with the value of k_{off} set to zero, and suggest an upper limit on the rate of mantADP release of 230 s^{-1}. This contrasts with the wild-type form of KHC407A, whose maximum mantADP release rate was not closely approached at microtubule concentrations up to 80 μM. The ratio $k_{max}/K_{50\text{-}Mt}$ estimates the apparent second order rate constant for microtubule binding by the mutant, 13 ± 0.2 $\mu M^{-1}s^{-1}$, almost 5-fold higher than that for wild-type KHC407A (2.9 $\mu M^{-1}s^{-1}$).

The rates of mantADP release from KHC407A-E237D were also measured, and fast-phase data are shown in figure 5.5. As with the wild-type enzyme, values of k_{obs} for this mutant do not appear to converge within the range of microtubule concentrations tested, but instead showed a linear relationship to the independent variable. The gradient of the linear fit, 0.9 ± 0.1 $\mu M^{-1}s^{-1}$, gives an estimate of the apparent second order rate constant governing the binding of the mutant kinesin to microtubules, and is comparable to the value obtained for the wild-type enzyme under similar conditions. Hence, the E237D mutation does not appear to have a significant effect on microtubule binding.

ATP dependence of mantADP Release from KHC407A-E200D and E237D. In the alternating-site model of conventional kinesin motility, two ADP release events are predicted to occur after the kinesin binds to microtubules [79;92;93]. In the experiment described in this section, the ATP dependence of mantADP release is examined. KHC407-E200D-mantADP complex was formed by mixing the two components to

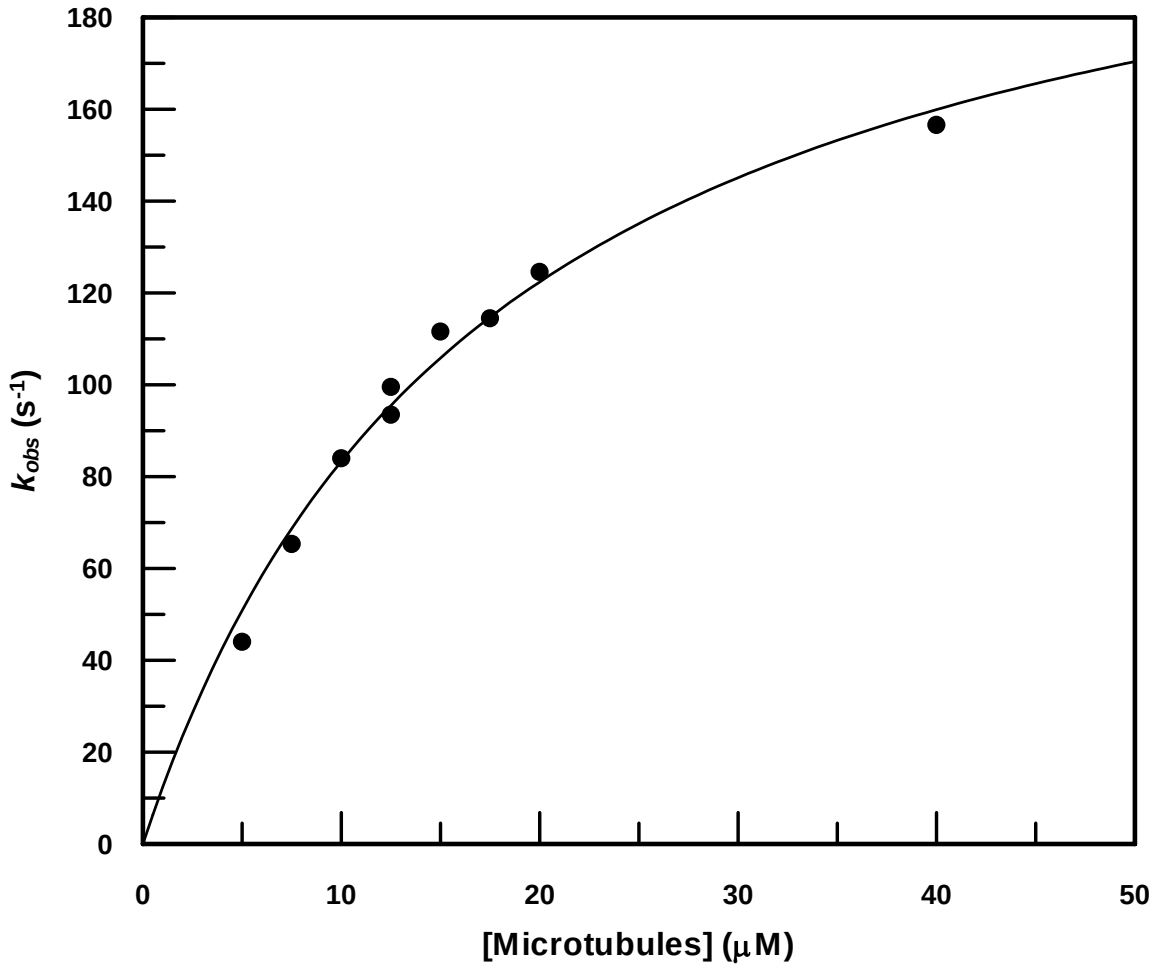

Figure 5.4: *Pre-steady-state release of mantADP from KHC407A-E200D.* Fluorescence decay from kinesin-mantADP complex (1 μM kinesin, 2 μM mantADP) upon rapid mixing with microtubules (5-40 μM) plus ATP (1 mM) was measured. Fitting of a double-exponential curve to data gave fast- and slow-phase rates of fluorescence decay at each microtubule concentration. Fast-phase rates are plotted along with a best-fit hyperbola. Fitting provides estimates of k_{max} at 230 ± 13 s^{-1} and $K_{50\text{-}Mt}$ of 18 ± 2 μM.

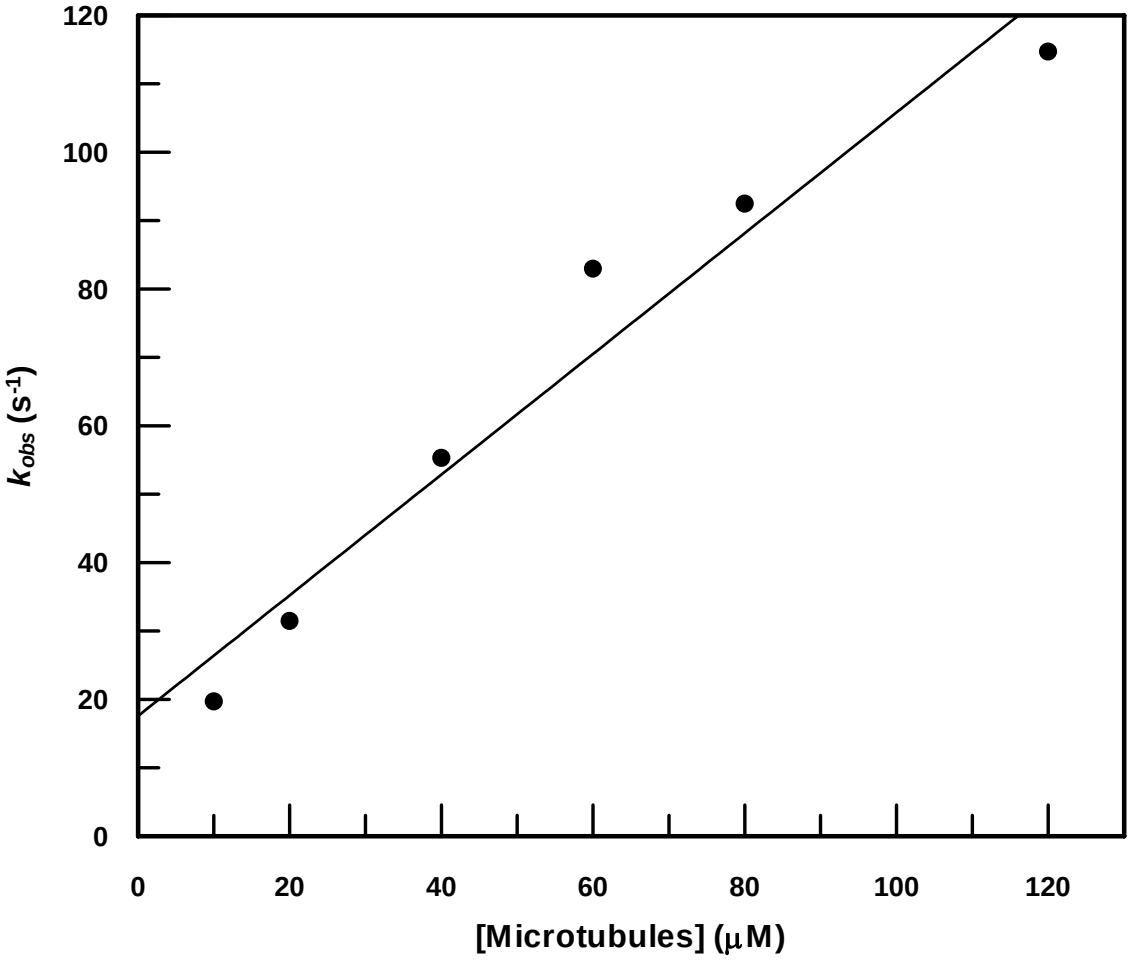

Figure 5.5: *Pre-steady-state release of mantADP from KHC407A-E237D.* Fluorescence decay from kinesin-mantADP complex (1 μM kinesin, 2 μM mantADP) upon rapid mixing with microtubules (10-120 μM) plus ATP (1 mM) was measured. Fitting of a double-exponential curve to data gave fast- and slow-phase rates of fluorescence decay at each microtubule concentration. Fast-phase rates shown in the graph fit a linear model with gradient of 0.9 ± 0.1 $\mu M^{-1}s^{-1}$, representing the apparent second order rate constant for kinesin-microtubule binding. A y-intercept of 18 ± 6 μM provides an estimate of the dissociation rate constant.

concentrations of 2 μM enzyme (by active-site titration) and 4 μM mantATP, and allowing the enzyme-substrate mixture to come to equilibrium. The complex was then rapidly mixed with microtubules (20 μM) plus nucleotide (ATP at 1, 2, 4, 7.5, 12.5, 17.5, and 22.5 μM, or ADP at 10 μM) in the stopped-flow instrument, and the fluorescence of the mixture monitored. Direct excitation of the fluorophore was accomplished using light at 360 nm, and the fluorescence output was measured through a 400 nm cutoff long-wave pass filter.

Figure 5.6 shows fluorescent traces (solid lines) from this experiment. A fit of the data with curves simulated using KINSIM are also plotted (dashed lines). Fitting was accomplished using the reaction in scheme 5.2, similar to that used for the fitting of mantADP release data for the wild-type enzyme. The uppermost trace represents mixing in the presence of 10 μM ADP, evaluated in simulations as the absence of any nucleotide. ADP was included here in order to minimize rebinding of mantADP once released.

Scheme 5.2: *Release of (mant)ADP by kinesin-microtubule complex after mixing with microtubules and ATP*

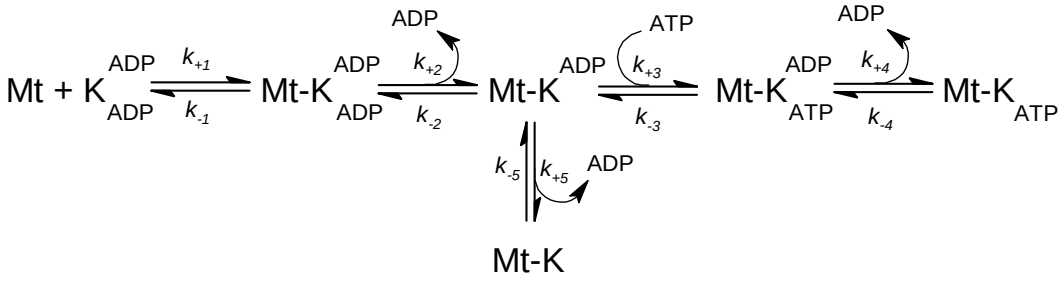

The release of mantADP from KHC407A-E237D was examined in the same fashion, with nucleotide concentrations tested at 1, 2, 4, 7.5, 12.5, 17.5, and 22.5 μM ATP and 10 μM ADP (figure 5.7). One feature worth noting in these two sets of data is

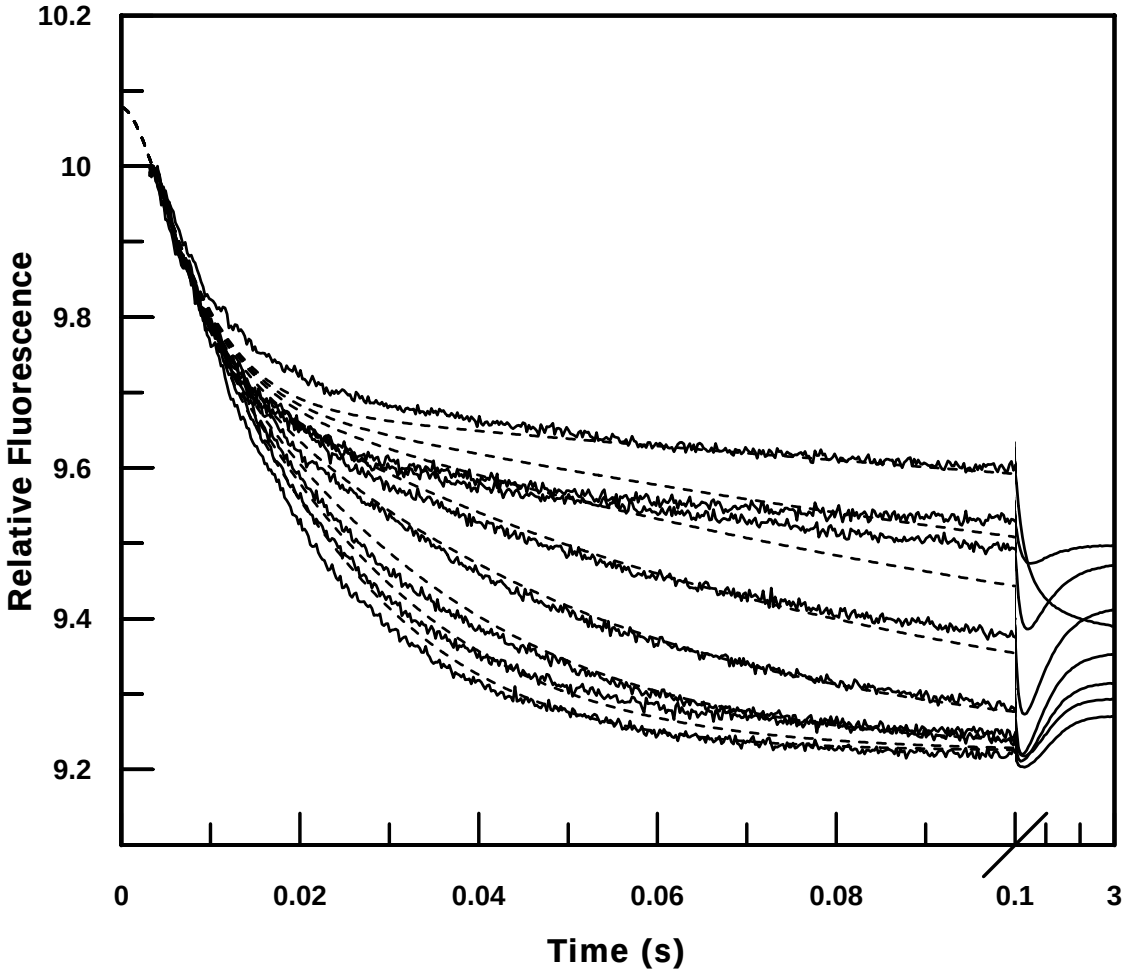

Figure 5.6: *ATP dependence of pre-steady-state release of mantADP from KHC407A-E200D.* Kinesin-mantADP complex was rapidly mixed with microtubules plus ATP or ADP in the stopped-flow instrument (1 μM kinesin, 2 μM mantADP, 16 μM microtubules plus nucleotide). Nucleotide concentrations were (top trace to bottom) 10 μM ADP, 1, 2, 4, 7.5, 12.5, 17.5, and 22.5 μM ATP. Solid lines are fluorescence traces, dashed lines are KINSIM simulations based on mechanism shown in scheme 5.2 and rate constants in table 5.1

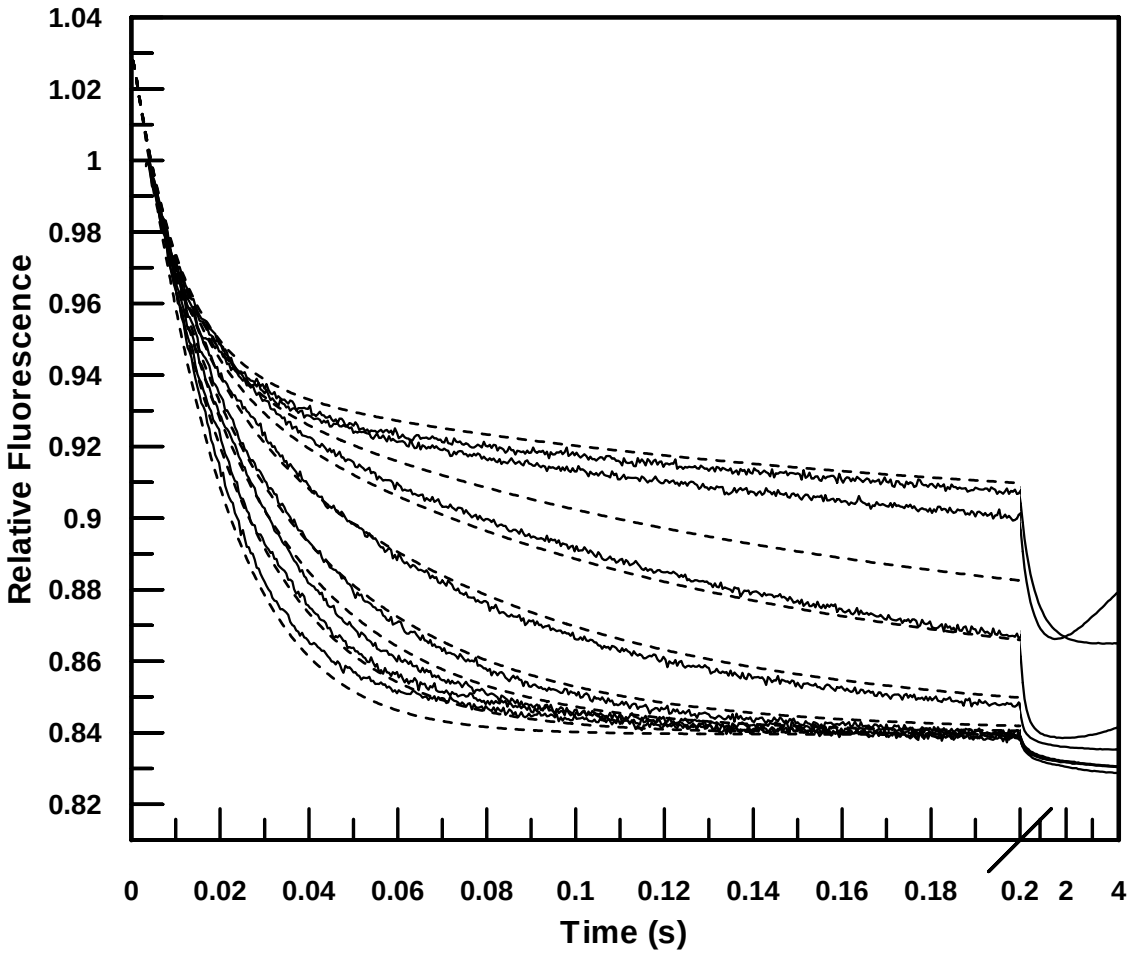

Figure 5.7: *ATP dependence of pre-steady-state release of mantADP from KHC407A-E237D.* Kinesin-mantADP complex was rapidly mixed with microtubules plus ATP or ADP in the stopped-flow instrument (1 μM kinesin, 2 μM mantADP, 16 μM microtubules plus nucleotide). Nucleotide concentrations were (top trace to bottom) 10 μM ADP, 1, 2, 4, 7.5, 12.5, 17.5, and 22.5 μM ATP. Solid lines are fluorescence traces, dashed lines are KINSIM simulations based on mechanism shown in scheme 5.2 and rate constants in table 5.1.

the reversal of fluorescence decay taking place after 0.1 second in each ATP trace in for the E200D mutant. This behavior is similar to that observed for the wild-type enzyme (figure 3.10) but absent in the E237D data. The reversal is likely to represent the rebinding of mantADP as ATP becomes exhausted and/or ADP accumulates as the reaction progresses. One possible explanation for the failure of the E237D data to show this reversal is the slow hydrolysis rate for the mutant enzyme (k_{cat} = 4.4 s^{-1}) versus the wild-type (62 s^{-1}), suggesting that the E237D mutant.

The fluorescence data for both E200D and E237D mutants fit by simulation of the reaction shown in scheme 5.2, similar to that used for kinetic simulations for the wild-type enzyme, and rate constants generating best-fit curves obtained (table 5.1). The kinetics of the observed reaction are similar to those of the wild-type except that the rate constants governing mantADP release (steps 2 and 4) are at least an order of magnitude smaller than they are in the wild-type enzyme. By contrast, the rate constants for the E237D mutant reveal no obvious defect in the kinetics of the mutant. It is difficult to explain based on these data alone why k_{cat} for the E237D mutant is so much lower than that of the wild-type.

ATP dependence of mantADP Release from KHC407A-E237A. The non-conservative switch II mutation E237A was prepared in KHC407A. Release of mantADP from this mutant after rapid mixing with microtubules plus ATP at various concentrations was tested, and the fluorescence traces are shown in figure 5.8. Fitting of kinetic simulations to the data provided estimates of rate constants, which are summarized in table 5.2. Corresponding estimates for KHC407A-E237D are also shown for comparison. The E237A mutation resulted in a kinesin that could not be assayed by active-site titration, as discussed previously, since no bound [α^{32}P]ADP could be

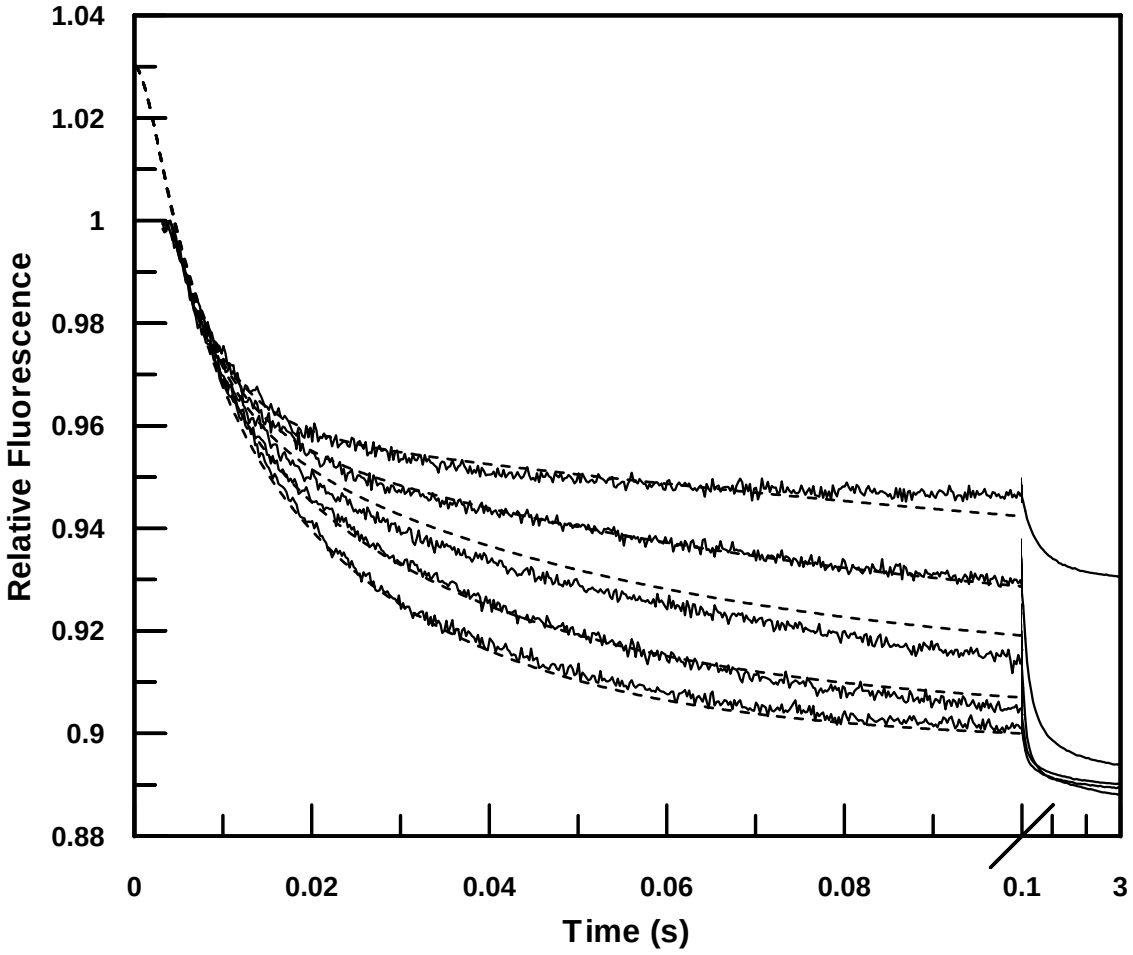

Figure 5.8: *ATP dependence of pre-steady-state release of mantADP from KHC407A-E237A.* Kinesin-mantADP complex was rapidly mixed with microtubules plus ATP or ADP in the stopped-flow instrument (1 μM kinesin, 2 μM mantADP, 16 μM microtubules plus nucleotide). Nucleotide concentrations were (top trace to bottom) 5 μM ADP, 2.5, 5, 10, and 15 μM ATP. Solid lines are fluorescence traces, dashed lines are KINSIM simulations based on mechanism shown in scheme 5.2 and rate constants in table 5.2.

Table 5.1: *Rate constants obtained by global fitting to mantADP release data.* Rate constants were obtained by fitting kinetic simulations of the reaction shown in scheme 5.2 using KINSIM. Some reverse reaction rates converged to zero during the fittings and are represented with a dash.

	KHC407A-W.t.		**KHC407A-E200D**		**KHC407A-E237D**	
Step	k_{+1}	k_{-1}	k_{+1}	k_{-1}	k_{+1}	k_{-1}
1	7.8 $\mu M^{-1}s^{-1}$	9.3 s^{-1}	18 $\mu M^{-1}s^{-1}$	-	5.5 $\mu M^{-1}s^{-1}$	60 s^{-1}
2	>3000 s^{-1}	43 $\mu M^{-1}s^{-1}$	200 s^{-1}	9 $\mu M^{-1}s^{-1}$	>1000 s^{-1}	90 $\mu M^{-1}s^{-1}$
3	1.7 $\mu M^{-1}s^{-1}$	18.4 s^{-1}	3.2 $\mu M^{-1}s^{-1}$	-	2 $\mu M^{-1}s^{-1}$	10 s^{-1}
4	>3000 s^{-1}	33 $\mu M^{-1}s^{-1}$	100 s^{-1}	11 $\mu M^{-1}s^{-1}$	>1000 s^{-1}	2 $\mu M^{-1}s^{-1}$
5	1 s^{-1}	-	1.8 s^{-1}	-	3.3 s^{-1}	-

detected. The results of the mantADP release experiments described here suggest that a nucleotide-binding site is present in this mutant. They suggest that two mantADP release events are possible, and that the presence of ATP accelerates the second event, while the first is microtubule-dependent. As in the case of the E237D mutant, the detectable rate of product release from KHC407A-E237A seems to contradict the depressed steady-state microtubule-dependent ATPase activity, which was undetectable by the assay used (figure 5.1).

DISCUSSION

In the experiments described in this section, two kinesin switch II mutants in which E237, thought to participate in an electrostatic interaction with switch I R204, was replaced, were examined using steady- and transient-state kinetic methods. Substitutions of E237 with either alanine or aspartate disrupted microtubule-dependent ATP hydrolysis by at least an order of magnitude, while substitutions at E200 were found to be less disruptive to ATPase activity. Both E200 and E237 reside within the phosphate sensor apparatus of the kinesin nucleotide-binding site, and have the capacity to form a salt-bridge with R204. The E237-R204 salt bridge is though to be necessary for ATP hydrolysis, and may form only in the presence of ATP, disengaging only after hydrolysis has occurred [47;138;186].

The disruption of the R204-E237 salt bridge with the E237D mutation reduced steady-state ATPase activity by tenfold, and the elimination of the acidic group with the mutation E237A reduced k_{cat} to nearly undetectable levels. The latter mutation may have rendered the nucleotide binding pocket catalytically inactive, since the salt bridge formed between switch I R204 and switch II E237 residues may be critical in stabilizing a water molecule required in the catalysis of the ATPase reaction [134;192-194]. Neither

mutation seems to have affected the ability of the binding pocket to bind nucleotide, since both mutants are capable of binding mantADP, and releasing it upon interaction with microtubules. Fitting of simulated data to fluorescence traces obtained from mantADP dissociation experiments suggest that the E237A mutation may be somewhat impaired in ADP release compared with E237D.

A different picture concerning the role of the E200 residue emerges from kinetic studies of E200A and E200D. The mutations do not affect steady-state ATP hydrolysis rates appreciably, and it is likely that whatever role played by the possible salt-bridge between E200 and R204 is minimal. Nevertheless, the E200D mutation exhibited a reduction in its mantADP release rate, suggesting that the residue in question participates in the destabilization of the kinesin-ADP complex during the motile cycle.

CHAPTER 6

Summary and Future Directions

Conventional kinesin is a dimeric, microtubule-dependent molecular motor that hydrolyzes ATP for each 8 nm step it takes towards the plus end of the microtubule filament to which it is bound [112;113]. The movement is processive, meaning that it remains bound to the microtubule during motility without dissociating, a process that requires at least one motor domain of the dimer to remain bound to the microtubule at all times [74-76]. This behavior requires a coordination between the two domains, as well as precise timing of microtubule binding, ATP hydrolysis, and product release.

Crystallographic studies of the motor domains of kinesin and kinesin-like proteins, as well as of structurally similar domains of myosin and G-proteins, has suggested the presence of mechanical coupling between events occurring at the nucleotide binding pocket and the site of microtubule interaction [133]. Specifically, two structures making contact with the gamma-phosphate of bound ATP are thought to mediate the conveyance of phosphorylation-state information from the binding site to other domains within the motor, and vice versa. In the experiments described in the previous chapters, mutations were introduced into the gamma-phosphate sensor apparatus, and kinetic analysis used to evaluate the effects of each mutation.

Analysis of the Wild-type Motor

A 407 residue N-terminal truncation of rat conventional kinesin was expressed in *E. coli*, and purified by ion-exchange chromatography. Sedimentation equilibrium experiments showed that the truncated molecule dimerizes in solution, with a K_d of 46

nM, consistent with a previously reported value determined for an N-terminal truncation of *Drosophila* conventional kinesin [21]. This experiment was done to verify that a length of the neck region sufficient for dimerization had been expressed. Steady-state activity assays and active-site titration confirmed the several expected properties of the protein: First, it has an active site capable of binding and hydrolyzing ATP in the absence of microtubules, and that in the absence of microtubules, this site is occupied by the product of hydrolysis. Second, the rate of ATPase activity by the motor is stimulated >1000-fold by microtubules. These results confirmed the catalytic properties expected from a kinesin.

Using the fluorescent nucleotide analogs mantATP and mantADP, which exhibit a fluorescence that is quenched in aqueous solution, and maximized in the hydrophobic microenvironment within the active site, nucleotide binding and dissociation could be probed. The stopped-flow instrument enabled the rapid mixing of reaction components, and subsequent monitoring of fluorescence changes at millisecond time scales. This technique, coupled with modeling of the motile cycle of the protein, made it possible to extract rate constants for substrate binding and product release from fluorescence data. Examination of the rates of mantADP release from the motor upon its binding to microtubules in the presence of ATP provided estimates of the rate constants governing ADP release; and by varying either microtubule or ATP concentrations, the response of mantADP release rate to changes in each variable could be determined. The response of mantADP release rate to increasing microtubule concentrations suggested rate constants governing kinesin-microtubule binding and dissociation; varying ATP generated traces from which information about ATP and dissociation could be extracted.

Kinesin-microtubule association and dissociation was also examined using a turbidity assay, which exploited a non-fluorescent optical change that accompanies the

reaction following mixing of the two components. The rate constants measured using this assay supported the results obtained from mantADP dissociation studies, and were consistent with them. This assay had the advantage that the step in question was isolated from subsequent steps by the optical measurement technique, to which steps subsequent to the initial binding step are thought to be invisible.

The optical traces from turbidity assays and mantADP dissociation experiments were found to be fit best by double-exponential models, which provided unexpected difficulties in the interpretation of the acquired data. In the turbidity assays, fast-phase rates were plotted against microtubule concentration and fit to a linear model, the slope and y-intercept of which provided estimates of the rate constants for association and dissociation, respectively; no interpretation of the slow phase data is made. Similarly, in mantADP release experiments where microtubule concentration was varied, both slow and fast phase rates were determined, but only the fast-phase data were responsive to the independent variable, the slow-phase data being essentially invariable. Thus, these two experiments provided, in addition to interpretable data, some information for which no interpretation was possible. While the slow-phase data may be represent experimental artifact, or else optical effects irrelevant to motor kinetics, it is possible that are relevant to the motile cycle.

Measurements of mantADP release from kinesin triggered by binding to microtubules in the presence of varying concentrations of ATP generated a series of traces that were best interpreted by fitting of simulated data rather than to exponential models. This was due to the complexity of the proposed enzymatic pathway, which made whatever simplifying assumptions that would have been required for fitting of analytic functions unrealistic. The KINSIM software package proved useful in determining rate constants that provided a best-fit set of simulated data.

Phosphate release kinetics were monitored using a fluorescent reporter consisting of the *E. coli* phosphate binding protein, to which was covalently attached a fluorophore in such a manner that the conformational change resulting from phosphate binding to the protein caused an increase in the fluorescence of the molecule. The release of phosphate is likely to be the rate-limiting step in the motile cycle.

Assembly of the rate constants governing the various steps in kinesin ATPase activity suggest that one important difference between rat and *Drosophila* conventional kinesin lies in the rate at which ADP is released during motility. For the *Drosophila* protein, the rate constants for both release events are ~300 s^{-1}; in rat kinesin these rates may be accelerated 10-fold over those of the *Drosophila* enzyme. The steady-state rate of rat kinesin is only twice that of its *Drosophila* counterpart, and the relationship to the dramatically improved rate of product release is not known.

Analysis of the N256K Mutant

A mutation that decoupled ATPase activity in the kinesin-like protein Kar3 from its microtubule binding function was identified in a yeast suppressor screen [62;187]. The Kar3-N650K mutant was able to hydrolyze ATP in the absence of microtubules at wild-type rates and was also able to bind microtubules. However, the mutant failed to demonstrate the microtubule-stimulated ATPase activity seen in the wild-type enzyme. This mutation falls in the α4 helix, just N-terminal to switch II of the gamma-phosphate sensor apparatus. The mutated residue is not believed to be directly involved in either microtubule or nucleotide interaction, and is instead thought to fall within a structure that provides mechanical coupling between the two sites. The structure is the α4 helix, just N-terminal to the switch II element of the gamma-phosphate sensor apparatus within the active site of the motor.

The homologous residue in rat kinesin was engineered into KHC407A to generate KHC407A-N256K. The resulting motor had a steady-state microtubule-stimulated ATPase rate that was reduced below that of wild-type by a factor of 10. ATP binding is not impaired, as evidenced directly by measurements of mantATP binding, as well as indirectly by simulation of mantADP release data. The binding of the mutant kinesin to microtubules is similarly unaffected. Instead, the primary defect caused by the N256K mutation appears to reside in the rate at which ADP is released, both after initial kinesin-microtubule interaction and after ATP binding. It is possible that the mutation affects the mechanical linkage between the active site and other domains within the motor, and prevents the appropriate conformational change required for the release of the hydrolyzed nucleotide from being transmitted to those structures that participate in product release.

Analysis of E200D and E200A

The secondary structures comprising the active site of kinesin include two elements that are thought to mediate the different conformational changes that occur in kinesin when ATP binds, is hydrolyzed, and ADP is released. These structures, called Switch I and Switch II, are conserved among the members of the kinesin superfamily, as well as within the myosins and G-proteins [142;143]. Central to the function of this apparatus is a salt bridge between a conserved switch I arginine and switch II glutamate that appears to be formed transiently in the ATP-like state of myosin. The corresponding residues in rat conventional kinesin, R204 and E237, appear to participate in the predicted electrostatic interaction only in one of the subunits of the crystal structure of the dimer [19]. In the other subunit, R204 is not associated with E237, but instead is positioned such that a salt bridge with the neighboring residue E200 is suggested. Two

mutants, E200D and E200A, were prepared and examined using rapid mixing kinetic techniques.

The effects of these mutations on ATPase activity were minor, reducing k_{cat} by about half in each case. The fact that the elimination of the carboxylic acid functional group by the E200A mutation had little effect beyond that brought about by E200D suggested that the formation of an R204-E200 salt bridge is of little consequence to kinesin function as measured in the steady-state ATPase assay. Nevertheless, in mantADP dissociation experiments, a ~10-fold reduction in the rate constant for mantADP dissociation below that for the wild-type was observed for the E200D mutant. It is possible that the mutation may cause a defect in some aspect of overall kinesin function that these kinetic experiments are not designed to detect, such as in force generation or regulation.

Analysis of E237D and E237A

Mutations at the conserved residue E237 nearly abolished steady-state ATPase activity. However, the rate constants estimated for microtubule binding, ATP binding and ADP release were nearly identical to those for wild-type in the case of E237D, while only the rate constants governing ADP release were reduced in E237A. This suggests that the kinetic defect caused by mutations at E237 affect a portion of the motility mechanism not detected in the assays used here. The rates of hydrolysis and phosphate release were not evaluated for these mutants, but it would not be surprising if either were found to be impaired. A mutation converting Switch I arginine to alanine in *Drosophila* conventional kinesin was found to be defective in ATP hydrolysis, as well as in microtubule detachment [190]. This mutation presumably disrupted the salt bridge between Switch I and Switch II, interfering with mechanical coupling between

microtubule- and ATP-binding elements in the motor. It is likely, therefore, that the E237A mutation may have a similar effect, but this was not tested.

Future Directions

For a more complete understanding of the mutants examined here, a rigorous examination of the hydrolysis step should be undertaken. Particularly in the case of the E237D mutant, whose rate constants for ATP and microtubule binding, and mantADP release were almost unchanged by the mutation, it would be instructive to know how the rate of ATP hydrolysis has been affected by the mutation. An examination of this parameter would involve rapid quench flow analysis of the hydrolysis step at varying concentrations of [α^{32}P]ATP in order to retrieve a reliable estimate of the rate constant governing this step. The E237A mutant was not characterized fully, and additional transient state kinetic experiments are warranted. This mutation appeared to reduce steady-state hydrolysis activity below detectable levels, yet the binding and release of ATP, ADP and microtubules seemed largely unaffected, suggesting that the defect caused by the mutation is in a step not directly examined by the experiments described in this work.

Most intriguing in the kinetics of the wild-type enzyme was the reversal of fluorescence observed in traces resulting from mantADP dissociation from the enzyme upon mixing with microtubules. This effect was not seen in the *Drosophila* construct, and had largely disappeared from the traces obtained with the E237D mutant. This reversal may be the result of mantADP re-binding to the motor after ATP has been exhausted, but this has not been directly demonstrated, and all attempts to simulate this behavior have failed. An answer to this problem may provide additional insight into the mechanism of the motility cycle of the motor.

References

[1] Vale,R.D. (2003) The molecular motor toolbox for intracellular transport. *Cell*, **112,** 467-480.

[2] Berg,J.S., Powell,B.C., & Cheney,R.E. (2001) A millennial myosin census. *Mol. Biol. Cell*, **12,** 780-794.

[3] Sellers,J.R. (2000) Myosins: a diverse superfamily. *Biochim. Biophys. Acta*, **1496,** 3-22.

[4] Kim,A.J. & Endow,S.A. (2000) A kinesin family tree. *J. Cell Sci.*, **113 Pt 21,** 3681-3682.

[5] Vaisberg,E.A., Grissom,P.M., & McIntosh,J.R. (1996) Mammalian cells express three distinct dynein heavy chains that are localized to different cytoplasmic organelles. *J. Cell Biol.*, **133,** 831-842.

[6] Desai,A., Verma,S., Mitchison,T.J., & Walczak,C.E. (1999) Kin I kinesins are microtubule-destabilizing enzymes. *Cell*, **96,** 69-78.

[7] Hunter,A.W., Caplow,M., Coy,D.L., Hancock,W.O., Diez,S., Wordeman,L., & Howard,J. (2003) The kinesin-related protein MCAK is a microtubule depolymerase that forms an ATP-hydrolyzing complex at microtubule ends. *Mol. Cell*, **11,** 445-457.

[8] Bringmann,H., Skiniotis,G., Spilker,A., Kandels-Lewis,S., Vernos,I., & Surrey,T. (2004) A kinesin-like motor inhibits microtubule dynamic instability. *Science*, **303,** 1519-1522.

[9] Bahler,M. (2000) Are class III and class IX myosins motorized signalling molecules? *Biochim. Biophys. Acta*, **1496,** 52-59.

[10] Montell,C. & Rubin,G.M. (1988) The Drosophila ninaC locus encodes two photoreceptor cell specific proteins with domains homologous to protein kinases and the myosin heavy chain head. *Cell*, **52,** 757-772.

[11] Ng,K.P., Kambara,T., Matsuura,M., Burke,M., & Ikebe,M. (1996) Identification of myosin III as a protein kinase. *Biochemistry*, **35,** 9392-9399.

[12] Chieregatti,E., Gartner,A., Stoffler,H.E., & Bahler,M. (1998) Myr 7 is a novel myosin IX-RhoGAP expressed in rat brain. *J. Cell Sci.*, **111 (Pt 24),** 3597-3608.

[13] Muller,R.T., Honnert,U., Reinhard,J., & Bahler,M. (1997) The rat myosin myr 5 is a GTPase-activating protein for Rho in vivo: essential role of arginine 1695. *Mol. Biol. Cell*, **8,** 2039-2053.

[14] Raftopoulou,M. & Hall,A. (2004) Cell migration: Rho GTPases lead the way. *Dev. Biol.*, **265,** 23-32.

[15] Vale,R.D., Reese,T.S., & Sheetz,M.P. (1985) Identification of a novel force-generating protein, kinesin, involved in microtubule-based motility. *Cell*, **42,** 39-50.

[16] Lasek,R.J. & Brady,S.T. (1985) Attachment of transported vesicles to microtubules in axoplasm is facilitated by AMP-PNP. *Nature*, **316,** 645-647.

[17] Yang,J.T., Laymon,R.A., & Goldstein,L.S. (1989) A three-domain structure of kinesin heavy chain revealed by DNA sequence and microtubule binding analyses. *Cell*, **56,** 879-889.

[18] Vale,R.D. & Fletterick,R.J. (1997) The design plan of kinesin motors. *Annu. Rev. Cell Dev. Biol.*, **13,** 745-777.

[19] Kozielski,F., Sack,S., Marx,A., Thormahlen,M., Schonbrunn,E., Biou,V., Thompson,A., Mandelkow,E.M., & Mandelkow,E. (1997) The crystal structure of dimeric kinesin and implications for microtubule-dependent motility. *Cell*, **91,** 985-994.

[20] Moyer,M.L., Gilbert,S.P., & Johnson,K.A. (1996) Purification and characterization of two monomeric kinesin constructs. *Biochemistry*, **35,** 6321-6329.

[21] Correia,J.J., Gilbert,S.P., Moyer,M.L., & Johnson,K.A. (1995) Sedimentation studies on the kinesin motor domain constructs K401, K366, and K341. *Biochemistry*, **34,** 4898-4907.

[22] Kohn,W.D., Mant,C.T., & Hodges,R.S. (1997) Alpha-helical protein assembly motifs. *J. Biol. Chem*, **272,** 2583-2586.

[23] Morii,H., Takenawa,T., Arisaka,F., & Shimizu,T. (1997) Identification of kinesin neck region as a stable alpha-helical coiled coil and its thermodynamic characterization. *Biochemistry*, **36,** 1933-1942.

[24] Tripet,B., Vale,R.D., & Hodges,R.S. (1997) Demonstration of coiled-coil interactions within the kinesin neck region using synthetic peptides. Implications for motor activity. *J. Biol. Chem*, **272,** 8946-8956.

[25] Tripet,B. & Hodges,R.S. (2002) Helix capping interactions stabilize the N-terminus of the kinesin neck coiled-coil. *J. Struct. Biol.*, **137,** 220-235.

[26] Seeberger,C., Mandelkow,E., & Meyer,B. (2000) Conformational preferences of a synthetic 30mer peptide from the interface between the neck and stalk regions of kinesin. *Biochemistry*, **39,** 12558-12567.

[27] Grummt,M., Woehlke,G., Henningsen,U., Fuchs,S., Schleicher,M., & Schliwa,M. (1998) Importance of a flexible hinge near the motor domain in kinesin-driven motility. *EMBO J.*, **17,** 5536-5542.

[28] Hunt,A.J. & Howard,J. (1993) Kinesin swivels to permit microtubule movement in any direction. *Proc. Natl. Acad. Sci. U. S. A*, **90,** 11653-11657.

[29] Hirokawa,N., Pfister,K.K., Yorifuji,H., Wagner,M.C., Brady,S.T., & Bloom,G.S. (1989) Submolecular domains of bovine brain kinesin identified by electron microscopy and monoclonal antibody decoration. *Cell*, **56,** 867-878.

[30] Hisanaga,S., Murofushi,H., Okuhara,K., Sato,R., Masuda,Y., Sakai,H., & Hirokawa,N. (1989) The molecular structure of adrenal medulla kinesin. *Cell Motil. Cytoskeleton*, **12,** 264-272.

[31] Hackney,D.D., Levitt,J.D., & Suhan,J. (1992) Kinesin undergoes a 9 S to 6 S conformational transition. *J. Biol. Chem*, **267,** 8696-8701.

[32] Hackney,D.D. & Stock,M.F. (2000) Kinesin's IAK tail domain inhibits initial microtubule-stimulated ADP release. *Nat. Cell Biol.*, **2,** 257-260.

[33] Stock,M.F., Guerrero,J., Cobb,B., Eggers,C.T., Huang,T.G., Li,X., & Hackney,D.D. (1999) Formation of the compact confomer of kinesin requires a COOH-terminal heavy chain domain and inhibits microtubule-stimulated ATPase activity. *J. Biol. Chem*, **274,** 14617-14623.

[34] Coy,D.L., Hancock,W.O., Wagenbach,M., & Howard,J. (1999) Kinesin's tail domain is an inhibitory regulator of the motor domain. *Nat. Cell Biol.*, **1,** 288-292.

[35] Verhey,K.J., Lizotte,D.L., Abramson,T., Barenboim,L., Schnapp,B.J., & Rapoport,T.A. (1998) Light chain-dependent regulation of Kinesin's interaction with microtubules. *J. Cell Biol.*, **143,** 1053-1066.

[36] Diefenbach,R.J., Mackay,J.P., Armati,P.J., & Cunningham,A.L. (1998) The C-terminal region of the stalk domain of ubiquitous human kinesin heavy chain contains the binding site for kinesin light chain. *Biochemistry*, **37,** 16663-16670.

[37] Steinberg,G. & Schliwa,M. (1995) The Neurospora organelle motor: a distant relative of conventional kinesin with unconventional properties. *Mol. Biol. Cell*, **6,** 1605-1618.

[38] Pfister,K.K., Wagner,M.C., Stenoien,D.L., Brady,S.T., & Bloom,G.S. (1989) Monoclonal antibodies to kinesin heavy and light chains stain vesicle-like structures, but not microtubules, in cultured cells. *J. Cell Biol.*, **108,** 1453-1463.

[39] Blatch,G.L. & Lassle,M. (1999) The tetratricopeptide repeat: a structural motif mediating protein-protein interactions. *Bioessays*, **21,** 932-939.

[40] Haimo,L.T. (1995) Regulation of kinesin-directed movements. *Trends Cell Biol.*, **5,** 165-168.

[41] Morfini,G., Szebenyi,G., Elluru,R., Ratner,N., & Brady,S.T. (2002) Glycogen synthase kinase 3 phosphorylates kinesin light chains and negatively regulates kinesin-based motility. *EMBO J.*, **21,** 281-293.

[42] Andrews,P.D., Ovechkina,Y., Morrice,N., Wagenbach,M., Duncan,K., Wordeman,L., & Swedlow,J.R. (2004) Aurora B regulates MCAK at the mitotic centromere. *Dev. Cell*, **6,** 253-268.

[43] Ohi,R., Sapra,T., Howard,J., & Mitchison,T.J. (2004) Differentiation of cytoplasmic and meiotic spindle assembly MCAK functions by Aurora B-dependent phosphorylation. *Mol. Biol. Cell*, **15,** 2895-2906.

[44] Donelan,M.J., Morfini,G., Julyan,R., Sommers,S., Hays,L., Kajio,H., Briaud,I., Easom,R.A., Molkentin,J.D., Brady,S.T., & Rhodes,C.J. (2002) Ca2+-dependent dephosphorylation of kinesin heavy chain on beta-granules in pancreatic beta-cells. Implications for regulated beta-granule transport and insulin exocytosis. *J. Biol. Chem.*, **277,** 24232-24242.

[45] Kull,F.J., Sablin,E.P., Lau,R., Fletterick,R.J., & Vale,R.D. (1996) Crystal structure of the kinesin motor domain reveals a structural similarity to myosin. *Nature*, **380,** 550-555.

[46] Kull,F.J., Vale,R.D., & Fletterick,R.J. (1998) The case for a common ancestor: kinesin and myosin motor proteins and G proteins. *J. Muscle Res. Cell Motil.*, **19,** 877-886.

[47] Vale,R.D. (1996) Switches, latches, and amplifiers: common themes of G proteins and molecular motors. *J. Cell Biol.*, **135,** 291-302.

[48] Miki,H., Setou,M., Kaneshiro,K., & Hirokawa,N. (2001) All kinesin superfamily protein, KIF, genes in mouse and human. *Proc. Natl. Acad. Sci. U. S. A*, **98,** 7004-7011.

[49] Hirokawa,N. (1998) Kinesin and dynein superfamily proteins and the mechanism of organelle transport. *Science*, **279,** 519-526.

[50] Endow,S.A. (1999) Microtubule motors in spindle and chromosome motility. *Eur. J. Biochem.*, **262,** 12-18.

[51] Hunter,A.W. & Wordeman,L. (2000) How motor proteins influence microtubule polymerization dynamics. *J. Cell Sci.*, **113 Pt 24,** 4379-4389.

[52] Scholey,J.M. (2003) Intraflagellar transport. *Annu. Rev. Cell Dev. Biol.*, **19,** 423-443.

[53] Pan,J. & Snell,W.J. (2002) Kinesin-II is required for flagellar sensory transduction during fertilization in Chlamydomonas. *Mol. Biol. Cell*, **13,** 1417-1426.

[54] Sack,S., Muller,J., Marx,A., Thormahlen,M., Mandelkow,E.M., Brady,S.T., & Mandelkow,E. (1997) X-ray structure of motor and neck domains from rat brain kinesin. *Biochemistry*, **36,** 16155-16165.

[55] Sindelar,C.V., Budny,M.J., Rice,S., Naber,N., Fletterick,R., & Cooke,R. (2002) Two conformations in the human kinesin power stroke defined by X-ray crystallography and EPR spectroscopy. *Nat. Struct. Biol.*, **9,** 844-848.

[56] Endow,S.A., Henikoff,S., & Soler-Niedziela,L. (1990) Mediation of meiotic and early mitotic chromosome segregation in Drosophila by a protein related to kinesin. *Nature*, **345,** 81-83.

[57] McDonald,H.B. & Goldstein,L.S. (1990) Identification and characterization of a gene encoding a kinesin-like protein in Drosophila. *Cell*, **61,** 991-1000.

[58] Sablin,E.P., Kull,F.J., Cooke,R., Vale,R.D., & Fletterick,R.J. (1996) Crystal structure of the motor domain of the kinesin-related motor ncd. *Nature*, **380,** 555-559.

[59] McDonald,H.B., Stewart,R.J., & Goldstein,L.S. (1990) The kinesin-like ncd protein of Drosophila is a minus end-directed microtubule motor. *Cell*, **63,** 1159-1165.

[60] Sablin,E.P., Case,R.B., Dai,S.C., Hart,C.L., Ruby,A., Vale,R.D., & Fletterick,R.J. (1998) Direction determination in the minus-end-directed kinesin motor ncd. *Nature*, **395,** 813-816.

[61] Foster,K.A., Mackey,A.T., & Gilbert,S.P. (2001) A mechanistic model for Ncd directionality. *J. Biol. Chem*, **276,** 19259-19266.

[62] Song,H. & Endow,S.A. (1998) Decoupling of nucleotide- and microtubule-binding sites in a kinesin mutant. *Nature*, **396,** 587-590.

[63] Endow,S.A. & Higuchi,H. (2000) A mutant of the motor protein kinesin that moves in both directions on microtubules. *Nature*, **406,** 913-916.

[64] Gulick,A.M., Song,H., Endow,S.A., & Rayment,I. (1998) X-ray crystal structure of the yeast Kar3 motor domain complexed with Mg.ADP to 2.3 A resolution. *Biochemistry*, **37,** 1769-1776.

[65] Endow,S.A., Kang,S.J., Satterwhite,L.L., Rose,M.D., Skeen,V.P., & Salmon,E.D. (1994) Yeast Kar3 is a minus-end microtubule motor protein that destabilizes microtubules preferentially at the minus ends. *EMBO J.*, **13,** 2708-2713.

[66] Yun,M., Zhang,X., Park,C.G., Park,H.W., & Endow,S.A. (2001) A structural pathway for activation of the kinesin motor ATPase. *EMBO J.*, **20,** 2611-2618.

[67] Kikkawa,M., Sablin,E.P., Okada,Y., Yajima,H., Fletterick,R.J., & Hirokawa,N. (2001) Switch-based mechanism of kinesin motors. *Nature*, **411,** 439-445.

[68] Gulick,A.M., Bauer,C.B., Thoden,J.B., & Rayment,I. (1997) X-ray structures of the MgADP, MgATPgammaS, and MgAMPPNP complexes of the Dictyostelium discoideum myosin motor domain. *Biochemistry*, **36,** 11619-11628.

[69] Smith,C.A. & Rayment,I. (1996) X-ray structure of the magnesium(II).ADP.vanadate complex of the Dictyostelium discoideum myosin motor domain to 1.9 A resolution. *Biochemistry*, **35,** 5404-5417.

[70] Kikkawa,M., Okada,Y., & Hirokawa,N. (2000) 15 A resolution model of the monomeric kinesin motor, KIF1A. *Cell*, **100,** 241-252.

[71] Okada,Y., Yamazaki,H., Sekine-Aizawa,Y., & Hirokawa,N. (1995) The neuron-specific kinesin superfamily protein KIF1A is a unique monomeric motor for anterograde axonal transport of synaptic vesicle precursors. *Cell*, **81,** 769-780.

[72] Howard,J. (1997) Molecular motors: structural adaptations to cellular functions. *Nature*, **389,** 561-567.

[73] Dillon,P.F. & Murphy,R.A. (1982) High force development and crossbridge attachment in smooth muscle from swine carotid arteries. *Circ. Res.*, **50,** 799-804.

[74] Hackney,D.D. (1994) The rate-limiting step in microtubule-stimulated ATP hydrolysis by dimeric kinesin head domains occurs while bound to the microtubule. *J. Biol. Chem*, **269,** 16508-16511.

[75] Gilbert,S.P., Webb,M.R., Brune,M., & Johnson,K.A. (1995) Pathway of processive ATP hydrolysis by kinesin. *Nature*, **373,** 671-676.

[76] Hackney,D.D. (1995) Highly processive microtubule-stimulated ATP hydrolysis by dimeric kinesin head domains. *Nature*, **377,** 448-450.

[77] Howard,J., Hudspeth,A.J., & Vale,R.D. (1989) Movement of microtubules by single kinesin molecules. *Nature*, **342,** 154-158.

[78] Block,S.M., Goldstein,L.S., & Schnapp,B.J. (1990) Bead movement by single kinesin molecules studied with optical tweezers. *Nature*, **348,** 348-352.

[79] Moyer,M.L., Gilbert,S.P., & Johnson,K.A. (1998) Pathway of ATP hydrolysis by monomeric and dimeric kinesin. *Biochemistry*, **37,** 800-813.

[80] Huxley,A.F. & Simmons,R.M. (1971) Proposed mechanism of force generation in striated muscle. *Nature*, **233,** 533-538.

[81] Uyeda,T.Q., Kron,S.J., & Spudich,J.A. (1990) Myosin step size. Estimation from slow sliding movement of actin over low densities of heavy meromyosin. *J. Mol. Biol.*, **214,** 699-710.

[82] Molloy,J.E., Burns,J.E., Kendrick-Jones,J., Tregear,R.T., & White,D.C. (1995) Movement and force produced by a single myosin head. *Nature*, **378,** 209-212.

[83] Ishijima,A., Kojima,H., Higuchi,H., Harada,Y., Funatsu,T., & Yanagida,T. (1996) Multiple- and single-molecule analysis of the actomyosin motor by nanometer-piconewton manipulation with a microneedle: unitary steps and forces. *Biophys. J.*, **70,** 383-400.

[84] Toyoshima,Y.Y., Kron,S.J., McNally,E.M., Niebling,K.R., Toyoshima,C., & Spudich,J.A. (1987) Myosin subfragment-1 is sufficient to move actin filaments in vitro. *Nature*, **328,** 536-539.

[85] Waller,G.S., Ouyang,G., Swafford,J., Vibert,P., & Lowey,S. (1995) A minimal motor domain from chicken skeletal muscle myosin. *J. Biol. Chem*, **270,** 15348-15352.

[86] deCastro,M.J., Ho,C.H., & Stewart,R.J. (1999) Motility of dimeric ncd on a metal-chelating surfactant: evidence that ncd is not processive. *Biochemistry*, **38,** 5076-5081.

[87] Foster,K.A. & Gilbert,S.P. (2000) Kinetic studies of dimeric Ncd: evidence that Ncd is not processive. *Biochemistry*, **39,** 1784-1791.

[88] Okada,Y. & Hirokawa,N. (1999) A processive single-headed motor: kinesin superfamily protein KIF1A. *Science*, **283,** 1152-1157.

[89] Okada,Y., Higuchi,H., & Hirokawa,N. (2003) Processivity of the single-headed kinesin KIF1A through biased binding to tubulin. *Nature*, **424,** 574-577.

[90] Mehta,A.D., Rock,R.S., Rief,M., Spudich,J.A., Mooseker,M.S., & Cheney,R.E. (1999) Myosin-V is a processive actin-based motor. *Nature*, **400,** 590-593.

[91] Reck-Peterson,S.L., Provance,D.W., Jr., Mooseker,M.S., & Mercer,J.A. (2000) Class V myosins. *Biochim. Biophys. Acta*, **1496,** 36-51.

[92] Hackney,D.D. (1994) Evidence for alternating head catalysis by kinesin during microtubule-stimulated ATP hydrolysis. *Proc. Natl. Acad. Sci. U. S. A*, **91,** 6865-6869.

[93] Gilbert,S.P., Moyer,M.L., & Johnson,K.A. (1998) Alternating site mechanism of the kinesin ATPase. *Biochemistry*, **37,** 792-799.

[94] Downing,K.H. & Nogales,E. (1998) Tubulin and microtubule structure. *Curr. Opin. Cell Biol.*, **10,** 16-22.

[95] Amos,L.A. & Hirose,K. (1997) The structure of microtubule-motor complexes. *Curr. Opin. Cell Biol.*, **9,** 4-11.

[96] Wade,R.H. & Hyman,A.A. (1997) Microtubule structure and dynamics. *Curr. Opin. Cell Biol.*, **9,** 12-17.

[97] Howard,J. & Hyman,A.A. (2003) Dynamics and mechanics of the microtubule plus end. *Nature*, **422,** 753-758.

[98] Nogales,E., Wolf,S.G., Khan,I.A., Luduena,R.F., & Downing,K.H. (1995) Structure of tubulin at 6.5 A and location of the taxol-binding site. *Nature*, **375,** 424-427.

[99] Nogales,E., Wolf,S.G., & Downing,K.H. (1998) Structure of the alpha beta tubulin dimer by electron crystallography. *Nature*, **391,** 199-203.

[100] Lowe,J., Li,H., Downing,K.H., & Nogales,E. (2001) Refined structure of alpha beta-tubulin at 3.5 A resolution. *J. Mol. Biol.*, **313,** 1045-1057.

[101] Sosa,H., Hoenger,A., & Milligan,R.A. (1997) Three different approaches for calculating the three-dimensional structure of microtubules decorated with kinesin motor domains. *J. Struct. Biol.*, **118,** 149-158.

[102] Unger,V.M. (2001) Electron cryomicroscopy methods. *Curr. Opin. Struct. Biol.*, **11,** 548-554.

[103] Hoenger,A., Sablin,E.P., Vale,R.D., Fletterick,R.J., & Milligan,R.A. (1995) Three-dimensional structure of a tubulin-motor-protein complex. *Nature*, **376,** 271-274.

[104] Kikkawa,M., Ishikawa,T., Wakabayashi,T., & Hirokawa,N. (1995) Three-dimensional structure of the kinesin head-microtubule complex. *Nature*, **376,** 274-277.

[105] Hoenger,A., Thormahlen,M., Diaz-Avalos,R., Doerhoefer,M., Goldie,K.N., Muller,J., & Mandelkow,E. (2000) A new look at the microtubule binding patterns of dimeric kinesins. *J. Mol. Biol.*, **297,** 1087-1103.

[106] Harrison,B.C., Marchese-Ragona,S.P., Gilbert,S.P., Cheng,N., Steven,A.C., & Johnson,K.A. (1993) Decoration of the microtubule surface by one kinesin head per tubulin heterodimer. *Nature*, **362,** 73-75.

[107] Kozielski,F., Arnal,I., & Wade,R.H. (1998) A model of the microtubule-kinesin complex based on electron cryomicroscopy and X-ray crystallography. *Curr. Biol.*, **8,** 191-198.

[108] Hirose,K., Lowe,J., Alonso,M., Cross,R.A., & Amos,L.A. (1999) Congruent docking of dimeric kinesin and ncd into three-dimensional electron cryomicroscopy maps of microtubule-motor ADP complexes. *Mol. Biol. Cell*, **10,** 2063-2074.

[109] Sosa,H., Dias,D.P., Hoenger,A., Whittaker,M., Wilson-Kubalek,E., Sablin,E., Fletterick,R.J., Vale,R.D., & Milligan,R.A. (1997) A model for the microtubule-Ncd motor protein complex obtained by cryo-electron microscopy and image analysis. *Cell*, **90,** 217-224.

[110] Hirose,K., Cross,R.A., & Amos,L.A. (1998) Nucleotide-dependent structural changes in dimeric NCD molecules complexed to microtubules. *J. Mol. Biol.*, **278,** 389-400.

[111] Ray,S., Meyhofer,E., Milligan,R.A., & Howard,J. (1993) Kinesin follows the microtubule's protofilament axis. *J. Cell Biol.*, **121,** 1083-1093.

[112] Coy,D.L., Wagenbach,M., & Howard,J. (1999) Kinesin takes one 8-nm step for each ATP that it hydrolyzes. *J. Biol. Chem*, **274,** 3667-3671.

[113] Schnitzer,M.J. & Block,S.M. (1997) Kinesin hydrolyses one ATP per 8-nm step. *Nature*, **388,** 386-390.

[114] Visscher,K., Schnitzer,M.J., & Block,S.M. (1999) Single kinesin molecules studied with a molecular force clamp. *Nature*, **400,** 184-189.

[115] Hua,W., Young,E.C., Fleming,M.L., & Gelles,J. (1997) Coupling of kinesin steps to ATP hydrolysis. *Nature*, **388,** 390-393.

[116] Astumian,R.D. (1997) Thermodynamics and kinetics of a Brownian motor. *Science*, **276,** 917-922.

[117] Schief,W.R., Clark,R.H., Crevenna,A.H., & Howard,J. (2004) Inhibition of kinesin motility by ADP and phosphate supports a hand-over-hand mechanism. *Proc. Natl. Acad. Sci. U. S. A*, **101,** 1183-1188.

[118] Yildiz,A., Tomishige,M., Vale,R.D., & Selvin,P.R. (2004) Kinesin walks hand-over-hand. *Science*, **303,** 676-678.

[119] Asbury,C.L., Fehr,A.N., & Block,S.M. (2003) Kinesin moves by an asymmetric hand-over-hand mechanism. *Science*, **302,** 2130-2134.

[120] Kaseda,K., Higuchi,H., & Hirose,K. (2003) Alternate fast and slow stepping of a heterodimeric kinesin molecule. *Nat. Cell Biol.*, **5,** 1079-1082.

[121] Hua,W., Chung,J., & Gelles,J. (2002) Distinguishing inchworm and hand-over-hand processive kinesin movement by neck rotation measurements. *Science*, **295,** 844-848.

[122] Schliwa,M. (2003) Kinesin: walking or limping? *Nat. Cell Biol.*, **5,** 1043-1044.

[123] Forkey,J.N., Quinlan,M.E., Shaw,M.A., Corrie,J.E., & Goldman,Y.E. (2003) Three-dimensional structural dynamics of myosin V by single-molecule fluorescence polarization. *Nature*, **422,** 399-404.

[124] Yildiz,A., Forkey,J.N., McKinney,S.A., Ha,T., Goldman,Y.E., & Selvin,P.R. (2003) Myosin V walks hand-over-hand: single fluorophore imaging with 1.5-nm localization. *Science*, **300,** 2061-2065.

[125] Rogers,K.R., Weiss,S., Crevel,I., Brophy,P.J., Geeves,M., & Cross,R. (2001) KIF1D is a fast non-processive kinesin that demonstrates novel K-loop-dependent mechanochemistry. *EMBO J.*, **20,** 5101-5113.

[126] Case,R.B., Pierce,D.W., Hom-Booher,N., Hart,C.L., & Vale,R.D. (1997) The directional preference of kinesin motors is specified by an element outside of the motor catalytic domain. *Cell*, **90,** 959-966.

[127] Endow,S.A. & Waligora,K.W. (1998) Determinants of kinesin motor polarity. *Science*, **281,** 1200-1202.

[128] Vale,R.D. & Milligan,R.A. (2000) The way things move: looking under the hood of molecular motor proteins. *Science*, **288,** 88-95.

[129] Hirose,K., Lockhart,A., Cross,R.A., & Amos,L.A. (1996) Three-dimensional cryoelectron microscopy of dimeric kinesin and ncd motor domains on microtubules. *Proc. Natl. Acad. Sci. U. S. A*, **93,** 9539-9544.

[130] Wendt,T.G., Volkmann,N., Skiniotis,G., Goldie,K.N., Muller,J., Mandelkow,E., & Hoenger,A. (2002) Microscopic evidence for a minus-end-directed power stroke in the kinesin motor ncd. *EMBO J.*, **21,** 5969-5978.

[131] Inoue,Y., Iwane,A.H., Miyai,T., Muto,E., & Yanagida,T. (2001) Motility of single one-headed kinesin molecules along microtubules. *Biophys. J.*, **81,** 2838-2850.

[132] Woehlke,G., Ruby,A.K., Hart,C.L., Ly,B., Hom-Booher,N., & Vale,R.D. (1997) Microtubule interaction site of the kinesin motor. *Cell*, **90,** 207-216.

[133] Sack,S., Kull,F.J., & Mandelkow,E. (1999) Motor proteins of the kinesin family. Structures, variations, and nucleotide binding sites. *Eur. J. Biochem.*, **262,** 1-11.

[134] Onishi,H., Mochizuki,N., & Morales,M.F. (2004) On the Myosin catalysis of ATP hydrolysis. *Biochemistry*, **43,** 3757-3763.

[135] Coleman,D.E., Berghuis,A.M., Lee,E., Linder,M.E., Gilman,A.G., & Sprang,S.R. (1994) Structures of active conformations of Gi alpha 1 and the mechanism of GTP hydrolysis. *Science*, **265,** 1405-1412.

[136] Pai,E.F., Krengel,U., Petsko,G.A., Goody,R.S., Kabsch,W., & Wittinghofer,A. (1990) Refined crystal structure of the triphosphate conformation of H-ras p21 at 1.35 A resolution: implications for the mechanism of GTP hydrolysis. *EMBO J.*, **9,** 2351-2359.

[137] Berchtold,H., Reshetnikova,L., Reiser,C.O., Schirmer,N.K., Sprinzl,M., & Hilgenfeld,R. (1993) Crystal structure of active elongation factor Tu reveals major domain rearrangements. *Nature*, **365,** 126-132.

[138] Kull,F.J. & Endow,S.A. (2002) Kinesin: switch I & II and the motor mechanism. *J. Cell Sci.*, **115,** 15-23.

[139] Endow,S.A. (2003) Kinesin motors as molecular machines. *Bioessays*, **25,** 1212-1219.

[140] Wittinghofer,A. & Pai,E.F. (1991) The structure of Ras protein: a model for a universal molecular switch. *Trends Biochem. Sci.*, **16,** 382-387.

[141] Rayment,I., Holden,H.M., Whittaker,M., Yohn,C.B., Lorenz,M., Holmes,K.C., & Milligan,R.A. (1993) Structure of the actin-myosin complex and its implications for muscle contraction. *Science*, **261,** 58-65.

[142] Fisher,A.J., Smith,C.A., Thoden,J.B., Smith,R., Sutoh,K., Holden,H.M., & Rayment,I. (1995) X-ray structures of the myosin motor domain of Dictyostelium discoideum complexed with MgADP.BeFx and MgADP.AlF4-. *Biochemistry*, **34,** 8960-8972.

[143] Dominguez,R., Freyzon,Y., Trybus,K.M., & Cohen,C. (1998) Crystal structure of a vertebrate smooth muscle myosin motor domain and its complex with the essential light chain: visualization of the pre-power stroke state. *Cell*, **94,** 559-571.

[144] Houdusse,A., Kalabokis,V.N., Himmel,D., Szent-Gyorgyi,A.G., & Cohen,C. (1999) Atomic structure of scallop myosin subfragment S1 complexed with MgADP: a novel conformation of the myosin head. *Cell*, **97,** 459-470.

[145] Houdusse,A., Szent-Gyorgyi,A.G., & Cohen,C. (2000) Three conformational states of scallop myosin S1. *Proc. Natl. Acad. Sci. U. S. A*, **97,** 11238-11243.

[146] Vale,R.D., Case,R., Sablin,E., Hart,C., & Fletterick,R. (2000) Searching for kinesin's mechanical amplifier. *Philos. Trans. R. Soc. Lond B Biol. Sci.*, **355,** 449-457.

[147] Rayment,I., Rypniewski,W.R., Schmidt-Base,K., Smith,R., Tomchick,D.R., Benning,M.M., Winkelmann,D.A., Wesenberg,G., & Holden,H.M. (1993) Three-dimensional structure of myosin subfragment-1: a molecular motor. *Science*, **261,** 50-58.

[148] Geeves,M.A. & Holmes,K.C. (1999) Structural mechanism of muscle contraction. *Annu. Rev. Biochem.*, **68,** 687-728.

[149] Gilbert,S.P. & Johnson,K.A. (1994) Pre-steady-state kinetics of the microtubule-kinesin ATPase. *Biochemistry*, **33,** 1951-1960.

[150] Hackney,D.D. (2002) Pathway of ADP-stimulated ADP release and dissociation of tethered kinesin from microtubules. Implications for the extent of processivity. *Biochemistry*, **41,** 4437-4446.

[151] Hancock,W.O. & Howard,J. (1999) Kinesin's processivity results from mechanical and chemical coordination between the ATP hydrolysis cycles of the two motor domains. *Proc. Natl. Acad. Sci. U. S. A*, **96,** 13147-13152.

[152] Klumpp,L.M., Brendza,K.M., Rosenberg,J.M., Hoenger,A., & Gilbert,S.P. (2003) Motor domain mutation traps kinesin as a microtubule rigor complex. *Biochemistry*, **42,** 2595-2606.

[153] Morfini,G., Szebenyi,G., Richards,B., & Brady,S.T. (2001) Regulation of kinesin: implications for neuronal development. *Dev. Neurosci.*, **23,** 364-376.

[154] Braman,J., Papworth,C., & Greener,A. (1996) Site-directed mutagenesis using double-stranded plasmid DNA templates. *Methods Mol. Biol.*, **57,** 31-44.

[155] Saiki,R.K., Gelfand,D.H., Stoffel,S., Scharf,S.J., Higuchi,R., Horn,G.T., Mullis,K.B., & Erlich,H.A. (1988) Primer-directed enzymatic amplification of DNA with a thermostable DNA polymerase. *Science*, **239,** 487-491.

[156] Studier,F.W. & Moffatt,B.A. (1986) Use of bacteriophage T7 RNA polymerase to direct selective high-level expression of cloned genes. *J. Mol. Biol.*, **189,** 113-130.

[157] Rosenberg,A.H., Lade,B.N., Chui,D.S., Lin,S.W., Dunn,J.J., & Studier,F.W. (1987) Vectors for selective expression of cloned DNAs by T7 RNA polymerase. *Gene*, **56,** 125-135.

[158] Studier,F.W., Rosenberg,A.H., Dunn,J.J., & Dubendorff,J.W. (1990) Use of T7 RNA polymerase to direct expression of cloned genes. *Methods Enzymol.*, **185,** 60-89.

[159] Shelanski,M.L., Gaskin,F., & Cantor,C.R. (1973) Microtubule assembly in the absence of added nucleotides. *Proc. Natl. Acad. Sci. U. S. A*, **70,** 765-768.

[160] Sloboda,R.D., Dentler,W.L., & Rosenbaum,J.L. (1976) Microtubule-associated proteins and the stimulation of tubulin assembly in vitro. *Biochemistry*, **15,** 4497-4505.

[161] Borisy,G.G., Olmsted,J.B., Marcum,J.M., & Allen,C. (1974) Microtubule assembly in vitro. *Fed. Proc.*, **33,** 167-174.

[162] Omoto,C.K. & Johnson,K.A. (1986) Activation of the dynein adenosinetriphosphatase by microtubules. *Biochemistry*, **25,** 419-427.

[163] Bradford,M.M. (1976) A rapid and sensitive method for the quantitation of microgram quantities of protein utilizing the principle of protein-dye binding. *Anal. Biochem.*, **72,** 248-254.

[164] Hiratsuka,T. (1983) New ribose-modified fluorescent analogs of adenine and guanine nucleotides available as substrates for various enzymes. *Biochim. Biophys. Acta*, **742,** 496-508.

[165] Woodward,S.K., Eccleston,J.F., & Geeves,M.A. (1991) Kinetics of the interaction of 2'(3')-O-(N-methylanthraniloyl)-ATP with myosin subfragment 1 and actomyosin subfragment 1: characterization of two acto-S1-ADP complexes. *Biochemistry*, **30,** 422-430.

[166] Brune,M., Hunter,J.L., Corrie,J.E., & Webb,M.R. (1994) Direct, real-time measurement of rapid inorganic phosphate release using a novel fluorescent probe and its application to actomyosin subfragment 1 ATPase. *Biochemistry*, **33,** 8262-8271.

[167] Brune,M., Hunter,J.L., Howell,S.A., Martin,S.R., Hazlett,T.L., Corrie,J.E., & Webb,M.R. (1998) Mechanism of inorganic phosphate interaction with phosphate binding protein from Escherichia coli. *Biochemistry*, **37,** 10370-10380.

[168] Willsky,G.R. & Malamy,M.H. (1976) Control of the synthesis of alkaline phosphatase and the phosphate-binding protein in Escherichia coli. *J. Bacteriol.*, **127,** 595-609.

[169] Gill,S.C. & von Hippel,P.H. (1989) Calculation of protein extinction coefficients from amino acid sequence data. *Anal. Biochem.*, **182,** 319-326.

[170] Gilbert,S.P. & Johnson,K.A. (1993) Expression, purification, and characterization of the Drosophila kinesin motor domain produced in Escherichia coli. *Biochemistry*, **32,** 4677-4684.

[171] Johnson,M.L., Correia,J.J., Yphantis,D.A., & Halvorson,H.R. (1981) Analysis of data from the analytical ultracentrifuge by nonlinear least-squares techniques. *Biophys. J.*, **36,** 575-588.

[172] Barshop,B.A., Wrenn,R.F., & Frieden,C. (1983) Analysis of numerical methods for computer simulation of kinetic processes: development of KINSIM--a flexible, portable system. *Anal. Biochem.*, **130,** 134-145.

[173] Zimmerle,C.T. & Frieden,C. (1989) Analysis of progress curves by simulations generated by numerical integration. *Biochem. J.*, **258,** 381-387.

[174] Johnson,K.A. (1986) Rapid kinetic analysis of mechanochemical adenosinetriphosphatases. *Methods Enzymol.*, **134,** 677-705.

[175] Cheng,J.Q., Jiang,W., & Hackney,D.D. (1998) Interaction of mant-adenosine nucleotides and magnesium with kinesin. *Biochemistry*, **37,** 5288-5295.

[176] Chen,J.T., Mayer,R.J., Fierke,C.A., & Benkovic,S.J. (1985) Site-specific mutagenesis of dihydrofolate reductase from Escherichia coli. *J. Cell Biochem.*, **29,** 73-82.

[177] Gardell,S.J., Craik,C.S., Hilvert,D., Urdea,M.S., & Rutter,W.J. (1985) Site-directed mutagenesis shows that tyrosine 248 of carboxypeptidase A does not play a crucial role in catalysis. *Nature*, **317,** 551-555.

[178] Robey,E.A., Wente,S.R., Markby,D.W., Flint,A., Yang,Y.R., & Schachman,H.K. (1986) Effect of amino acid substitutions on the catalytic and regulatory properties of aspartate transcarbamoylase. *Proc. Natl. Acad. Sci. U. S. A*, **83,** 5934-5938.

[179] Schnell,J.R., Dyson,H.J., & Wright,P.E. (2004) Structure, dynamics, and catalytic function of dihydrofolate reductase. *Annu. Rev. Biophys. Biomol. Struct.*, **33,** 119-140.

[180] Hackney,D.D. (1988) Kinesin ATPase: rate-limiting ADP release. *Proc. Natl. Acad. Sci. U. S. A*, **85,** 6314-6318.

[181] Hackney,D.D., Malik,A.S., & Wright,K.W. (1989) Nucleotide-free kinesin hydrolyzes ATP with burst kinetics. *J. Biol. Chem.*, **264,** 15943-15948.

[182] Huang,T.G. & Hackney,D.D. (1994) Drosophila kinesin minimal motor domain expressed in Escherichia coli. Purification and kinetic characterization. *J. Biol. Chem.*, **269,** 16493-16501.

[183] Ma,Y.Z. & Taylor,E.W. (1995) Kinetic mechanism of kinesin motor domain. *Biochemistry*, **34,** 13233-13241.

[184] Ma,Y.Z. & Taylor,E.W. (1997) Kinetic mechanism of a monomeric kinesin construct. *J. Biol. Chem.*, **272,** 717-723.

[185] Xing,J., Wriggers,W., Jefferson,G.M., Stein,R., Cheung,H.C., & Rosenfeld,S.S. (2000) Kinesin has three nucleotide-dependent conformations. Implications for strain-dependent release. *J. Biol. Chem*, **275,** 35413-35423.

[186] Sablin,E.P. & Fletterick,R.J. (2001) Nucleotide switches in molecular motors: structural analysis of kinesins and myosins. *Curr. Opin. Struct. Biol.*, **11,** 716-724.

[187] Hoyt,M.A., He,L., Totis,L., & Saunders,W.S. (1993) Loss of function of Saccharomyces cerevisiae kinesin-related CIN8 and KIP1 is suppressed by KAR3 motor domain mutations. *Genetics*, **135,** 35-44.

[188] Naber,N., Rice,S., Matuska,M., Vale,R.D., Cooke,R., & Pate,E. (2003) EPR Spectroscopy Shows a Microtubule-Dependent Conformational Change in the Kinesin Switch 1 Domain. *Biophys. J.*, **84,** 3190-3196.

[189] Rice,S., Lin,A.W., Safer,D., Hart,C.L., Naber,N., Carragher,B.O., Cain,S.M., Pechatnikova,E., Wilson-Kubalek,E.M., Whittaker,M., Pate,E., Cooke,R., Taylor,E.W., Milligan,R.A., & Vale,R.D. (1999) A structural change in the kinesin motor protein that drives motility. *Nature*, **402,** 778-784.

[190] Farrell,C.M., Mackey,A.T., Klumpp,L.M., & Gilbert,S.P. (2002) The role of ATP hydrolysis for kinesin processivity. *J. Biol. Chem*, **277,** 17079-17087.

[191] Klumpp,L.M., Mackey,A.T., Farrell,C.M., Rosenberg,J.M., & Gilbert,S.P. (2003) A Kinesin switch I arginine to lysine mutation rescues microtubule function. *J. Biol. Chem*, **278,** 39059-39067.

[192] Minehardt,T.J., Cooke,R., Pate,E., & Kollman,P.A. (2001) Molecular dynamics study of the energetic, mechanistic, and structural implications of a closed phosphate tube in ncd. *Biophys. J.*, **80,** 1151-1168.

[193] Muller,J., Marx,A., Sack,S., Song,Y.H., & Mandelkow,E. (1999) The structure of the nucleotide-binding site of kinesin. *Biol. Chem*, **380,** 981-992.

[194] Song,Y.H., Marx,A., Muller,J., Woehlke,G., Schliwa,M., Krebs,A., Hoenger,A., & Mandelkow,E. (2001) Structure of a fast kinesin: implications for ATPase mechanism and interactions with microtubules. *EMBO J.*, **20,** 6213-6225.

Vita

Scott David Auerbach was born in Brookline Massachusetts on August 9, 1965, the son of Gabriel Auerbach and Gloria Auerbach. He graduated from Brookline High School in 1983, and attended the University of Pennsylvania, from which he received a Bachelor of Arts degree in December 1986. During the following years he was employed as a research assistant at the University of Iowa department of Biological Sciences, and the University of Iowa College of Medicine. In September 1998 he entered the Graduate School at the University of Texas.

Permanent Address: 1044 Camino La Costa, Austin TX 78752

This dissertation was typed by the author